12-1-2022 2:30 PM

On the Spatial Modelling of Biological Invasions

Tedi Ramaj, *The University of Western Ontario*

Supervisor: Zou, Xingfu, *The University of Western Ontario*

A thesis submitted in partial fulfillment of the requirements for the Doctor of Philosophy degree in Applied Mathematics

Abstract

We investigate problems of biological spatial invasion through the use of spatial modelling. We begin by examining the spread of an invasive weed plant species through a forest by developing a system of partial differential equations (PDEs) involving an invasive weed and a competing native plant species. We find that extinction of the native plant species may be achieved by increasing the carrying capacity of the forest as well as the competition coefficient between the species. We also find that the boundary conditions exert long-term control on the biomass of the invasive weed and hence should be considered when implementing control measures. We then consider biological invasion on a smaller scale – the spread of melanoma, an invasive cancer. We investigate oncolytic virotherapy using adenoviruses as a treatment modality by using a system of ordinary differential equations (ODEs). Our model incorporates the oxygen concentration of the tumour microenvironment, as it is well known that hypoxic conditions reduce the efficacy of adenoviruses. As in the case of invasive weed spreading, our modelling highlights the importance of a favourable environment. In particular, our investigation into the infection rate of the virus and the oncolysis rate supports the notion of bounding the oncolysis rate for optimal clinical outcomes. Furthermore, our modelling suggests that the virus' oncolytic potency should be increased under hypoxic conditions, but should not be too large, so as to avoid inhibiting the replication of the virus. We find that these results are consistent after extending the model to a regional model which accounts for spreading of the melanoma via the lymphatic system. We then continue our investigation of oncolytic virotherapy by analyzing a PDE model of melanoma spreading through the skin. We find results which are consistent with our ODE model. Namely, placing infection rate-dependent bounds on the oncolysis rate leads to more favourable clinical outcomes. We provide some quantitative estimates on how to determine these bounds. Our theoretical modelling provides further evidence to suggest that auxiliary topical (regenerative) treatment of the skin can be a useful complement to virotherapy.

Keywords: spatial modelling, travelling wave solutions, mathematical ecology, invasive weed spreading, oncolytic virotherapy, hypoxia, PDE modelling, ODE modelling, lattice

Summary for Lay Audience

Using mathematical and computational tools can offer new insights on existing problems in biology. We consider some problems of biological invasion from a mathematical perspective: (i) The spread of an invasive weed plant species through a forest, taking up the resources of the pre-existing native plants and (ii) the spread of melanoma, an invasive skin cancer with high a mortality rate when diagnosed at an advanced stage. Even though these problems may seem very disconnected, very similar mathematical tools can be used to analyze them and to determine the similarities which exist between them. When investigating invasive plants with this approach, we find some potentially useful control measures to reduce the harm caused by invasive weeds. In particular, we find that taking control measures at the *boundaries* of where the weeds grow rather than throughout the entire forest can help control the spreading. When investigating the spread of melanoma, we consider the possible outcomes of treating the cancer with an oncolytic virus. This is a genetically engineered virus that attacks cancer cells, uses them to replicate, then destroys them while leaving healthy tissue unharmed. We build models which let us make suggestions on how to engineer these viruses by determining what features the viruses need. In particular, we find that a useful oncolytic virus should be effective at infecting the cancer cells, but *not too potent* at destroying these cancer cells. Why is that? Because if the virus kills the cancer cells faster than it may infect them, then it won't have any hosts through which to replicate. We find that there is a very delicate balance between how infectious the virus is and how efficient it is at killing the cancer cells. Our models give guidance on how to build these viruses under various conditions, such as the available oxygen at the tumour site. By using math to investigate these biological problems and using computers to run simulations, we can make predictions on how to mitigate the negative impacts of biological invasions without having to wait for months or years. Of course this approach cannot replace ecological field work or clinical trials, but it can help guide them.

Acknowledgements

First and foremost, I would like to thank my supervisor, Professor Xingfu Zou. Professor Zou has been incredibly inspiring, supportive, and patient during my time in his lab group. Without his immense knowledge and guidance, especially during some very difficult times, producing this thesis certainly would not have been possible. Thank you, Professor Zou, this experience has meant a lot to me and it was only so incredible thanks to you.

I would also like to extend my sincere gratitude to the entire Applied Math (and Math) department at Western University for providing me with this incredible opportunity. The invaluable experience and skills I have picked up during my time here is something I would not trade for the world. In particular, I would like to thank Prof. Yu and Prof. Wahl for their courses on nonlinear dynamics and mathematical biology which were pivotal to the production of this thesis.

I would also like to thank the entire Zou lab group, past and present, as well as the Applied Dynamical Systems seminar group, for the very interesting and thought-provoking discussions.

Another special thanks goes to Dr. Joseph Geraci. I doubt I would have started down this path if it wasn't for you. Seeing the type of work you did was my first introduction to the world of mathematical research and I keep those early moments with me to this day.

My thanks also go out to the province of Ontario for the funding provided via two Ontario Graduate Scholarships.

Last but certainly not least, I would like to thank my family for their continued love and support. Teuta and Ardian. Of course you already know that words cannot express how much you both mean to me. Now and forever. Iggy. I could never forget to thank you. Finally, my brother Albi. Spending time with you always gets me through the day. Thank you.

Dedicated to Ymer.

(1931 – 2022)

Co-Authorship Statement

I, Tedi Ramaj, declare that this thesis titled "On the spatial modelling of biological invasions" has been written by me under the supervision of Dr. Xingfu Zou.

Chapter 2 of this thesis has been published in the Bulletin of Mathematical Biology as Ramaj, T. (2021). On the Mathematical Modelling of Competitive Invasive Weed Dynamics. Bulletin of Mathematical Biology, 83(2), 1-25.

Chapter 3 of this thesis, "On the treatment of melanoma: a mathematical model of oncolytic virotherapy," is being prepared for submission for publication. The draft of the paper was prepared by Tedi Ramaj and then revised by Tedi Ramaj and Dr. Xingfu Zou.

Chapter 4 of this thesis, "A continuous spatial model of melanoma treatment via oncolytic virotherapy," is being prepared for submission for publication. The draft of the paper was prepared by Tedi Ramaj and then revised by Tedi Ramaj and Dr. Xingfu Zou.

Contents

List of Figures

List of Tables

List of Appendices

Chapter 1

Introduction

Spatial modelling of biological phenomena has seen widespread application in various fields such as ecology, epidemiology, population dynamics, and immunology [2, 17, 24, 29]. When used in combination with time-dependent dynamical models, spatial modelling can provide new insights on the underlying biological systems in a way which may drive policy decisions and suggest unique methodologies for dealing with classical biological problems. At the same time, these biological problems may offer new insights on the mathematical methodologies by presenting challenging problems and encouraging the use of complicated modelling techniques.

Some examples of spatial modelling include the modelling of the spread of invasive plant species [17], spatial modelling of infectious disease spread [24], and the modelling of various cancer treatment modalities, such as oncolytic virotherapy [2]. The mathematical tools used to develop and analyze these models can include delay differential equations (DDEs), ordinary differential equations (ODEs) on lattices, and partial differential equations (PDEs). The use of computational tools to perform numerical analyses and run simulations is also integrated into spatial modelling.

Broadly, the goal of this thesis is to develop and analyze spatial models in two separate biological contexts: an invasive plant species competition model and the modelling of melanoma

skin cancer treatment via oncolytic virotherapy. In both cases, we make use of PDE modelling and in the latter case, we also make use of ODE modelling on a spatial lattice. Ultimately, we provide a synthesis of the two seemingly disparate biological problems by connecting them through the mathematical framework. The underlying theme is the concept of biological invasion – the invasion of a native forest by an invasive plant species, the invasion of a healthy extracellular matrix by an invasive cancer, and even the invasion of melanoma cancer cells by an oncolytic virus in an attempt at treatment.

The rest of this chapter is devoted to providing the relevant biological background and motivations, as well as the relevant mathematical and computational techniques which will be used throughout this thesis.

1.1 *Tradescantia fluminensis*: An Invasive Weed

We begin by considering the case of ecological invasion on a population level. An invasive species is typically defined as a non-native species that threatens ecosystems and native species [32]. Invasive species can be animals, plants, fungi, and other living organisms. Along with climate change, invasive species have historically been implicated as the one of the greatest drivers of biodiversity loss [26, 50]. Invasive species may be introduced to an ecosystem through a variety of ways, such as natural dispersal. The most common method of the introduction of invasive species is through direct human intervention, either accidentally or deliberately [30]. For instance, exotic animals might be introduced for the purpose of trade and plant species may be introduced for the purpose of gardening, decorations, or foraging. These species typically display strong colonization characteristics and are able to establish in the new habitats, often at the cost of displacing the pre-existing native species [30]. It should be noted that not all non-native species are invasive. Along with the threat posed to native animal and plant species, the impacts which invasive species have on biodiversity also trigger cascading effects which can ultimately culminate in harm of human well-being through depletion of natural resources

and the effect on agricultural industries [32]. It is therefore crucial to assess the risk posed by invasive species in order to inform policy decisions, both environmental and economical.

Invasive weed plant species pose a significant environmental risk. By depleting the resources of native plants, these weeds may displace native species [42]. This can lead to a cascading effect, in which animal species which rely on the native plants as important parts of their habitats are also negatively impacted and displaced, potentially devastating an entire ecosystem as a result.

The plant species *Tradescantia fluminensis, T. fluminensis,* is a herb which is native to South America. In countries such as New Zealand, Australia, and (parts of) the United States, *T. fluminensis* acts as an invasive weed, competing with these countries' native plant species and leading to depletion of the naturally existing forests [17, 41, 42]. This occurs as a result of competition over resources, such as nutrients and water. Previous studies have found that the presence of this weed can cause an exponential decrease in the native plant biomass [42].

Finding new ways to control the spread of invasive weeds is essential in the preservation of many ecosystems. Many methods, such as the application of herbicides, have been suggested and applied in the control of invasive plant species. As an example, Standish et al. have suggested that decreasing the biomass of *T. fluminensis* below some critical threshold may lead to the regeneration of many native forests [42]. Aside from herbicide use, other control measures against the invasion of weed species include manual techniques such as cutting/pulling, animal grazing, and biocontrols (animals and insects), and even prescribed fires [44]. We explore a different option: Are there any alterations we may make to the environment of native plant species to provide them with advantages which may lead to out-competing the invasive weeds?

There is much need to approach the problem of invasive weed species in new ways. More recently, mathematical modelling has seen use in addressing this problem, In Chapter 2, we add to the existing literature by formulating and analyzing a new PDE model of competition between native plants and *T. fluminensis*. By comparing the results of the model to the relevant ecological literature, we are able to make some suggestions concerning less invasive methods

of controlling the spread of *T. fluminensis*. For example, as we will see in Chapter 2, our modelling predicts that increasing the carrying capacity of the forests (i.e., through stricter nature preservation policies) may lead to a reduction of the extinction of native plant species [43].

1.2 Melanoma: An Invasive Cancer

Despite ongoing advances in treatment, cancer remains one of the deadliest and most challenging group of diseases, particularly at more advanced stages. While survival rates have greatly improved for certain cancers such as cancers of the prostate and breast, the survival rates unfortunately remain depressingly low for other cancers such as glioblastoma and pancreatic cancer (particularly adenocarcinomas of the pancreas) [40]. Late detection due to lack of feasible screening methods is one of the major reasons for this disparity of outcomes [15]. Another major reason is due to a lack of quantity and efficacy of available treatments, particularly in the metastatic (cancer that has spread to distant organs or bones) setting. For example, as of 2022, there are typically only two lines of treatment available to Canadian patients with metastatic unresectable pancreatic cancer (FOLFIRINOX and Gemcitabine + Abraxane) [5] and many patients are too weak to even begin a single chemo regimen. Therefore, there is great interest not only in the development of *more* treatment protocols, but of less toxic ones such as immunotherapies.

Not all cancers are invasive – many cancers are noninvasive. Noninvasive cancers remain *in situ*, remaining in the original tissue in which they originated rather than spreading throughout the body (see, i.e., [47]). Treatment of these cancers is still typically required as they have the potential to become invasive over time if not promptly identified and eradicated. At this stage, often considered stage 0, treatment tends to involve surgery or radiation, but rarely more toxic modalities such as chemotherapy. Invasive cancers are cancers which have announced their intention to spread throughout the entire organism. Upon invading distant regions of the

body, the cancer cells may form new tumours and interfere with the necessary function of vital organs, leading to death. The analogy between metastatic invasive cancer and invasive weeds is clear: tumour cells, like invasive plants, have spread to a different part of the body where they are essentially exotic and interfere with the delicate balance of the pre-existing system (i.e., organ or ecosystem). An example of an invasive skin cancer is melanoma.

Melanoma is considered a deadly form of skin cancer, which is known for high mortality rates when diagnosed at advanced stages [39]. It begins in the melanocytes – the cells responsible for producing melanin – and can begin in various parts of the body such as the arms, legs, or trunk [38, 45]. It is the fifth most common cancer in adults in the United States [37]. Fortunately, due to increases in early detection and increased protection against UV radiation, there have been significant improvements in its treatment and in patient outcomes [39]. However, treatment becomes much more difficult in the metastatic setting at which point the disease generally becomes incurable. This has driven the need for additional treatment modalities.

Like many other cancers, melanoma typically spreads through two possible routes: the bloodstream and the lymphatic system. Generally, melanoma is more likely to first spread into nearby lymph nodes before spreading into the bloodstream [51] and toward distant organs, i.e., metastasis. In this thesis, we consider the case of spread through the lymphatic system. Once the primary melanoma tumour grows larger and deeper into the skin, there is a higher probability of it reaching the lymphatic system [3, 28]. At this point, lymphatic fluid carries the cancer cells to the lymph nodes [23]. Typically, a greater number of lymph nodes effected at the time of diagnosis is associated with a worse prognosis. From here, the tumour cells may go on to invade distant organs.

1.2.1 Oncolytic Virotherapy

Oncolytic virotherapy refers the use of genetically modified viruses to selectively infect and destroy cancer cells via both direct and indirect mechanisms [12, 36]. This treatment modality has a significantly reduced toxicity compared to a conventional treatment method such as

chemotherapy. The use of oncolytic virotherapy in tandem with chemotherapy can lead to even more promising results in terms of prognosis. For example, ONYX-015, an oncolytic adenovirus, has been used in clinical trials for the treatment of metastatic pancreatic cancer [48]. Maintaining quality of life is an important aspect of treatment for patients with terminal cancer and so the use of such a virus comes with the benefit of reduced toxicity compared to some traditional therapies.

An oncolytic virus, the modified herpes simplex virus Talimogene laherparepvec (T-VEC), has been use in the clinical setting to treat inoperable melanoma [20, 35]. The virus is typically administered via direct subcutaneous injection into the melanoma lesion [14]. The treatment is frequently performed in combination with other therapies such as radiotherapy and chemotherapy. The virus selectively infects and destroys melanoma tumour cells, hijacking their replication machinery, proliferating, and moving on to infect additional tumour cells. Furthermore, the virus can also activate the immune system, stimulating an immune response against cancer cells which have already spread [10, 12]. Other onclytic viruses used in the treatment of melanoma include adenoviruses such as ONYX-015 and ZD55-IL-24 [18].

In Chapter 3, we propose and analyze an ODE model of oncolytic virotherapy. We then extend this model to a regional model which incorporates spread of the cancer through the lymphatic system, hence incorporating spatial structure. The goal is to analyze the potential systemic therapy properties of oncolytic viruses. In Chapter 4, we propose and analyze a continuous PDE model of oncolytic virotherapy. In both cases, we make predictions concerning the mechanism of cancer cell infection by oncolytic viruses. We also make some suggestions concerning optimization of the treatment protocol.

1.2.2 Cell-to-Cell Viral Spreading

In Chapters 3 and 4, we make use of cell-to-cell spreading of viruses in our modelling of oncolytic virotherapy. This is a mechanism used by oncolytic viruses, also known as oncolysis, in which the virus infects and destroys cancer cells via necrosis. Viral progeny are then released

and go on to infect surrounding cancer cells via cell-to-cell spreading [16].

In contrast, much of the mathematical modelling of viral infections considers the use of a free virus variable [34, 46]. To consider the case of cell-to-cell spreading of viruses, we may adopt the approach used in [6, 22]. We can consider the density of cells which are uninfected by the virus, $u(t)$, and the density of cells which are infected by the virus, $n(t)$. As in [6], we assume that α gives the rate at which infected cells are able to infect the uninfected cells and that β/α is the fraction of cells which survive the incubation period. Then we may model the infection by using the following system of integro-differential equations [6]:

$$\frac{\mathrm{d}u}{\mathrm{d}t} = -\alpha u n, \tag{1.1}$$

$$\frac{\mathrm{d}n}{\mathrm{d}t} = \beta \int_{-\infty}^{t} u(\xi) n(\xi) F(t-\xi) \mathrm{d}\xi, \tag{1.2}$$

where $F(\xi)$ is the delay kernel probability distribution. For biological realism, we assume that the initial values of u and n are positive for $\xi \in (-\infty, 0]$. The above system assumes that cells which are infectious at time t were infected ξ units in the past. As in Section 3 of [6], we assume that $F(\xi)$ is given by the Dirac delta function, $F(\xi) = \delta(\xi)$. Making this substitution into system (1.1) - (1.2) yields

$$\frac{\mathrm{d}u}{\mathrm{d}t} = -\alpha u(t) n(t), \tag{1.3}$$

$$\frac{\mathrm{d}n}{\mathrm{d}t} = \beta u(t) n(t), \tag{1.4}$$

which resembles predation in population models. This is the mode of infection which will be considered as an important feature of the models we develop in Chapters 3 and 4. This form of infection has previously been considered in mathematical models of oncolytic virotherapy such as in [49]. For more on cell-to-cell spreading of viruses, one may read [6, 16, 22].

1.3 Mathematical Methodologies

In subsequent chapters, we make use of various mathematical methodologies concerning spatial modelling. Even though the biological context of Chapter 2 may seem dissimilar to that of Chapters 3 and 4, the common factor between the chapters is the physical property of invasion. Invasive weeds spread throughout natural forests and disrupt naturally existing plants. Invasive cancers spread throughout an organism and disrupt the function of naturally existing organs. Oncolytic viruses invade their target cancer cells and disrupt their function. The common theme here is invasion via spatial spreading. To that end, we may use similar tools to perform spatial modelling of these *seemingly* vastly different scenarios.

1.3.1 Stability of Steady States

When constructing mathematical models, adding complexity to the model can help capture richer dynamics of real-world phenomena. In general, as the complexity of a model is increased, the mathematical tractability tends to decrease. Typically, finding explicit solutions to the problems posed is very difficult and, frequently, impossible. While the use of numerical simulations in approximating solutions to the models may be used as a very useful alternative to finding exact solutions, it is often preferable to be able to analytically establish some exact results by using mathematical theories. Aside from providing information on how the systems will behave, these analytic results may also be used to guide numerical simulations by offering suggestions on numerical values of the model parameters.

In this thesis, we are primarily concerned with modelling via autonomous ODEs. Even when considering PDEs, our analytic investigations are frequently concerned with the existence of travelling wave solutions. For our purposes, as in Subsection 1.3.2, this type of analysis typically involves investigating a system of autonomous ODEs which describes the dynamics of the travelling wave. To that end, we review some relevant results regarding stability of steady states of autonomous ODEs.

We will consider first-order ODEs. The following theory will also be relevant for n^{th}-order ODEs as such higher-order ODEs may be expressed as systems of first-order ODEs. For more details on the following definitions see [33] or most texts on nonlinear dynamical systems theory.

Definition 1.3.1 A system of n first-order ODEs is **autonomous** if it may be written in the form

$$\frac{\mathrm{d}\mathbf{x}}{\mathrm{d}t} = \mathbf{f}(\mathbf{x}), \quad \text{for } \mathrm{x} \in \Omega, \tag{1.5}$$

where we consider the open subset $\Omega \subset \mathbb{R}^n$ and $\mathbf{f} : \Omega \to \mathbb{R}^n$ is continuously differentiable. If $\tilde{\mathbf{x}} \in \Omega$ is a point such that $\mathbf{f}(\tilde{\mathbf{x}}) = \mathbf{0}$, then $\tilde{\mathbf{x}}$ is a **steady state** (or *equilibrium*) of system (1.5).

If a system is initially at the steady state, it will remain there for all values of the independent variable. A wide range of behaviours of solutions of system (1.5) can be characterized by the *stability* of the system's steady states. It is therefore useful to formally define stability.

Definition 1.3.2 Consider system (1.5) with initial conditions $\mathbf{x}(0) = \mathbf{x}_0$ which has solution $\mathbf{x}(t)$. If for all $\epsilon > 0$ there exists a $\delta > 0$, so that for all $\mathbf{x}_0$ such that

$$\|\mathbf{x}_0 - \tilde{\mathbf{x}}\| < \delta \implies \|\mathbf{x}(t) - \tilde{\mathbf{x}}\| < \epsilon \quad \forall t > 0,$$

then the steady state $\tilde{\mathbf{x}}$ is **locally stable**. In this case, $\|\cdot\|$ denotes the standard Euclidean norm. Moreover, if in addition to the steady state being locally stable, it also holds that

$$\lim_{t\to\infty} \mathbf{x}(t) = \tilde{\mathbf{x}},$$

then the steady state $\tilde{\mathbf{x}}$ is said to be locally **asymptotically** stable. If $\tilde{\mathbf{x}}$ is not locally stable, then we say it is **unstable.**

The definition of local stability of a given steady state considers solution trajectories with initial conditions near the steady state. If in addition to being locally stable, all solutions with

initial conditions in Ω converge to the steady state as $t \to \infty$, then we say that the steady state is **globally asymptotically stable**.

From a biological perspective, being able to establish stability of a favourable steady state (such as an weed-free or a cancer-free steady state) of one's model is typically preferable. Establishing local asymptotic stability tends to be easier as it can often be accomplished through linearization of a nonlinear system about the steady state. Since the stability of steady states of linear systems are well understood, we can study stability of hyperbolic steady states of nonlinear systems by use of tools such as the Hartman-Grobman Theorem [33]. Global asymptotic stability is a stronger result but tends to be harder to prove, particularly in higher dimensions. Techniques such as constructing Lyapunov functions over trapping regions can be useful in establishing global stability results.

We now consider the construction of a Lyapunov function in order to establish global asymptotic stability of the steady state $\tilde{\mathbf{x}}$.

Definition 1.3.3 *If $V : \Omega \to \mathbb{R}$ is a continuously differentiable function, then we say that V is a **Lyapunov function** of system (1.5) if*

1. *V is positive definite on Ω, i.e., $V(\tilde{\mathbf{x}}) = 0$ and $V(\mathbf{x}) > 0$ for all $\mathbf{x} \in \Omega \setminus \{\tilde{\mathbf{x}}\}$;*

2. *$\dot{V}(\tilde{\mathbf{x}}) \leq 0$ for all $\mathbf{x} \in \Omega$.*

Theorem 1.3.1 (LaSalle's Invariance Principle) *Assume that $\tilde{\mathbf{x}}$ is a steady state of system (1.5) and that there exists a Lyapunov function of this system in the sense of Definition 1.3.3. If $U := \{\mathbf{x} \in \Omega : \dot{V}(\mathbf{x}) = 0\}$ and $W \subset U$ is the largest positively invariant (with respect to system (1.5)) subset of U, then all bounded solutions of system (1.5) in Ω approach W as $t \to \infty$.*

An important corollary of Theorem 1.3.1 is that if the set W contains only the locally stable steady state $\tilde{\mathbf{x}}$, then all bounded solutions approach $\tilde{\mathbf{x}}$ as $t \to \infty$ and so $\tilde{\mathbf{x}}$ is globally asymptotically stable.

Throughout this thesis, we frequently make use of stability analysis as it comes up in various contexts. The study of travelling wave solutions of PDE models is one such example, as we will see in the next subsection.

1.3.2 Travelling Wave Solutions

Travelling wave solutions of partial differential equations have been studied extensively in the context of modelling various biological phenomena [7, 13, 25, 27]. We consider a system of reaction-diffusion-advection equations of the form

$$\frac{\partial \mathbf{u}(x,t)}{\partial t} + V\frac{\partial \mathbf{u}(x,t)}{\partial x} = D\frac{\partial^2 \mathbf{u}(x,t)}{\partial x^2} + \mathbf{F}(\mathbf{u}(x,t)), \tag{1.6}$$

where $x \in \mathbb{R}$, $\mathbf{u} \in \mathbb{R}^n$, $V = \text{diag}(v_1, v_2, \ldots, v_n)$, $D = \text{diag}(D_1, D_2, \ldots, D_n)$, and $\mathbf{F} : \mathbb{R}^n \to \mathbb{R}^n$ is a continuously differentiable function. In Chapter 2, we consider the case where $D = 0$ and in Chapter 4, we consider the case where $V = 0$. To find a travelling wave solution of this system, we consider a solution of the form

$$\mathbf{u}(x,t) = \mathbf{U}(x - ct) = \Big[U_1(x - ct), \quad U_2(x - ct), \quad \cdots, \quad U_n(x - ct)\Big]^T,$$

where $c > 0$. We call such a solution a right-travelling travelling wave solution. By setting $\xi := x - ct$, where ξ is also called the travelling wave variable, the travelling wave solution may be written as $\mathbf{U}(\xi)$. By substituting the ansatz into system (1.6), we obtain the following system of ordinary differential equations:

$$-c\frac{\mathrm{d}\mathbf{U}}{\mathrm{d}\xi} + V\frac{\mathrm{d}\mathbf{U}}{\mathrm{d}\xi} = D\frac{\mathrm{d}^2\mathbf{U}}{\mathrm{d}\xi^2} + \mathbf{F}(\mathbf{U}(\xi)). \tag{1.7}$$

Let $E_0 = (a_1, a_2, \ldots, a_n)$ and $E_1 = (b_1, b_2, \ldots, b_n)$ be steady states of system (1.7). We set the additional condition that the solution, $\mathbf{U}(\xi)$, approaches E_0 as $\xi \to -\infty$ and approaches E_1 as $\xi \to \infty$. With this additional condition, we have properly defined a travelling wave solution of

system (1.6).

Usually considered the classical example of the study of travelling wave solutions is the so-called Fisher-KPP equation [11, 21]. This is given by the reaction-diffusion equation

$$\frac{\partial u}{\partial t} = D\frac{\partial^2 u}{\partial x^2} + ru\left(1 - \frac{u}{K}\right), \tag{1.8}$$

where D is the diffusion coefficient, r is the logistic growth rate, and K is the carrying capacity, i.e., of some population with density u. This is an example of a reaction-diffusion equation. In order to obtain this equation from system (1.7), we set $n = 1$ and $V = 0$. This equation may be non-dimensionalized to give

$$\frac{\partial u}{\partial t} = \frac{\partial^2 u}{\partial x^2} + u\,(1 - u)\,. \tag{1.9}$$

We note that equation (1.9) has two steady states, $u = 0$ and $u = 1$. A travelling wave solution of equation (1.9) takes the form $u(x, t) = U(\xi)$, where we define $\xi := x - ct$, and c is a positive constant. The solution satisfies $\lim_{\xi\to-\infty} U(\xi) = 1$ and $\lim_{\xi\to\infty} U(\xi) = 0$. That is, the solution connects the two steady states. Through a standard phase portrait analysis, it can be shown that for $c \geq 2$, there exists a travelling wave solution of the Fisher-KPP equation [9]. If $c < 2$, then the Fisher-KPP equation does not possess any non-negative travelling wave solutions and, therefore, it does not possess any biologically relevant travelling wave solutions. We now give a brief outline of the standard approach used to show these results.

We can show the existence of a travelling wave solution by using standard Poincaré-Bendixson theory. To begin, substituting $u(x, t) = U(x - ct) = U(\xi)$ into equation (1.9) yields the following travelling wave ordinary differential equation:

$$-c\frac{\mathrm{d}U}{\mathrm{d}\xi} = \frac{\mathrm{d}^2 U}{\mathrm{d}\xi^2} + U(1 - U). \tag{1.10}$$

Setting $V(\xi) := U'(\xi)$, we may write equation (1.10) as the following system of first order

differential equations:

$$U'(\xi) = V, \tag{1.11}$$

$$V'(\xi) = -cV - U(1-U). \tag{1.12}$$

Linearizing the system at the steady states $(U, V) = (0, 0)$ and $(U, V) = (1, 0)$ gives the matrices

$$J(0,0) = \begin{pmatrix} 0 & 1 \\ -1 & -c \end{pmatrix}, \quad J(1,0) = \begin{pmatrix} 0 & 1 \\ 1 & -c \end{pmatrix},$$

which respectively have eigenvalues $(-c \pm \sqrt{c^2-4})/2$ and $(-c \pm \sqrt{c^2+4})/2$. Since $J(1,0)$ always has one negative eigenvalue and one positive eigenvalue, the steady state $(1,0)$ is a saddle point. On the other hand, $J(0,0)$ may have either real or non-real complex eigenvalues. In all cases, the eigenvalues have negative real part and therefore, $(0,0)$ is (locally) stable. If $c < 2$, the origin is a stable spiral and the solution $U(\xi)$ becomes negative for some values of ξ. Hence, no biologically feasible travelling wave solution exists for $c < 2$, as we require non-negative solutions. On the other hand, if $c \geq 2$, then there exists a heteroclinic orbit connecting $(1,0)$ to $(0,0)$ for which $U(\xi)$ remains non-negative. Trajectories for different values of c are given in Figure 1.1. See [9] for more details. We can conclude that $c_{\min} = 2$ is the *minimal* wave speed for which a travelling wave solution exists and such a solution exists for all $c \geq 2$.

Since we are considering a right-travelling wave, we note that as $t \to \pm\infty$, we have $\xi \to \mp\infty$. Hence, the long-term dynamics of this system tend to the $U = 1$ steady state. In the context of a population undergoing logistic growth and spreading via diffusion, this solution corresponds to the potential of the population to move from near extinction to a level approaching the carrying capacity. We will consider travelling wave solutions of more complicated models, but we will see that just as in the Fisher-KPP equation, linearization at the steady states plays a major role in establishing our results.

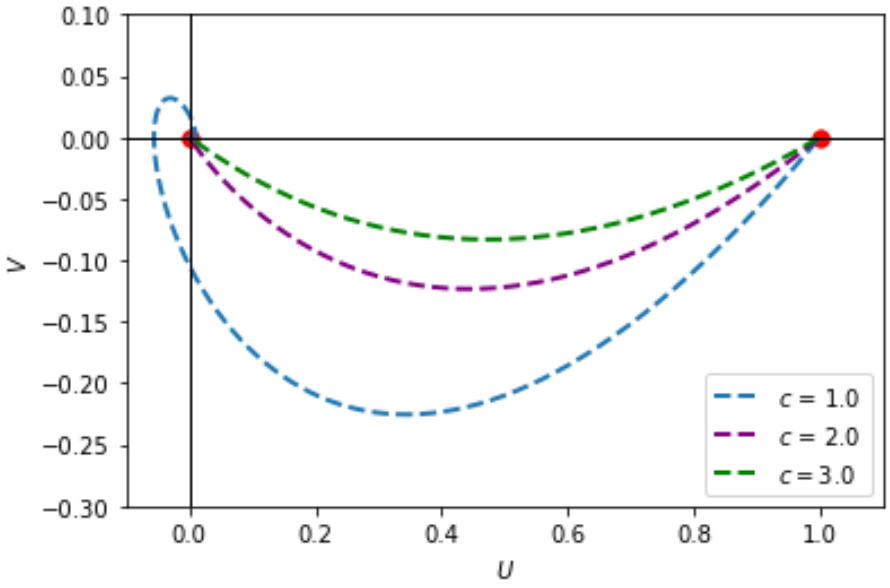

Figure 1.1: Heteroclinic orbits of the Fisher-KPP equation connecting $(1, 0)$ to $(0, 0)$ for different wave speeds, c. When $c = 1.0$, U crosses the V-axis and becomes negative, leading to a non-biological solution. For $c \geq 2$, U remains non-negative and we have a biologically feasible travelling wave solution.

1.4 Contributions of this Thesis

We now have the simplified yet sufficient biological background to tackle some problems of biological invasion from a mathematical perspective. Unsurprisingly, these forms of biological invasion contain spatial structure which should be considered. In the context of spreading invasive weeds, the spatial structure corresponds to a forest mat across which the weed spreads. In the context of oncolytic virotherapy treatment of melanoma, the spatial structure corresponds to the position of the tumour cells (and the virus) within the organism. The overarching goal of this thesis is to develop and investigate spatial mathematical models and further establish a connection between the ecological invasion of weeds and the malignant invasion of cancer. The particular contribution of each chapter is summarized below.

- **Chapter 2:** We begin this chapter by revisiting a two-variable PDE model of *T. fluminensis* spreading [4]. We consider some special cases of this model which have not previously been considered and analytically solve the corresponding initial and bound-

ary value problems. From these solutions, we can make some biological predictions concerning control measures to avoid uncontrolled weed spreading. Namely, we predict that in forests in which invasive weeds are spreading *very* fast, controlling the weed biomass **only** at a boundary (such as beside a river) is more effective and more feasible than taking control measures (like herbicide application) throughout the entire forest. In other words, controlling the original boundary of the weed is more effective than taking extreme measures throughout the entire forest mat. These results are consistent with some of the existing ecological literature [19]. We then extend the model further by introducing a pre-established native plant species which can also spread through the forest and competes with the invading weed. In our analysis, we determine some conditions on the system parameters which lead to co-existence of the species and preclude the extinction of the native species. Among many results, we find that the carrying capacity of the forest is one of the most important parameters and that maintaining a greater carrying capacity can lead to co-existence. Perhaps more surprisingly, we find that the same is true of the rate of competition between the weed and the native species – greater competition rates leads to co-existence of the species. When considering travelling wave solutions of our system, we also prove that the infimal (rather than minimal) wave speed required for a co-existence transition wave is given by the advection (*creeping* speed of the invasive weed. In this regard, the result of our extended model agrees with and further supports the result of the original model proposed by Hogan and Myerscough [4].

- **Chapter 3:** In this chapter, we develop a model of oncolytic virotherapy which takes into account the oxygen concentration of the tumour microenvironment. We model the use of an adenovirus which has decreased infection and oncolysis (i.e., cancer cell destroying) functioning under hypoxic conditions. Compared to much of the existing modelling literature, we model the virus' infection and oncolysis rates as a functions of the available oxygen concentration rather than as constants. We then extend this model even further by considering a regional model of melanoma spreading to the adjacent lymph nodes

through the lymphatic system by constructing a system of ODEs on a one-dimensional lattice, with each vertex representing a lymph node and each edge representing a lymphatic vessel. Through our analysis and computational work, our findings may grant some insight on the engineering of oncolytic viruses. Namely, we establish some important relationships between the infection capabilities of the virus and its oncolytic (killing) capabilities which depend on the oxygen conditions of the tumour microenvironment. We are led to conjecture that under hypoxic conditions, the preferential virus characteristic would be increased oncolytic capacity, but under oxygen-rich conditions, the oncolytic capacity should be reduced relative to the infection capacity. In all cases, our theoretical work indicates that the delicate balance between how potent a virus is at infecting and how potent a virus is at killing is at the forefront of successful treatment. Importantly, we determine that the oncolytic capabilities of the virus must **never** be too great as this will lead to failure of the treatment as more cancer cells are killed than can be infected. This work can hopefully lead to some potential directions regarding engineering oncolytic adenoviruses.

- **Chapter 4:** We continue with the theme of oncolytic virotherapy in this chapter. The spatial aspect of Chapter 3 comes from the lattice model which incorporates lymph nodes. On the other hand, the spatial structure of Chapter 4 comes from the use of a three-variable PDE system to model the *local* spread of a melanoma tumour on the surface of the skin in the presence of oncolytic virus treatment. That is, we consider continuous space rather than discrete space. We build these models by building upon the work of [4, 8] – which just consider melanoma growth – and extending the models by considering the impact of treatment with an oncolytic virus. We investigate the existence of travelling wave solutions, both analytically and numerically. We once again assess the importance of the infection and oncolysis capabilities of the virus, as in Chapter 3. While many characteristics of this new mechanistic model differ from those of Chapter 3, we find consistent results regarding preferential virus characteristics. That is, we once

again find that the oncolysis rate of the virus must not be too great, consistent both with Chapter 3 and the existing literature (i.e., see [1]). Our investigation also suggest that a useful complementary treatment may include non-invasive topical treatments such as wound dressing of the damaged skin, a technique which has also been investigated in the oncology literature [31]. We further provide evidence of the importance of wound dressing as an important part of melanoma treatment.

- **Chapter 5:** In the final chapter, we make some concluding remarks and discuss possible future work regarding the modelling of biological invasion.

Bibliography

[1] Bhatt, D. K., Janzen, T., Daemen, T., & Weissing, F. J. (2022). Modelling the spatial dynamics of oncolytic virotherapy in the presence of virus-resistant tumor cells. bioRxiv.

[2] Cassidy, T., & Craig, M. (2019). Determinants of combination GM-CSF immunotherapy and oncolytic virotherapy success identified through in silico treatment personalization. *PLoS computational biology*, 15(11), e1007495.

[3] Chen, L. L., Nolan, M. E., Silverstein, M. J., Mihm Jr, M. C., Sober, A. J., Tanabe, K. K., ... & Michaelson, J. S. (2009). The impact of primary tumor size, lymph node status, and other prognostic factors on the risk of cancer death. *Cancer: Interdisciplinary International Journal of the American Cancer Society*, 115(21), 5071-5083.

[4] Colson, C., Sánchez-Garduño, F., Byrne, H. M., Maini, P. K., & Lorenzi, T. (2021). Travelling-wave analysis of a model of tumour invasion with degenerate, cross-dependent diffusion. *Proceedings of the Royal Society A*, 477(2256), 20210593.

[5] Conroy, T., Bachet, J. B., Ayav, A., Huguet, F., Lambert, A., Caramella, C., ... & Ducreux, M. (2016). Current standards and new innovative approaches for treatment of pancreatic cancer. *European Journal of Cancer*, 57, 10-22.

[6] Culshaw, R. V., Ruan, S., & Webb, G. (2003). A mathematical model of cell-to-cell spread of HIV-1 that includes a time delay. *Journal of Mathematical Biology*, 46(5), 425-444.

[7] Dunbar, S. R. (1983). Travelling wave solutions of diffusive Lotka-Volterra equations. *Journal of Mathematical Biology*, 17(1), 11-32.

[8] El-Hachem, M., McCue, S. W., & Simpson, M. J. (2021). Travelling wave analysis of cellular invasion into surrounding tissues. *Physica D: Nonlinear Phenomena*, 428, 133026.

[9] Fife, P.C., *Mathematical Aspects of Reaction and Diffusion Systems*, Lecture Notes in Biomathematics, Vol.28, Springer, Berlin, New York, 1979.

[10] Filley, A. C., & Dey, M. (2017). Immune system, friend or foe of oncolytic virotherapy?. *Frontiers in oncology*, 7, 106.

[11] Fisher, R. A. (1937). The wave of advance of advantageous genes. *Annals of Eugenics*, 7(4), 355-369.

[12] Fountzilas, C., Patel, S., & Mahalingam, D. (2017). Oncolytic virotherapy, updates and future directions. *Oncotarget*, 8(60), 102617.

[13] Harko, T., & Mak, M. K. (2014). Travelling wave solutions of the reaction-diffusion mathematical model of glioblastoma growth: An Abel equation based approach. arXiv preprint arXiv:1409.0605.

[14] Harrington, K. J., Puzanov, I., Hecht, J. R., Hodi, F. S., Szabo, Z., Murugappan, S., & Kaufman, H. L. (2015). Clinical development of talimogene laherparepvec (T-VEC): A modified herpes simplex virus type-1–derived oncolytic immunotherapy. *Expert Review of Anticancer Therapy*, 15(12), 1389-1403.

[15] Hidalgo, M., Cascinu, S., Kleeff, J., Labianca, R., Löhr, J. M., Neoptolemos, J., ... & Heinemann, V. (2015). Addressing the challenges of pancreatic cancer: future directions for improving outcomes. *Pancreatology*, 15(1), 8-18.

[16] Hill, C., & Carlisle, R. (2019). Achieving systemic delivery of oncolytic viruses. *Expert Opinion on Drug Delivery*, 16(6), 607-620.

[17] Hogan, A. B., & Myerscough, M. R. (2017). A model for the spread of an invasive weed, Tradescantia fluminensis. *Bulletin of Mathematical Biology*, 79(6), 1201-1217.

[18] Hu, H. J., Liang, X., Li, H. L., Du, C. M., Hao, J. L., Wang, H. Y., ... & Liu, X. Y. (2020). The armed oncolytic adenovirus ZD55-IL-24 eradicates melanoma by turning the tumor cells from the self-state into the nonself-state besides direct killing. *Cell Death & Disease*, 11(11), 1-21.

[19] James A, Molloy SM, Ponder-Sutton A, Plank MJ, Lamoureaux SL, Bourdôt GW, Kelly D. (2015), Modelling Tradescantia fluminensis to assess long term survival. *PeerJ* 3:e1013 https://doi.org/10.7717/peerj.1013

[20] Johnson, D. B., Puzanov, I., & Kelley, M. C. (2015). Talimogene laherparepvec (T-VEC) for the treatment of advanced melanoma. *Immunotherapy*, 7(6), 611-619.

[21] Kolmogorov, A.N., Petrovskii I.G., Piskunov N.S., Study of a diffusion equation that is related to the growth of a quality of matter, and its application to a biological problem, Byul.Mosk.Gos.Univ.Ser.A, Mat.Mekh.1 (1937) 1–26.

[22] Lai, X., & Zou, X. (2014). Modeling HIV-1 virus dynamics with both virus-to-cell infection and cell-to-cell transmission. *SIAM Journal on Applied Mathematics*, 74(3), 898-917.

[23] Leong, S. P., Pissas, A., Scarato, M., Gallon, F., Pissas, M. H., Amore, M., ... & Lund, A. W. (2021). The lymphatic system and sentinel lymph nodes: conduit for cancer metastasis. *Clinical & Experimental Metastasis*, 1-19.

[24] Li, A., & Zou, X. (2021). Evolution and Adaptation of Anti-predation Response of Prey in a Two-Patchy Environment. *Bulletin of Mathematical Biology*, 83(5), 1-27.

[25] Ma, S., & Zou, X. (2005). Existence, uniqueness and stability of travelling waves in a discrete reaction–diffusion monostable equation with delay. *Journal of Differential Equations*, 217(1), 54-87.

[26] Mainka, S. A., & Howard, G. W. (2010). Climate change and invasive species: double jeopardy. *Integrative Zoology*, 5(2), 102-111.

[27] Marchant, B. P., Norbury, J., & Sherratt, J. A. (2001). Travelling wave solutions to a haptotaxis-dominated model of malignant invasion. *Nonlinearity*, 14(6), 1653.

[28] Mays, M. P., Martin, R. C., Burton, A., Ginter, B., Edwards, M. J., Reintgen, D. S., ... & Scoggins, C. R. (2010). Should all patients with melanoma between 1 and 2 mm Breslow thickness undergo sentinel lymph node biopsy?. Cancer: *Interdisciplinary International Journal of the American Cancer Society*, 116(6), 1535-1544.

[29] Neuhauser, C. (2001). Mathematical challenges in spatial ecology. *Notices of the AMS*, 48(11), 1304-1314.

[30] Parker, M., Thompson, J. N., & Weller, S. G. (2001). The population biology of invasive species. *Annu. Rev. Ecol. Syst*, 32, 305-32.

[31] Pavel, T. I., Chircov, C., Rădulescu, M., & Grumezescu, A. M. (2020). Regenerative wound dressings for skin cancer. *Cancers*, 12(10), 2954.

[32] Pejchar, L., & Mooney, H. A. (2009). Invasive species, ecosystem services and human well-being. *Trends in Ecology & Evolution*, 24(9), 497-504.

[33] Perko, L. (2013). *Differential equations and dynamical systems* (Vol. 7). Springer Science & Business Media.

[34] Pooladvand, P., Yun, C. O., Yoon, A. R., Kim, P. S., & Frascoli, F. (2021). The role of viral infectivity in oncolytic virotherapy outcomes: A mathematical study. *Mathematical Biosciences*, 334, 108520.

[35] Puzanov, I., Milhem, M. M., Minor, D., Hamid, O., Li, A., Chen, L., ... & Andtbacka, R. H. (2016). Talimogene laherparepvec in combination with ipilimumab in previously

untreated, unresectable stage IIIB-IV melanoma. *Journal of Clinical Oncology*, 34(22), 2619.

[36] Russell, S. J., Peng, K. W., & Bell, J. C. (2012). Oncolytic virotherapy. *Nature Biotechnology*, 30(7), 658-670.

[37] Saginala, K., Barsouk, A., Aluru, J. S., Rawla, P., & Barsouk, A. (2021). Epidemiology of melanoma. *Medical Sciences*, 9(4), 63.

[38] Shain, A., Bastian, B. From melanocytes to melanomas. Nat Rev Cancer 16, 345–358 (2016). https://doi.org/10.1038/nrc.2016.37

[39] Schadendorf, D., van Akkooi, A. C., Berking, C., Griewank, K. G., Gutzmer, R., Hauschild, A., ... & Ugurel, S. (2018). Melanoma. *The Lancet*, 392(10151), 971-984.

[40] Siegel, R. L., Miller, K. D., Fuchs, H. E., & Jemal, A. (2021). Cancer statistics, 2021. Ca Cancer J Clin, 71(1), 7-33.

[41] Standish, R. J. (2002), Experimenting with methods to control Tradescantia fluminensis, an invasive weed of native forest remnants in New Zealand. *New Zealand Journal of Ecology*, 161-170.

[42] Standish, R. J., Robertson, A. W. and Williams, . P. (2001), The impact of an invasive weed Tradescantia fluminensis on native forest regeneration. *Journal of Applied Ecology*, 38: 1253-1263. doi:10.1046/j.0021-8901.2001.00673.x.

[43] Ramaj, T. (2021). On the Mathematical Modelling of Competitive Invasive Weed Dynamics. *Bulletin of Mathematical Biology*, 83(2), 1-25.

[44] Tu, M., Hurd, C., & Randall, J. M. (2001). Weed control methods handbook: tools & techniques for use in natural areas.

[45] Uong, A., & Zon, L. I. (2010). Melanocytes in development and cancer. *Journal of Cellular Physiology*, 222(1), 38–41. https://doi.org/10.1002/jcp.21935.

[46] Wang, Z., Guo, Z., & Smith, H. (2019). A mathematical model of oncolytic virotherapy with time delay. *Mathematical Biosciences and Engineering*, 16(4), 1836-1860.

[47] Ward, E. M., DeSantis, C. E., Lin, C. C., Kramer, J. L., Jemal, A., Kohler, B., ... & Gansler, T. (2015). Cancer statistics: breast cancer in situ. *CA: a cancer journal for clinicians*, 65(6), 481-495.

[48] Wennier, S., Li, S., & McFadden, G. (2011). Oncolytic virotherapy for pancreatic cancer. *Expert Reviews in Molecular Medicine*, 13.

[49] Wodarz, D. (2001). Viruses as antitumor weapons: defining conditions for tumor remission. *Cancer Research*, 61(8), 3501-3507.

[50] Wilcove, D. S., Rothstein, D., Dubow, J., Phillips, A., & Losos, E. (1998). Quantifying threats to imperiled species in the United States. *BioScience*, 48(8), 607-615.

[51] Zbytek, B., Carlson, J. A., Granese, J., Ross, J., Mihm, M., & Slominski, A. (2008). Current concepts of metastasis in melanoma. *Expert Review of Dermatology*, 3(5), 569-585.

Chapter 2

On the Mathematical Modelling of Competitive Invasive Weed Dynamics

2.1 Introduction

This work is motivated by the work of Hogan and Myerscough [4], in which the authors investigated the spreading of an invasive weed. In their paper, PDE models were used to explore the dynamics of the weed *Tradescantia fluminensis*. *T. fluminensis* is an herb native to South America which acts as an invasive weed species in countries such as New Zealand, Australia, and parts of the United States [4, 10, 11]. This weed invades the floor of depleted forests and competes with native plants for resources [11]. In turn, this prevents re-growth of the native plants. Biological research has shown that the presence of this weed causes an exponential decrease in native plant biomass. Standish et al. predicted that increasing the native plant biomass will suppress the growth of *T. fluminensis* [11]. Furthermore, this paper suggested that reducing the biomass of *T. fluminensis* below some critical amount could lead to regeneration of the native forest [11].

Motivated by the ideas of these previous papers, we seek to study the dynamics *T. fluminensis* both in isolation and in competition with neighbouring native plant species by expanding

on previous mechanistic modelling. One of the goals of this modelling is to offer ideas for implementing controls on the invasive weed growth in order to reduce or prevent native forest depletion, as well as the deleterious side effects this may have on animal species native to these habitats.

The mathematical modelling of invasive weed dynamics has previously seen success in offering insights on mechanisms of weed growth [4] as well as proposing ideas for controls [3]. Research conducted by Standish [10] suggests a positive correlation between light exposure and regrowth of *T. fluminensis*. This idea is an important aspect of the work of Hogan and Myerscough [4], in which the authors proposed a model which accounts for light availability and self-shading, the process by which a plant's own leaves will inhibit the amount of light to which neighbouring leaves are exposed. This is an idea we continue using throughout this chapter.

We also propose some ideas for implementing controls for *T. fluminensis* growth. Gourley et al. [3] and James et al. [6] have previously proposed the use of insects as bio-controls for invasive weed growth. We will instead consider the idea of using a physical boundary as a control. This would involve working on a small area of a forest instead of an entire forest mat, an approach which may be more feasible.

Another important feature we incorporate in this modelling is competition between a native plant species and *T. fluminensis*. This type of competition between invasive weeds and native plants has previously been observed [7]. These types of competitive dynamics are dependent on photosynthetic activity and hence on self-shading, so this modelling is a natural extension of the work of Hogan and Myerscough. Mathematical modelling of plant competition has also been used to find conditions which yield co-existence/persistence of multiple species [12]. We take a similar approach in this chapter. In particular, we use the competition model to suggest necessary conditions for the two competing species to coexist, based on factors such as weed leaf biomass, competition, native species carrying capacity, etc. In summary, this lets us propose some ideas of altering parameters which may lead to native forest regeneration.

2.1.1 Model and Methods

We will begin by exploring the use of the method of characteristics on a simplified version of the original, successful model proposed by Hogan and Myerscough [4] to explore the model from a different perspective. We will do this in two cases: a forest mat *without* a boundary and a forest mat with a boundary. Biologically, the second case corresponds to some physical boundary in the forest which exerts control on the plant growth, such as a river/body of water. The first case, while less realistic, will yield a solution which will be relevant to the second case and therefore be considered with great detail. The main simplification we will make in comparison to the original model of Hogan and Myerscough is the assumption that the effect of self-shading (a type of intraspecies competition in which a plant competes with itself for resources [1], i.e., sunlight) is negligible [4]. We will then propose some PDE models of competition between native plants and the invasive weed in an attempt to capture the dynamics of the interspecies competition. We then use these models as a basis for exploring the existence of travelling wave fronts. In particular, we will find *necessary* conditions for the existence of a travelling wave. This type of solution of the PDE model will imply the existence of a solution between steady states of the system, hence implying a transition from one state of the forest to a different state over sufficiently long time. In the context of weed invasion, this could offer many interesting interpretations. For instance, the transition from a co-existence equilibrium to an extinction equilibrium explains how altering parameters will affect the long-term behaviour of the forest.

The master equations, the different cases of which we will be studying throughout this chapter, are

$$\begin{cases} \dfrac{\partial n}{\partial t} &= -v\dfrac{\partial n}{\partial x} + \beta\alpha(\ell)n - \sigma n - \gamma nu, \\ \dfrac{\partial \ell}{\partial t} &= m\alpha(\ell)n - \phi\ell, \\ \dfrac{\partial u}{\partial t} &= -v_u\dfrac{\partial u}{\partial x} + ru\left(1 - \dfrac{n+u}{K}\right) - \gamma nu. \end{cases} \tag{2.1}$$

This system is based on the model proposed by Hogan and Myerscough [4]. We will consider different definitions of $\alpha(\ell)$ and ϕ and we have incorporated a third variable which represents a competing native plant species. The quantities n, ℓ, and u respectively represent biomasses of the weed stem, weed leaves, and native plant. As in [4], we consider the case where both the weed species and native plant species spread across the forest via advection. β represents a rate of stem apex growth, m represents an effect of stem biomass on leaf growth, σ represents the rate of stem apex death, and ϕ represents the weed leaf natural death rate. As in Hogan and Myerscough's model, $\alpha(\ell)$ can be interpreted as factoring in the effect of photosynthesis, which depends on the leaf density. This dependence accounts for *self-shading* [4] - a mode of intraspecies competition which many plants exhibit wherein newly grown apical leaves inhibit the amount of light available to older leaves on the same plant by casting a shadow over these older leaves [1]. In different sections of this chapter, we will consider different forms of $\alpha(\ell)$ which account for different dependences on the leaf biomass in different physical situations. The constants v and v_u represent the rates of weed spreading and native plant spreading, respectively. It is also clear that the native plant growth is modelled via a logistic growth term with rate r and carrying capacity K. The weed stem biomass appears in the logistic term to account for the weed consuming the native plant's resources. Finally, γ is the competition coefficient between the two species.

In Sections 2.2 and 2.3, we consider the case where $U = 0$. This represents the growth of the weed species in the absence of a competing species. This case with self-shading incorporated and a non-constant weed leaf death rate was studied in detail in [4], in particular via a travelling-wave analysis. We will instead consider the case where self-shading is negligible, i.e., $\alpha(\ell)$ is held constant for all $\ell \geq 0$. We will explore a different technique, namely the method of characteristics, to gain some new insights on this case. We will consider both a case with purely initial conditions and a case with both initial and boundary conditions which correspond to different ecological situations.

In Section 2.4, we first consider the case where $v_u = v$ and $\alpha(\ell)$ is again held constant. This

corresponds to the case where the native plant species also spreads through the forest mat via advection, at the *same* speed as the weed species. Furthermore, self-shading is still taken to be negligible for the mathematical tractability of the system. This represents the case where there is sufficient photosynthetic input, independent of the weed leaf biomass.

In Section 2.4.1, we consider the case of an established forest, i.e., the native plant species does *not* spread via advection as in the previous case. In this case, only the weed species is spreading. Hence, we take $v_u = 0$. We will not consider self-shading to be negligible and we will define the function $\alpha(\ell)$ to not be constant on its domain.

2.2 The Method of Characteristics on the Whole Space $\mathbb{R}$

In the spirit of chapter 2 of Logan [8], we will begin our analysis by applying the method of characteristics. We consider the case where $U = 0$ in system (2.1), i.e., the case where the native plant species is absent. Furthermore, we take $\alpha(\ell) = \alpha$ to be constant. Note that a very similar system was studied in [4], which was given by

$$\begin{cases} \dfrac{\partial n}{\partial t} &= -\dfrac{\partial}{\partial x}(nv) + \beta\alpha(\ell)n - \sigma n, \\ \dfrac{\partial \ell}{\partial t} &= m\alpha(\ell)n - \phi(\ell)\ell, \end{cases} \tag{2.2}$$

where $n = n(x,t), \ell = \ell(x,t) : \mathbb{R} \times \mathbb{R}_+ \to \mathbb{R}$ respectively represent the non-dimensionalized densities of the weed's stem apices and leaves at position x at time t. This PDE system models the growth of the weed via advection, with constant rate v, rather than seed dispersal [9], i.e., through insects, wind, etc. This mechanism of spread is also referred to the *creeping* of the weed species through the forest mat. The authors considered the case where $\alpha(\ell)$ grows to some maximum value as the leaf density approaches a critical value, then decreases as the leaf density continues to increase past this critical value. Furthermore, they took the leaf-density death rate ϕ to be a linear function of the leaf density. The authors performed a travelling-wave

analysis to explore the dynamics of their model.

For the remainder of Section 2.2 and in Section 2.3, we will instead apply the method of characteristics to gain some new insights on an altered version of this model. In this section, we consider the case of system (2.2) where both $\alpha(\ell) = \alpha$ and $\phi(\ell) = \phi$ are taken to be positive constants. This represents the case where self-shading has been removed as a limiting agent, i.e., via some artificial light source for constant, sufficient photosynthetic activity. This system is given by

$$\begin{cases} \dfrac{\partial n}{\partial t} &= -v\dfrac{\partial}{\partial x}(n) + (\beta\alpha - \sigma)n, \\ \dfrac{\partial \ell}{\partial t} &= m\alpha n - \phi\ell. \end{cases} \tag{2.3}$$

We will consider n and ℓ to represent the stem apex biomass and the leaf biomass, respectively. Observe that making our assumption of *no* self-shading decouples the first equation of system (2.3) from the second equation. We will first consider this equation in the domain $\mathbb{R} \times \mathbb{R}_+$. Doing so, we impose the following initial conditions:

$$n(x, 0) = n_0(x) \geq 0, \quad \ell(x, 0) = \ell_0(x) \geq 0, \qquad x \in \mathbb{R}, \tag{2.4}$$

where n_0 and ℓ_0 give the initial distributions of stem and leaf biomasses, respectively. Therefore, these functions represent the initial state of weed biomass in some forest/biological system.

Using the method of characteristics, it holds that $n'(t) = (\beta\alpha - \sigma)n$ on the characteristic curves given by $x'(t) = v$. That is, the characteristics are given by $x - vt = \xi$, for all $\xi \in \mathbb{R}$. Hence, the characteristics are the lines on the xt-plane with slope $1/v$. Using separation of variables:

$$\int_{s=0}^{s=t} \frac{\mathrm{d}n}{n} = \int_{s=0}^{s=t} (\beta\alpha - \sigma)\,\mathrm{d}s,$$

$$\implies \ln|n(x,t)| - \ln|\underbrace{n(\xi,0)}_{=n_0(\xi)}| = (\beta\alpha - \sigma)\, t \implies n = n_0(\xi)e^{(\beta\alpha-\sigma)t}.$$

Hence, by making the substitution $\xi = x - vt$, it follows that

$$n(x,t) = n_0(x - vt) \cdot e^{(\beta\alpha-\sigma)t}. \tag{2.5}$$

Remark 2.2.1 *In the case where α is not held to be constant, while explicitly solving for $n(x,t)$ may not be feasible, it is still simple to show the positivity of the solution $n(x,t)$. It can be shown, as above, that if there exists some solution vector $[n(x,t), \ell(x,t)]^T$ to (2.2), then*

$$n(x,t) = n_0(x - vt) \exp\left(\int_0^t \left[\beta\alpha(\ell\,(x(s), s)) - \sigma\right] \mathrm{d}s\right).$$

Therefore, $n(x,t) \geq 0$ for all $(x,t) \in \mathbb{R} \times \mathbb{R}_+$, showing the positivity of stem apex biomass - this is a necessary condition for well-posedness.

The second PDE in system (2.3) may now be solved by substituting (2.5) into the PDE and using a suitable integrating factor. In this case, we can use the integrating factor $e^{\phi t}$. Then,

$$\ell_t + \phi\ell = m\alpha \cdot n_0(x - vt)e^{(\beta\alpha-\sigma)t},$$

$$\implies \int_0^t \frac{\partial}{\partial s}\left(e^{\phi s}\ell\right)\mathrm{d}s = m\alpha \int_0^t n_0(x - vs)e^{(\beta\alpha-\sigma+\phi)s}\mathrm{d}s,$$

$$\implies e^{\phi t}\ell(x,t) - \ell(x,0) = m\alpha \int_0^t n_0(x - vs)e^{(\beta\alpha-\sigma+\phi)s}\mathrm{d}s.$$

Making use of the initial conditions (2.4), we obtain the following solution:

$$\ell(x,t) = e^{-\phi t}\ell_0(x) + m\alpha e^{-\phi t} \int_0^t n_0(x - vs)e^{(\beta\alpha-\sigma+\phi)s}\mathrm{d}s. \tag{2.6}$$

Biologically, we are interested in determining the long-term behaviour of the system, i.e., to

determine the future state of a forest in which the weed is spreading. While this information is easy to determine from equation (2.5), the asymptotic behaviour of ℓ, described by equation (2.6), may be less clear. To that end, we consider taking $t \to \infty$ in the following theorem.

Theorem 2.2.1 *Let $n_0, \ell_0 \in C(\mathbb{R})$ be strictly positive functions. Furthermore, let n_0 be a bounded function, i.e., there exists some $M > 0$ such that $0 < n_0(x) \leq M$. Then the solution of system (2.3) with initial conditions $n(x,0) = n_0(x)$ and $\ell(x,0) = \ell_0(x)$ is given by (2.5) and (2.6). Furthermore,*

1. *If $\beta\alpha < \sigma$, then $\forall x \in \mathbb{R} : \lim_{t\to\infty} n(x,t) = \lim_{t\to\infty} \ell(x,t) = 0$.*

2. *If $\beta\alpha = \sigma$, then $n(x,t) = n_0(x - vt)$.*

Proof We have previously shown that (2.5) and (2.6) give solutions to (2.3) by deriving the solutions. This completes the proof of the first part of the theorem.

Next, we consider the case where $\beta\alpha < \sigma$ and that the integral term on the right-hand side of (2.6) converges, say, to limit $0 < L < \infty$ as $t \to \infty$. Note that L is a function of x. In this case, since $0 \leq n_0(\xi) \leq M$ for all $\xi \in \mathbb{R}$, it must hold that $\lim_{t\to\infty} n(x,t) = 0$, i.e., by the Squeeze Theorem:

$$0 \leq n_0(x - vt)e^{(\beta\alpha-\sigma)t} \leq Me^{(\beta\alpha-\sigma)t} \quad \text{and} \quad \lim_{t\to\infty} 0 = \lim_{t\to\infty} Me^{(\beta\alpha-\sigma)t} = 0,$$

$$\implies \lim_{t\to\infty} n_0(x - vt)e^{(\beta\alpha-\sigma)t} = 0.$$

Next, it holds that

$$\begin{aligned}\lim_{t\to\infty} \ell(x,t) &= \ell_0(x) \cdot \lim_{t\to\infty} e^{-\phi t} + m\alpha \cdot \lim_{t\to\infty} e^{-\phi t} \int_0^t n_0(x - vs)e^{(\beta\alpha-\sigma+\phi)s} \mathrm{d}s \\ &= \ell_0(x) \cdot 0 + m\alpha \cdot 0 \cdot L = 0\end{aligned}$$

In the case where the integral diverges (to ∞), at any fixed x, we may apply L'Hopital's rule

and the Fundamental Theorem of Calculus as follows:

$$\begin{aligned}\lim_{t\to\infty}\frac{1}{e^{\phi t}}\int_0^t n_0(x-vs)e^{(\beta\alpha-\sigma+\phi)s}\mathrm{d}s &= \lim_{t\to\infty}\frac{n_0(x-vt)e^{(\beta\alpha-\sigma+\phi)t}}{\phi e^{\phi t}}\\ &= \frac{1}{\phi}\lim_{t\to\infty} n_0(x-vt)\cdot\exp\left[(\beta\alpha-\sigma)t\right]\\ &= 0,\end{aligned}$$

where the last equality again follows from the fact that $e^{(\beta\alpha-\sigma)t}\to 0$ for $\beta\alpha-\sigma<0$ and n_0 is a bounded function. Combining the above results, we conclude that at some fixed x, we have $n(x,t),\ell(x,t)\to 0$ as $t\to 0$ when $\beta\alpha<\sigma$.

If $\beta\alpha=\sigma$, it then follows by direct substitution into (2.5) that $n(x,t)=n_0(x-vt)$. ∎

We now consider the biological significance of Theorem 2.2.1. If $\beta\alpha<\sigma$, at all points $x\in\mathbb{R}$, the weed biomass will tend to 0. That is, if there is a low rate of stem apex formation or of photosynthesis, relative to the stem apex death rate, then both the stem biomass and the leaf biomass will asymptotically tend to zero and the weed will go extinct. This should be expected due to the larger death rate.

If $\beta\alpha=\sigma$, then at any point (x,t), the stem biomass will be exactly equal to $n_0(x-vt)$, the initial distribution. Biologically, this means that if the growth rates equal the death rate, then over all time, the distribution of stem biomass will mimic the initial distribution, as a right-travelling wave with speed $v>0$. That is, at point (x,t) the distribution of stem biomass will be given by the initial distribution at position $x-vt$, i.e., at any point t in time, we can obtain the weed biomass at position x by the initial distribution shifted vt units to the left. This means that at time t, the initial distribution of $n_0(x)$ at time $t=0$ has been shifted vt units to the right, i.e., travelling right with constant speed v. Therefore, in forward time, the initial distribution of the forest will shift to the right with a constant speed v. This is the direction of advection and so it is biologically consistent that the weeds shift in this direction. There is no effect of growth or death and so the model simply gives advection ($n_t+vn_x=0$) with no source.

We have not yet addressed the case where $\beta\alpha > \sigma$. One might initially expect that in this case, where the death rate is sufficiently low, stem biomass would tend to infinity as $t \to \infty$. This is clearly the case when the initial leaf biomass distribution is a positive constant for all x. However, this is not generally the case. One can easily see this by considering the counter-example where $n_0(x) = 0$. As it turns out, even in the case where $n_0(x) > 0 \ \ \forall x \in \mathbb{R}$, it does not necessarily hold that $n(x,t) \to \infty$ as $t \to \infty$. To see this, we can consider the following *counter-example*:

Example 2.2.1 For all $x \in \mathbb{R}$ let $n_0(x) := e^{2(\beta\alpha-\sigma)x} > 0$. If $\beta\alpha > \sigma$, then we have

$$\lim_{t\to\infty} n(x,t) = \lim_{t\to\infty} e^{2(\beta\alpha-\sigma)(x-t)} \cdot e^{(\beta\alpha-\sigma)t} = e^{2(\beta\alpha-\sigma)x} \cdot \lim_{t\to\infty} e^{-(\beta\alpha-\sigma)t} = 0.$$

The above example illustrates that the form of the initial distribution n_0 exerts control on the long-term behaviour of the stem apex biomass, $n(x,t)$. This implies the following biological insight: even if the weeds have a greater rate of growth and experience sufficient photosynthetic input compared to their death rate, extinction is still possible. In order to study the case where $\beta\alpha > \sigma$, we will consider the special case where $n_0(x)$ has compact support. In particular, we consider the following initial stem apex biomass distribution:

$$n_0(x) := \begin{cases} K, & \text{if } \ x \in [a,b], \\ 0, & \text{else.} \end{cases}$$

This initial condition yields the following solution:

$$n(x,t) = \begin{cases} Ke^{(\beta\alpha-\sigma)t}, & \text{if } \ a+vt \le x \le b+vt, \\ 0, & \text{else,} \end{cases}$$

where $a, b \in \mathbb{R}$ and $K > 0$ with $a < b$. Graphically, we can see this in Figure 2.1.

In the regions *outside* the region $a + vt \le x \le b + vt$, the stem biomass remains zero for all

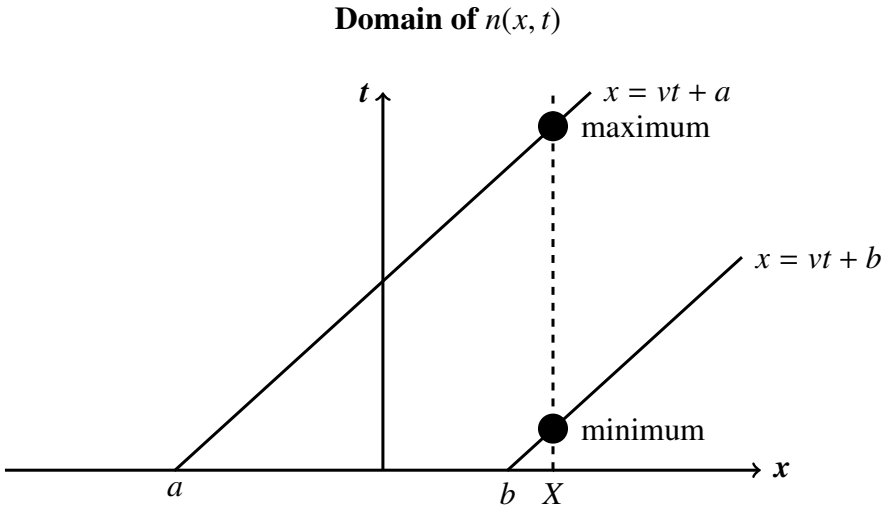

Figure 2.1: Given a point $X \geq b$ in the forest, a vertical line through $(X, 0)$ will achieve its minimum on the line $x = b + vt$ and will achieve its maximum on the line $x = a + vt$.

time at all positions. We are more interested in the behaviour of the stem biomass inside this region. For any fixed position $X \geq a$, the stem biomass will eventually become positive for some finite time before once again reducing to 0. That is, $\exists\, t > 0$ such that $n(X, t) \neq 0$.

This situation corresponds to the case where the weed spreads (in the positive direction) while experiencing exponential growth. No growth occurs to the left of the position $x = a$. The weeds will grow at a given position for some amount of time - the precise amount predicted by the model can easily be found via basic analytic geometry - while the boundaries of the weed shift to the right with speed v.

Furthermore, we can find the minimum and maximum amounts of weed stem biomass which will be present at a given position $X \geq a$:

$$\max_{t \geq 0} n(X, t) = K \exp\left[\frac{(\beta\alpha - \sigma)(X - a)}{v}\right]$$

and $\min_{t \geq 0} n(X, t) = 0$. However, if we take $t_* := (X - b)/v$ and $t^* := (X - a)/v$, then the more

interesting minimum at $X \geq b$ is given by

$$\min_{t\in[t_*,t^*]} n(X,t) = K\exp\left[\frac{(\beta\alpha-\sigma)(X-b)}{v}\right],$$

These values can be used to predict the weed stem biomass at a particular position in the forest as well as to approximate the amount of time it will take for the forest to reach that state and how long it will be maintained.

We can now determine the leaf biomass, $\ell(x,t)$. To this end, we begin by defining

$$I(x,t) := \int_0^t n_0(x-vs)e^{(\beta\alpha-\sigma+\phi)s}\mathrm{d}s.$$

In the case where $x \leq a$, we have $I(x,t) = 0$ since $x - vs \leq a - vs$ for all $s \geq 0$.

In the case where $a < x < b$, we first consider $0 \leq t \leq (x-a)/v$. Then, we may write

$$I(x,t) = \int_0^t Ke^{(\beta\alpha-\sigma+\phi)s}\mathrm{d}s = \tilde{K}\left[e^{(\beta\alpha-\sigma+\phi)t} - 1\right],$$

where we define

$$\tilde{K} := \frac{K}{\beta\alpha-\sigma+\phi}.$$

In the case where $t > (x-a)/v$, it can be similarly shown that

$$I(x,t) = \tilde{K}\left[e^{(\beta\alpha-\sigma+\phi)(x-a)/v} - 1\right].$$

Finally, we can consider $b \leq x$. In this case, we have

$$I(x,t) = \begin{cases} 0, & \text{if } 0 \leq t \leq \dfrac{x-b}{v}, \\ \tilde{K}\left[e^{(\beta\alpha-\sigma+\phi)t} - e^{(\beta\alpha-\sigma+\phi)(x-b)/v}\right], & \text{if } \dfrac{x-b}{v} < t < \dfrac{x-a}{v}, \\ \tilde{K}\left[e^{(\beta\alpha-\sigma+\phi)(x-a)/v} - e^{(\beta\alpha-\sigma+\phi)(x-b)/v}\right], & \text{if } \dfrac{x-a}{v} \leq t. \end{cases}$$

Let $\rho := \beta\alpha - \sigma + \phi$. Combining the above results with (2.6), we obtain the following solution for ℓ:

$$\ell(x,t) = e^{-\phi t}\ell_0(x) + \tilde{L}(x,t),$$

where $\tilde{L}(x,t)$ is given by

$$\tilde{L}(x,t) := \begin{cases} 0, & \text{if } x \le a,\ 0 \le t, \\ \tilde{K}m\alpha e^{-\phi t}\left[e^{\rho t} - 1\right], & \text{if } a < x < b,\ 0 \le t \le \dfrac{x-a}{v}, \\ \tilde{K}m\alpha e^{-\phi t}\left[e^{\rho(x-a)/v} - 1\right], & \text{if } a < x < b,\ \dfrac{x-a}{v} < t, \\ 0, & \text{if } b \le x,\ 0 \le t \le \dfrac{x-b}{v}, \\ \tilde{K}m\alpha e^{-\phi t}\left[e^{\rho t} - e^{\rho(x-b)/v}\right], & \text{if } b \le x,\ \dfrac{x-b}{v} < t < \dfrac{x-a}{v}, \\ \tilde{K}m\alpha e^{-\phi t}\left[e^{\rho(x-a)/v} - e^{\rho(x-b)/v}\right], & \text{if } b \le x,\ \dfrac{x-a}{v} \le t. \end{cases}$$

We can now address the *global* dynamics of the stem and leaf biomasses. We impose the following asymptotic symmetry boundary condition on the initial distribution:

$$\lim_{x\to-\infty} n_0(x) = \lim_{x\to\infty} n_0(x) = n^* > 0. \tag{2.7}$$

In this case, we can show that when $\beta\alpha = \sigma$, the stem biomass in the forest will remain constant over all time. To that end, let $N(t)$ give the total stem biomass at time t. Then,

$$N(t) := \int_{-\infty}^{\infty} n(x,t)\mathrm{d}x. \tag{2.8}$$

Assuming the proper conditions on n (i.e., continuous differentiability, convergence of the

integrals, etc.) for the application of the Leibniz Rule, it follows that

$$N'(t) = \frac{\mathrm{d}}{\mathrm{d}t}\int_{-\infty}^{\infty} n(x,t)\mathrm{d}x = \int_{-\infty}^{\infty} \frac{\partial}{\partial t} n(x,t)\mathrm{d}x$$

$$= \int_{-\infty}^{\infty} -v\frac{\partial}{\partial x} n(x,t)\mathrm{d}x = -v \cdot e^{(\beta\alpha-\sigma)t} \cdot \Big[n_0(x-vt)\Big]_{-\infty}^{\infty}$$

$$= -ve^{(\beta\alpha-\sigma)t} \cdot (n^* - n^*) = 0.$$

Hence, if both *boundaries* initially have the same stem apex biomass, we should expect no change in the net biomass. This is expected in the case of advection in the absence of a source or sink.

Finally, if $\beta\alpha > \sigma$ and (2.7) holds, both the stem apex and leaf biomasses will grow without bound at a fixed point x as $t \to \infty$. In this case, the weeds will dominate the forest floor.
We can similarly define the total leaf biomass as

$$L(t) := \int_{-\infty}^{\infty} \ell(x,t)\mathrm{d}x. \tag{2.9}$$

Since the method of characteristics previously gave us *explicit* solutions for n and ℓ, we can re-express the above formulas, by using (2.5) and (2.6), as

$$N(t) = \int_{-\infty}^{\infty} n_0(x-vt)e^{(\beta\alpha-\sigma)t}\mathrm{d}x, \tag{2.10}$$

$$L(t) = e^{-\phi t}\int_{-\infty}^{\infty} \ell_0(x)\mathrm{d}x + m\alpha e^{-\phi t}\int_{-\infty}^{\infty}\int_0^t n_0(x-vs)e^{(\beta\alpha-\sigma+\phi)s}\mathrm{d}s\mathrm{d}x. \tag{2.11}$$

Using the definitions in (2.8) and (2.9) in tandem with system (2.3), we can also *analytically* obtain more information about the total forest biomass. To do this, we again make use of the asymptotic symmetry assumption on n_0, namely (2.7), as well as the assumption that all

improper integrals converge. Once again, we will assume that n and ℓ are sufficiently well defined to justify an interchange of differentiation and integration. Differentiating:

$$\begin{aligned}
\frac{\mathrm{d}N}{\mathrm{d}t} &= \int_{-\infty}^{\infty} \frac{\partial}{\partial t} n(x,t)\mathrm{d}x = \int_{-\infty}^{\infty} \left(-v\frac{\partial}{\partial x} n(x,t) + (\beta\alpha - \sigma)n \right) \mathrm{d}x \\
&= -v \int_{-\infty}^{\infty} \frac{\partial}{\partial x} n(x,t)\mathrm{d}x + (\beta\alpha - \sigma) \int_{-\infty}^{\infty} n(x,t)\mathrm{d}x \\
&= -v \cdot e^{(\beta\alpha-\sigma)t} \left[n^* - n^* \right] + (\beta\alpha - \sigma)N(t) \\
&= (\beta\alpha - \sigma)N(t).
\end{aligned}$$

Similarly,

$$\frac{\mathrm{d}L}{\mathrm{d}t} = m\alpha \int_{-\infty}^{\infty} n(x,t)\mathrm{d}x - \phi \int_{-\infty}^{\infty} \ell(x,t)\mathrm{d}x = m\alpha N(t) - \phi L(t).$$

Hence, we have the following initial value problem:

$$\begin{cases}
N'(t) = (\beta\alpha - \sigma)N, \\
L'(t) = m\alpha N - \phi L, \\
N(0) = \displaystyle\int_{-\infty}^{\infty} n_0(x)\mathrm{d}x, \quad L(0) = \int_{-\infty}^{\infty} \ell_0(x)\mathrm{d}x.
\end{cases} \tag{2.12}$$

This is a decoupled linear system of ordinary differential equations (ODEs) with constant coefficients. Note that the steady state is either a stable node or a saddle point depending on $\mathrm{sgn}(\beta\alpha - \sigma)$. The solution of the initial value problem (2.12) is given by

$$\begin{pmatrix} N(t) \\ L(t) \end{pmatrix} = \frac{1}{\beta\alpha - \sigma + \phi} \int_{-\infty}^{\infty} n_0(x)\mathrm{d}x \cdot e^{(\beta\alpha-\sigma)t} \begin{pmatrix} \beta\alpha - \sigma + \phi \\ m\alpha \end{pmatrix} + \dots \\ \cdots + \left(\int_{-\infty}^{\infty} \ell_0(x)\mathrm{d}x - \frac{m\alpha}{\beta\alpha - \sigma + \phi} \int_{-\infty}^{\infty} n_0(x)\mathrm{d}x \right) e^{-\phi t} \begin{pmatrix} 0 \\ 1 \end{pmatrix}. \tag{2.13}$$

It follows that $N(t), L(t) \geq 0$ for all $t \geq 0$; this is a necessary condition for the well-posedness of the system.

If $\beta\alpha < \sigma$, then $(0, 0)$ is a stable node and we have $N, L \to 0$ as $t \to \infty$. Hence, the total biomasses will also tend to 0, implying extinction. Similarly, if $\beta\alpha > \sigma$ then $N \to \infty$ as $t \to \infty$, except in the cases where $N(0) = 0$. Moreover, an examination of the phase portrait of this system reveals that, as the steady state will be a saddle, all trajectories not initially on the stable manifold will asymptotically tend towards the unstable manifold and so $N, L \to \infty$. Near the steady state, the stable manifold is tangent to the span of $[N, L]^T = [0, 1]^T$ and the unstable manifold is tangent to the span of the eigenvector $[N, L]^T = [\beta\alpha - \sigma + \phi, m\alpha]^T$, which lies in the first quadrant as $\beta\alpha > \sigma$.

The results seen here are biologically sensible, as they correspond to the *net* long-term behaviour of the forest mimicking the long-term behaviour at particular positions, x, in the forest as was revealed by the method of characteristics.

2.3 The Method of Characteristics on $\mathbb{R}_+$: A Boundary Condition

At this point we have given a thorough treatment to the case of an infinite string, $x \in \mathbb{R}$. We will now consider the case with boundary conditions in addition to the initial conditions. Biologically, this may correspond, for example, to a system where there may be a river at the

edge of a forest, exerting control on weed growth on this boundary. We will consider this boundary to be given by $x = 0$. We denote our new domain of interest as $\Omega := \mathbb{R}^2_+$, i.e., the first quadrant. In this section, as in the previous section, we continue to consider the effect of self-shading to be negligible. Hence, the first PDE of (2.3) is decoupled from the second PDE. For this reason, we will primarily consider only the first PDE in this section. Once a solution, $n(x,t)$, has been obtained, i.e., via the method of characteristics, the remaining, linear, scalar PDE can be solved to obtain $\ell(x,t)$, just as in Section 2.2.

With this in mind, we proceed to prescribe initial and boundary conditions and we may formulate the model as follows:

$$\begin{cases} n_t + vn_x = (\beta\alpha - \sigma)n, & x > 0, \quad t > 0, \\ n(x,0) = n_0(x), & x > 0, \\ n(0,t) = f(t), & t > 0. \end{cases} \tag{2.14}$$

The function $f(t) \geq 0$ represents the control exerted by the boundary on the plant's dynamics, i.e., the effect of a river on the edge of the forest. The characteristic curves are again given by $x - vt = \xi$ for $\xi \in \mathbb{R}$.

We will first consider the region $x > vt$. In this case, we have the initial condition:

$$x = \xi > 0, \quad n = n_0(\xi), \quad \text{at } t = 0. \tag{2.15}$$

This is just the case considered in Section 2.2 and hence, the method of characteristics once again gives (2.5) to be the solution satisfying (2.15). We can now consider the region $x < vt$. In this case, we have the boundary condition:

$$t = \tau > 0, \quad n = f(\tau), \quad \text{at } x = 0. \tag{2.16}$$

The characteristic curves are in the form $t = \tau + x/v$. Recall that on the characteristics, we have

$n'(t) = (\beta\alpha - \sigma)n$. Hence, by using separation of variables, we find the following solution in this region:

$$n(x,t) = f\left(t - \frac{x}{v}\right)e^{(\beta\alpha-\sigma)(x/v)},$$

where we used the fact that $t - \tau = x/v$. In summary, we have the following solution of (2.14):

$$n(x,t) = \begin{cases} n_0(x - vt)e^{(\beta\alpha-\sigma)t}, & x > vt, \\ f\left(t - \frac{x}{v}\right)e^{(\beta\alpha-\sigma)x/v}, & x < vt. \end{cases} \tag{2.17}$$

Biologically, this means that points above $x = vt$ are influenced by f whereas points below $x = vt$ are influenced by n_0. We can ask what happens as v, the rate of advection, is increased. The line separating the two regions, $t = x/v$, becomes less steep as v is increased (see Figure 2.2).

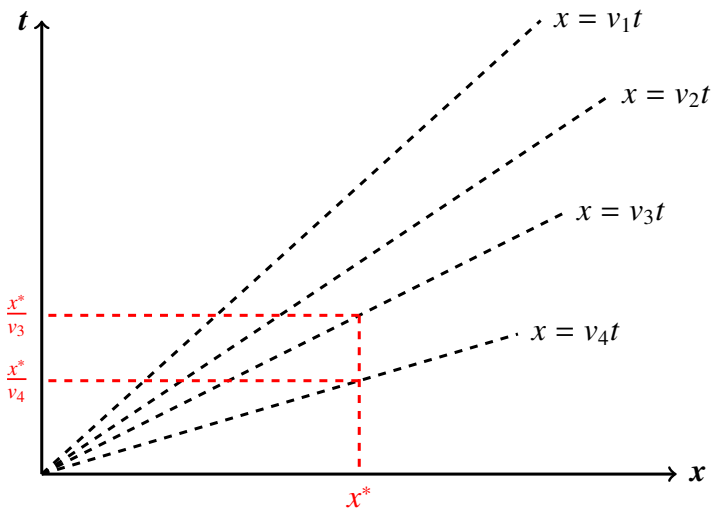

Figure 2.2: Characteristic curves through the origin on Ω as v is increased.

In Figure 2.2, we have $v_1 < v_2 < v_3 < v_4$. Hence, as v is increased, the area of region $x > vt$ is *decreased* on any interval of the form $x \in [0, x^*], \forall x^* > 0$.

Next, if we consider some $v_j > v_i$, then as v_j is increased, it also follows that there is an

increase in the area of the trapezoid with coordinates $(x,t) = (0,0),(0,x^*/v_i),(x^*,x^*/v_i)$, and $(x^*,x^*/v_j)$. We can physically interpret this result as follows: as the rate of advection or *stem biomass spreading* is increased, there is a greater region of forest over which the river/boundary exerts control in shorter periods of time. Hence, we may propose the following approach to deal with *unwanted* weed growth based on this insight: If we may implement a mechanism for controlling the stem apex biomass at the boundary and keeping it low (i.e., we have a choice of the function f and we make it small for all $t > 0$), then if we can sufficiently *speed up* the rate of advection (i.e., increasing v sufficiently) we will have greater control of the weed stem biomass, because a greater region near the origin will have biomass given by $f(t-x/v)e^{(\beta\alpha-\sigma)(x/v)} \approx f(t)$ as $v \to \infty$. Intuitively, we expect to have much more control over the boundary condition than we would on the initial condition as we cannot exert much influence over *far-away* regions $x >> 0$. It should be noted that this requires the strong assumption that advection is only in one direction.

On a final note, we may write a closed form for the total population of stem apices, $N(t)$, by using the definition $N(t) := \int_{\mathbb{R}_+} n(x,t)\mathrm{d}x$ and (2.17) as follows:

$$N(t) = \int_0^{vt} f\left(t - \frac{x}{v}\right) e^{(\beta\alpha-\sigma)x/v}\mathrm{d}x + \int_{vt}^{\infty} n_0(x-vt)e^{(\beta\alpha-\sigma)t}\mathrm{d}x. \tag{2.18}$$

This equation may be used to calculate the stem apex biomass given the initial and boundary conditions.

This concludes the sections on applying the method of characteristics. We have shown that even though the method used is simple, it can give a great deal of insight on first order PDE models and the dynamics of a system can vary greatly depending on the boundary and initial conditions. For instance, in the case of the proliferation and advection of weeds, if a boundary is imposed on the system we can have drastically different dynamics, compared to the case of no boundary, i.e., if we choose f and n_0 to have different qualitative behaviour. While this method has proven to be invaluable, we will now consider systems of PDEs in which equations

cannot be *completely* decoupled (but they will be partially decoupled) and explore the existence of travelling wave solutions.

2.4 Travelling Wave Solutions of a Competition Model

Just as in [4], we will consider the existence of travelling wave solutions (TWS) and apply relevant methods in order to analyze a competition model between weeds and native plants. We propose a new competition model based on [4]. We may then proceed to apply the methodology found in chapters 5 and 6 of Logan [8]. We introduce a native plant species biomass, $u(x,t)$. We will look at two cases: First, we consider the case where this species is also spreading through advection, with the same speed as the invasive weed, v. Next, we assume that this native species has already been established in the forest and hence drop the advection term which is present in the weed species. We begin with the former case. Observe that this case is obtained by setting $v_u = v$ to be constant in system (2.1). We will assume that self-shading is once again negligible, just as in Sections 2 and 3. That is, $\alpha(\ell) = \alpha$ for all $\ell \geq 0$ in system (2.1). This assumption will allow us to decouple the first two equations in system (2.1) and hence allow us to consider the following system:

$$\begin{cases} n_t &= -vn_x + \beta\alpha n - \sigma n - \gamma nu, \\ u_t &= -vu_x + ru\left(1 - \dfrac{n+u}{K}\right) - \gamma nu, \end{cases} \tag{2.19}$$

where $r > 0$ is the logistic growth rate of the competing native species, $K > 0$ is the carrying capacity, and $\gamma > 0$ is the mass-action competition coefficient. We consider right-travelling TWS, with wave speed c, of the form

$$n(x,t) = N(\xi), \quad u(x,t) = U(\xi), \quad \xi := x - ct, \ c > 0. \tag{2.20}$$

Substituting equations (2.20) into system (2.19) yields the following system of ODEs:

$$\begin{cases} -cN' &= -vN' + \beta\alpha N - \sigma N - \gamma NU, \\ -cU' &= -vU' + rU\left(1 - \dfrac{N+U}{K}\right) - \gamma NU. \end{cases} \tag{2.21}$$

We here consider the case where $c \neq v$, i.e., the solutions have a speed not equal to the speed of advection. In this case, system (2.21) may be written as

$$\begin{cases} N' = \dfrac{\beta\alpha - \sigma}{v-c} N - \dfrac{\gamma}{v-c} NU, \\ U' = \dfrac{r}{v-c} U\left(1 - \dfrac{N+U}{K}\right) - \dfrac{\gamma}{v-c} NU. \end{cases} \tag{2.22}$$

Two of the steady states of this system are $(N, U) = (0, 0)$ and $(N, U) = (0, K)$. Biologically, the steady state $(0, 0)$ represents a *mutual extinction* steady state where the biomasses of both the weed and the native plant are zero. The steady state $(0, K)$ represents a steady state where only the native plants survive (and have reached the carrying capacity) and the weeds go extinct.

There is also an additional, *positive*, steady state, which we will denote by (N^*, U^*), in the case where $\beta\alpha - \sigma < \gamma K$. If $N^* > 0, U^* > 0$, this steady state is known as a *co-existence* steady state where both species survive. We can find an explicit form for this steady state by making use of the nullclines and the fact that steady states occur at the intersection of nullclines.

To do so, we set $N' = 0$ and $U' = 0$. The N-nullclines are given by the equations

$$N = 0, \quad U = \frac{\beta\alpha - \sigma}{\gamma}, \tag{2.23}$$

and the U-nullclines are given by the equations

$$U = 0, \quad U = K - \left(1 + \frac{\gamma K}{r}\right) N. \tag{2.24}$$

To find (N^*, U^*), we find the point of intersection of the appropriate N-nullcline with the ap-

propriate U-nullcline:

$$U = \frac{\beta\alpha - \sigma}{\gamma} = K - \left(1 + \frac{\gamma K}{r}\right) N.$$

Solving this equation for N yields N^*, which is hence given by

$$N^* = \frac{\gamma K - (\beta\alpha - \sigma)}{\gamma} \cdot \frac{r}{r + \gamma K}. \tag{2.25}$$

Observe that $N^* > 0$ since $\gamma K > \beta\alpha - \sigma$. If this inequality were *not* true, then this steady state would not be biological (not positive). Therefore, for the rest of our analysis, we assume this inequality holds true. Furthermore, U^* is given by

$$U^* = \frac{\beta\alpha - \sigma}{\gamma}. \tag{2.26}$$

For the positivity of U^*, we will also impose the condition $\beta\alpha > \sigma$, i.e., for the biological validity of this steady state. We proceed to plot the nullclines (2.23), (2.24) and indicate the direction of the vector field at relevant points in Figure 2.3.

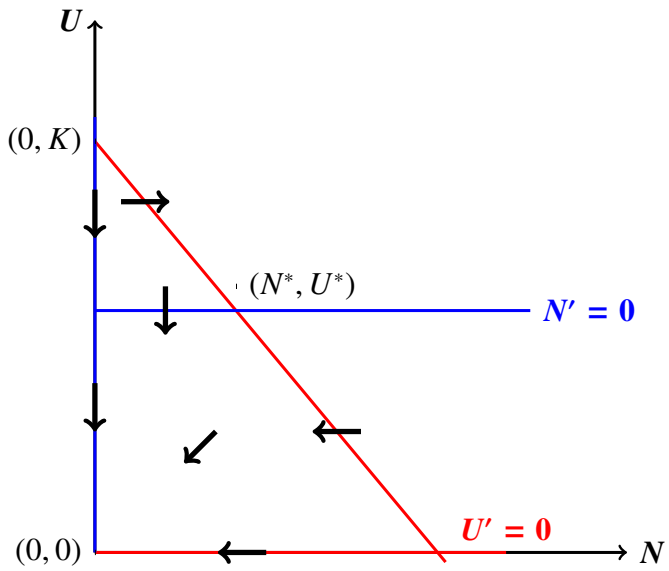

Figure 2.3: Nullclines and vector field of the TWS ODE system when $v < c$.

Observe that in Figure 2.3, we are considering $v < c$. In the case where $v > c$, the direction

of the vectors at each point in the phase portrait are reversed as the term $v - c$ occurs in all of the terms in system (2.22). Biologically, this represents the case in which the travelling wave speed is greater than the advection speed of the weed.

The following proposition will allow us to conclude the existence of a TWS between (N^*, U^*) and $(0, 0)$ in the case where $v < c$. That is, there exists a TWS of system (2.19), $[N(\xi), U(\xi)]^T$, which satisfies the conditions

$$\lim_{\xi\to\infty} N(\xi) = 0, \quad \lim_{\xi\to\infty} U(\xi) = 0, \tag{2.27}$$

and

$$\lim_{\xi\to-\infty} N(\xi) = \frac{\gamma K - (\beta\alpha - \sigma)}{\gamma} \cdot \frac{r}{r + \gamma K}, \tag{2.28}$$

$$\lim_{\xi\to-\infty} U(\xi) = \frac{\beta\alpha - \sigma}{\gamma}. \tag{2.29}$$

Proposition 2.4.1 *Consider system (2.22). If* $0 < \beta\alpha - \sigma < \gamma K$ *and* $v < c$*, then the following statements concerning the steady states of this system are true:*

1. *The steady state* $(0, 0)$ *is a stable node.*
2. *The steady state* $(0, K)$ *is an unstable node.*
3. *The steady state* (N^*, U^*) *is a saddle point.*

Proof The Jacobian matrix of (2.22) is given by

$$J(N, U) = \begin{pmatrix} \dfrac{\beta\alpha - \sigma - \gamma U}{v - c} & -\dfrac{\gamma N}{v - c} \\ \left(-\dfrac{r}{k(v - c)} - \dfrac{\gamma}{v - c}\right) U & \dfrac{r - \dfrac{rN}{K} - \dfrac{2rU}{K} - \gamma N}{v - c} \end{pmatrix}. \tag{2.30}$$

We linearize the system at the steady states $(0,0)$ and $(0,K)$:

$$J(0,0) = \begin{pmatrix} \dfrac{\beta\alpha - \sigma}{v-c} & 0 \\ 0 & \dfrac{r}{v-c} \end{pmatrix}, \tag{2.31}$$

$$J(0,K) = \begin{pmatrix} \dfrac{\beta\alpha - \sigma - \gamma K}{v-c} & 0 \\ \dfrac{-r - K\gamma}{v-c} & -\dfrac{r}{v-c} \end{pmatrix}. \tag{2.32}$$

Since $J(0,0)$ is a diagonal matrix, its eigenvalues are $\lambda_1^0 = (\beta\alpha - \sigma)/(v-c) < 0$ and $\lambda_2^0 = r/(v-c) < 0$. Since both of these eigenvalues are negative, it follows that $(0,0)$ is a stable node.

The matrix $J(0,K)$ is a lower-triangular matrix and so its eigenvalues are given by

$$\lambda_1^K = \frac{\beta\alpha - \sigma - \gamma K}{v-c} > 0, \quad \lambda_2^K = -\frac{r}{v-c} > 0.$$

Since both of these eigenvalues are real and positive, it follows that $(0,K)$ is an unstable node. Finally, we compute the determinant of $J^* := J(N^*, U^*)$:

$$\det J^* = -\frac{\gamma}{v-c} \cdot \frac{r}{\gamma K + r} \cdot \frac{K\gamma - (\beta\alpha - \sigma)}{\gamma} \cdot \left(\frac{r}{K(v-c)} + \frac{\gamma}{v-c} \right) \cdot \frac{\beta\alpha - \sigma}{\gamma}.$$

Since $\det J^* < 0$, it follows that (N^*, U^*) is a saddle point, thus completing the proof. ∎

Remark 2.4.1 *If we were to instead consider the case where $v > c$, then $(0,0)$ would become an unstable node and $(0,K)$ would become a stable node. In this case, (N^*, U^*) would remain a saddle point but the stability of the manifolds would reverse, compared to the case where $v < c$. That is, the stable manifold will become unstable and the unstable manifold will become stable.*

We can also use **Mathematica** to numerically show these results by plotting the phase portrait (see Figure 2.4). In this plot, the following parameter values were used: $v = 1, c =$

$2, \beta = \alpha = r = K = \gamma = 1$, and $\sigma = 0.5$. We can see that the point (N^*, L^*) is a saddle point, $(0, 0)$ is a stable node, and $(0, K)$ is an unstable node.

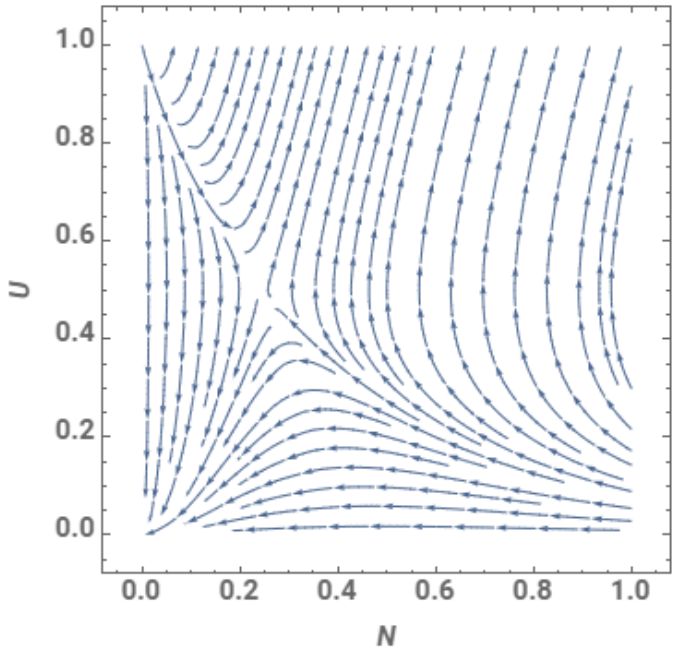

Figure 2.4: Phase portrait of system (2.22) in the case where $v < c$. Note that following a trajectory on this phase portrait gives the evolution of the forest state in backward-time. This is because we are considering right-travelling waves. To see the evolution of the forest state in forward time, a trajectory must be followed backwards on this plot.

In summary, the following theorem follows from Proposition 2.4.1, the vector field (see Figure 2.3), and the Poincaré-Bendixson Theorem:

Theorem 2.4.1 *If $0 < \beta\alpha - \sigma < \gamma K$, then for all $c > v$, there exists a solution of system (2.22) satisfying the boundary conditions (2.27) - (2.29).*

Remark 2.4.2 *It can be shown (via direct substitution) that if $c = v$, there does not exist a solution of system (2.22) which connects (N^*, U^*) and $(0, 0)$. Therefore, v is not a minimum travelling wave speed. Furthermore, if $c < v$, then it is clear (i.e., by reversing the direction of the trajectories in Figure 2.4) that there exists a TWS connecting $(0, 0)$ to (N^*, U^*) as $\xi \to \infty$. These solutions correspond to co-extinction waves, as the biomasses of both the native species and invasive weed biomasses tend to 0 as $t \to \infty$. This is not ecologically favourable.*

Hence, we have shown that there exists a TWS of system (2.19) satisfying the boundary conditions (2.27) - (2.29). The wave profiles are plotted in Figure 2.5.

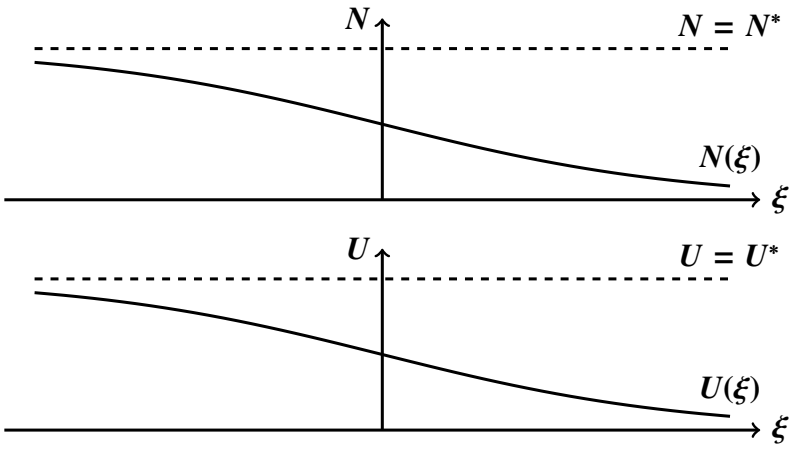

Figure 2.5: The wave profiles, i.e., solutions of the travelling wave ODE system. The long-term behaviour of the system is determined by taking $\xi \to -\infty$. These graphs show that the forest will asymptotically tend to co-existence steady state, (N^*, U^*).

Notice in Figure 2.5 that as $t \to \infty$ we have $\xi \to -\infty$ as the waves are travelling to the *right* since $c > 0$. Hence, we should expect that over sufficiently long periods of time, the biomasses of both the stem apices and the native plant species will tend to the co-existence steady state, not the extinction steady state. We can discuss the biological meaning of the conditions leading to this co-existence. Since $v < c$, the wave speed is greater than the advection speed. Since $\beta\alpha > \sigma$, this means that the growth and photosynthetic rate of the weed is greater than the death rate and since $\gamma K > \beta\alpha - \sigma$, there is a relatively large carrying capacity *or* a high rate of competition between the species. This means that a higher carrying capacity leads to co-existence; i.e., if there are more nutrients, both species may coexist. Less intuitive is the fact that a greater competition term can also lead to co-existence.

2.4.1 Travelling Wave Solutions: An Established Forest and Self-Shading

We now consider the case where $v_u = 0$ and $\alpha(\ell)$ is no longer constant, i.e., the wild-type species does not spread via advection and self-shading is not negligible. This corresponds to

the case where the forest mat is established prior to the weed invasion and follows a standard logistic growth model in the absence of the invasive weed. We place the following assumptions on α: $\alpha(0) = \alpha_0 > 0$ and $\lim_{z\to\infty} \alpha(z) = \alpha_\infty < \infty$, i.e., there is some saturating value. Furthermore, we assume that α is smooth on $(0, \infty)$. Finally, we assume that α is increasing on $[0, \infty)$.

We are interested in investigating right-travelling wave solutions and hence we seek solutions of the form $[N(\xi), L(\xi), U(\xi)]^T$ where $\xi := x - ct$ and $c > 0$. Making this substitution into system (2.1) yields the following system of ODEs:

$$\begin{cases} (v-c)N' &= \beta\alpha(L)N - \sigma N - \gamma NU, \\ -cL' &= m\alpha(L)N - \phi L, \\ -cU' &= rU\left(1 - \dfrac{N+U}{K}\right) - \gamma NU. \end{cases} \tag{2.33}$$

Note that $(N, L, U) = (0, 0, K)$ is a steady state of this system. We now seek steady states in which the native species have gone extinct, i.e., $U = 0$. Making this substitution into (2.33) yields the following system of algebraic equations:

$$\beta\alpha(L) - \sigma = 0,$$
$$m\alpha(L)N - \phi L = 0.$$

For this system to have a solution, the first equation in the system must have some solution, say L^*, i.e., $\alpha(L^*) = \sigma/\beta$. Recall that α is a continuous, increasing function with saturating value (horizontal asymptote) α_∞. Then to guarantee the existence of the (unique) solution L^* to this equation, we have the following sufficient and necessary condition:

$$\alpha_0 < \frac{\sigma}{\beta} < \alpha_\infty. \tag{2.34}$$

In this case, we also have some N^* given by

$$N^* = \frac{\phi L^*}{m\alpha(L^*)} = \frac{\phi\beta}{m\sigma}L^*.$$

In summary, we seek a TWS of (2.33) which satisfies

$$\lim_{\xi\to\infty}\left[N(\xi), L(\xi), U(\xi)\right]^T = [0, 0, K]^T, \tag{2.35}$$

$$\lim_{\xi\to-\infty}\left[N(\xi), L(\xi), U(\xi)\right]^T = [N^*, L^*, 0]^T. \tag{2.36}$$

To make biological sense of the above conditions, we recall that we are studying *right*-travelling waves. Hence, solutions satisfying these conditions correspond to solutions travelling from $(0, 0, K)$ to $(N^*, L^*, 0)$ as $t \to \infty$. This corresponds to an event in which the invasive weed drives the native plant to extinction over sufficiently long time.

Computing the Jacobian matrix of system (2.33) yields

$$J(N, L, U) = \begin{pmatrix} \dfrac{\beta\alpha(L) - \sigma - \gamma U}{v - c} & \dfrac{\beta\alpha'(L)N}{v - c} & -\dfrac{\gamma N}{v - c} \\ -\dfrac{m\alpha(L)}{c} & \dfrac{\phi - m\alpha'(L)N}{c} & 0 \\ \dfrac{(r + K\gamma)U}{Kc} & 0 & \dfrac{2rU + rN + \gamma KN - rK}{Kc} \end{pmatrix}.$$

We first consider the case where $c > v$. Linearizing (2.33) about the steady state $(0, 0, K)$ yields the matrix $J(0, 0, K)$. This is a lower-triangular matrix with eigenvalues $\phi/c, r/c$ and

$$\frac{\beta\alpha_0 - \sigma - \gamma K}{v - c} > 0,$$

since $\beta\alpha_0 - \sigma < 0$. Hence, the steady state $(0, 0, K)$ is an unstable node and we can rule out the existence of travelling waves satisfying the boundary conditions (2.35) - (2.36). Biologically, this implies that there are no TWS leading to *extinction of the native plant species* when the advection rate of the invasive weed across the forest is sufficiently small.

We now consider the case where $c < v$. Linearizing system (2.33) about the steady state $(N^*, L^*, 0)$ yields the following matrix:

$$J(N^*, L^*, 0) = \begin{pmatrix} 0 & \dfrac{\beta\alpha'(L^*)N^*}{v-c} & -\dfrac{\gamma N^*}{v-c} \\ -\dfrac{m\sigma}{\beta c} & \dfrac{\phi - m\alpha'(L^*)N^*}{c} & 0 \\ 0 & 0 & \dfrac{rN^* + \gamma KN^* - rK}{Kc} \end{pmatrix}, \tag{2.37}$$

where we use the fact that $\alpha(L^*) = \sigma/\beta$. Note that $\alpha'(L^*) > 0$. The characteristic polynomial of $J(N^*, L^*, 0)$ is given by

$$P(\lambda) = \left(\lambda - \frac{rN^* + \gamma KN^* - rK}{Kc}\right)\left[\lambda\left(\lambda - \frac{\phi - m\alpha'(L^*)N^*}{c}\right) + \frac{m\sigma\alpha'(L^*)N^*}{c(v-c)}\right].$$

The roots of this polynomial are given by

$$\lambda_1 = \frac{rN^* + \gamma KN^* - rK}{Kc},$$

and

$$\lambda_{2,3} = \frac{\phi - m\alpha'(L^*)N^*}{2c} \pm \frac{1}{2}\sqrt{\left(\frac{m\alpha'(L^*)N^* - \phi}{c}\right)^2 - \frac{4m\sigma\alpha'(L^*)N^*}{c(v-c)}}.$$

If the weed-invasion steady state has no unstable manifold, then there is no solution satisfying (2.35) - (2.36). Hence, if *all* the eigenvalues computed above have *negative real parts*, then we can rule out the existence of a TWS. Combining these results on the local stability of both steady states, we have the following theorem:

Theorem 2.4.2 *If $c > v$, then there is no solution of system (2.33) with boundary conditions (2.35) - (2.36).*

The above theorem gives us an upper bound on the travelling wave speed to any possible TWS (if any exist). The next theorem gives us conditions on the parameters which rule out the

existence of a TWS, hence leading to further necessary conditions.

Theorem 2.4.3 *If $c < v$ and the following inequalities holds:*

$$\frac{\sigma}{\beta\alpha'(L^*)} < L^* < \frac{\sigma mrK}{\beta\phi(r+\gamma K)}.$$

Then there is no solution of system (2.33) with boundary conditions (2.35) - (2.36).

The above theorem provides us with some biological insights from this model. If the competition rate between the species is sufficiently large, then we should not expect an extinction event to occur. Furthermore, if the rate of weed leaf biomass death is sufficiently large, then we once again would not expect the invasive weed to drive the native species to extinction. Both of these conclusions are biologically reasonable. In the former case, the model reflects the *resilience* of the native plant species when faced with competition. In the latter case, the model reflects the idea that if photosynthetic input into the weed is sufficiently low, then we should not expect the weed species to successfully drive the native species to extinction as the weed species itself will find survival more difficult.

2.5 Conclusion and Discussion

In Sections 2.2 and 2.3 of this chapter, we studied a case of the model proposed in [4] in which self-shading is negligible and the weed leaf death rate is constant. We did this in both the case of purely initial conditions and the case of mixed initial and boundary conditions. In the former case, we found closed form solutions for both the stem apex and leaf biomasses as functions of position and time. In the latter case, these solutions are also easily obtained via the method of characteristics. We further suggested a method of control for the weed in the case of a boundary via changing the rate of stem apex biomass advection, v.

Of particular interest is the main result of Section 2.3: an increased rate of the weed spreading *away* from the boundary results in a greater control of the weed biomass in regions farther

away from this boundary. This intuitively represents the fact that the effects of the boundary will *wear off* after the weed has travelled a larger distance from its initial locations. This led us to suggest that using the boundary as a control can be more effective in the cases where the weed is spreading faster - this would be fortunate for rapidly depleting native forests. This suggestion is an agreement with James et al. [6], which suggested that inhibiting weed growth at the stem base is more effective than inhibiting branching. In both cases, the idea is to control the original boundary rather than focus on far-away regions of spread. Furthermore, this agrees with the findings of Standish [10] that herbicide use or hand-weeding of *T. fluminensis* is not an effective method of control, particularly for regions far away from the boundary. However, Standish also found that light availability, mathematically represented by the variable α in our model, can also be used as a control. In particular, increasing shading resulted in decreased weed biomass. The boundary value problem presented in Section 2.3 reinforces this idea, as a constant and low value of α gives control of the weed biomass to the function f, i.e., the controllable boundary condition.

The advantage of the modelling done in Sections 2.2 and 2.3 is in the simplicity of the models, namely the use of first order PDEs with natural boundary and initial conditions while still yielding results that are intuitive and compatible with biological observations. Furthermore, they offer potential ideas for control measures which are also intuitive and physically tractable. The disadvantage of this modelling is that its simplicity can fail to capture some of the more realistic features of invasive weed spread. Furthermore, this modelling has only taken into account one-dimensional weed spreading, when we would more realistically expect two-dimensional spreading.

In Section 2.4, we proposed two competition models between the invasive weed and a wild-type plant species. In the first case, we were able to look at a two-variable system by uncoupling the N equation from the L equation. This was again accomplished by ignoring the affect of self-shading described in [4]. In the second case, we did not ignore this effect and studied a three-variable system of PDEs. We once again studied the existence of a TWS. In this

case, we found that a necessary condition for the existence of a TWS was that the advection, or *creeping*, speed of the weed stem must be greater than the travelling wave speed, c, for an extinction event to occur. This is consistent with the case studied by Hogan and Myerscough, where $v > c$, i.e., single weeds must expand faster than the entire weed mat [4]. Furthermore, as in [4], we found that the ratio σ/β plays an important rule in determining the dynamics of the system. In particular, Theorem 2.4.1 shows that if this ratio is too high, then an extinction event (of the wild-type species) will not occur. This seems to imply that increasing the death rate of the weed stem (or decreasing its birth rate) above (below) the critical value given in this theorem will allow the wild-type species to exist in the forest (though not necessarily at the co-existence steady state).

The advantage of the modelling done in Section 2.4 is that the theory of two-variable (and monotone) dynamical systems is well established and can provide many interesting insights on competition between the invasive weed and native plant, allowing us to capture more interesting dynamics. The limitations of the modelling from this section generally come from the difficulty in proving the existence of a travelling wave front in a three-variable model, as Poincaré-Bendixson theory is no longer applicable. More advanced analytical tools, such as the Banach Fixed Point Theorem, are required to better explore the dynamics of these models.

There is a great deal of future work which may be done. As noted by Froude [2], the model uses advection to incorporate a so-called *creeping* effect. Another mechanism of weed invasion is dispersal which incorporates diffusion [9]. Hence, the following PDE might give a possible model for this mechanism:

$$n_t + vn_x = Dn_{xx} + \beta\alpha(\ell)n - \sigma n - \gamma nu. \tag{2.38}$$

One may transform this new system into a system of four first-order ODEs, i.e., by letting $M(\xi) := N'(\xi)$ where $\xi := x - ct$, when seeking travelling wave solutions . Once again, necessary conditions may be obtained for the existence of a TWS. One may use the Routh-

Hurwitz criteria or the Gershgorin Disc Theorem [13] as tools for obtaining information on the eigenvalues of the new system in the case where directly computing the eigenvalues is non-feasible. These methods can give bounds on the parameters which will be sufficient in ruling out the existence of TWS, such as extinction waves. This may provide insights on implementing control strategies to prevent extinction of native forest biomass.

Invasive weeds, such as *T. fluminensis*, can also have a negative impact on wild-type animal species living in the area of invasion [2]. A next step can also incorporate a herbivorous animal species into the model, which preys on the wild-type plant species. Furthermore, invasive weeds have also been shown to interact mutualistically with carnivorous animal species [2]; a cooperative interaction which may also be appended to the model.

The next step will be to find sufficient conditions for the existence of a TWS to (2.33), (2.35) - (2.36). As this is a system of three variables, finding these conditions is considerably more difficult. An approach similar to the one outlined by Huang [5] may be considered. In this case, one may look at system (2.33) in reverse *time* (ξ) and construct a Lyapunov function as in [5]. If successful, this approach, combined with the necessary conditions in Section 2.4 of this chapter, will give sufficient and necessary conditions for the existence of an extinction wave in which the wild-type species is completely driven to extinction via the introduction of a spatially advective weed species. Therefore, finding such conditions are not only mathematically important but also biologically significant. We leave it for future exploration.

Bibliography

[1] Duursma, R. A., Mäkelä, A., Reid, D. E., Jokela, E. J., Porté, A. J., & Roberts, S. D. (2010). Self-shading affects allometric scaling in trees. *Functional Ecology*, 24(4), 723-730.

[2] Froude, V. (2002), *Biological control options for invasive weeds of New Zealand protected areas*. Wellington: Department of Conservation.

[3] Gourley, S. A., Li, J., & Zou, X. (2016). A mathematical model for biocontrol of the invasive weed Fallopia japonica. *Bulletin of Mathematical Biology*, 78(8), 1678-1702.

[4] Hogan, A. B., & Myerscough, M. R. (2017). A model for the spread of an invasive weed, Tradescantia fluminensis. *Bulletin of Mathematical Biology*, 79(6), 1201-1217.

[5] Huang, W. (2012). Traveling wave solutions for a class of predator–prey systems. *Journal of Dynamics and Differential Equations*, 24(3), 633-644.

[6] James, A., Molloy, S. M., Ponder-Sutton, A., Plank, M. J., Lamoureaux, S. L., Bourdôt, G. W., & Kelly, D. (2015). Modelling Tradescantia fluminensis to assess long term survival. *PeerJ*, 3, e1013.

[7] Knuesting, J., Brinkmann, M. C., Silva, B., Schorsch, M., Bendix, J., Beck, E., & Scheibe, R. (2018). Who will win where and why? An ecophysiological dissection of the competition between a tropical pasture grass and the invasive weed Bracken over an elevation range of 1000 m in the tropical Andes. *PloS one*, 13(8), e0202255.

[8] Logan, J. David. (2007) *An Introduction to Nonlinear Differential Equations*, Second Edition.Wiley-Interscience. John Wiley & Sons.

[9] Portnoy, S., & Willson, M. F. (1993). Seed dispersal curves: behavior of the tail of the distribution. *Evolutionary Ecology*, 7(1), 25-44.

[10] Standish, R. J. (2002). Experimenting with methods to control Tradescantia fluminensis, an invasive weed of native forest remnants in New Zealand. *New Zealand Journal of Ecology*, 161-170.

[11] Standish, R. J., Robertson, A. W., & Williams, P. A. (2001). The impact of an invasive weed Tradescantia fluminensis on native forest regeneration. *Journal of Applied Ecology*, 38(6), 1253-1263.

[12] Vance, R. R., & Nevai, A. L. (2007). Plant population growth and competition in a light gradient: a mathematical model of canopy partitioning. *Journal of Theoretical Biology*, 245(2), 210-219.

[13] Weisstein, Eric W. "Gershgorin Circle Theorem." From MathWorld–A Wolfram Web Resource. http://mathworld.wolfram.com/GershgorinCircleTheorem.html

[14] Wolfram Research, Inc., Mathematica, Version 12.0, Champaign, IL (2019).

Chapter 3

On the Treatment of Melanoma: A Mathematical Model of Oncolytic Virotherapy

3.1 Introduction

Melanoma is considered the most deadly type of skin cancer. Melanoma begins in melanocytes - the cells responsible for producing melanin - and can develop in various parts of the body [28, 36]. Melanoma is the fifth most common cancer in adults in the United States [27]. While melanoma rates have been steadily rising, mortality has not followed this same trend. This decreased mortality is attributed to various factors such as early detection, increased protection against UV radiation, and improvements in treatment [30]. Metastatic melanoma continues to be a major issue contributing the cancer mortality, due to the increased difficulty of treating the disease once it has spread beyond its original site [29]. Various forms of therapy, including chemotherapy, immunotherapy, and radiotherapy are used in the treatment of advanced melanoma. Developing new forms of therapy and enhancing existing therapy is always desirable in increasing survival rates of the disease.

Oncolytic virotherapy is a method of cancer treatment in which genetically modified viruses are used to selectively infect and destroy cancer cells via a variety of direct and indirect mechanisms, while leaving surrounding healthy cells unharmed [10, 26]. These viruses are called oncolytic viruses (OVs). The genetically modified herpes simplex virus Talimogene laherparepvec (T-VEC) has been used in clinical trials to treat inoperable melanoma [17, 25]. The treatment is often performed in combination with other therapies, such as being followed up with the use of adjuvant radiotherapy. The oncolytic virus is typically administered via direct subcutaneous injection into the lesion [12]. The idea is for the virus to selectively infect cancer cells and use them to replicate and perform oncolysis to destroy the neoplasm. The viral infection may also destroy the cancer cells through indirect mechanisms such as activating the immune system and aiding the immune response against the cancer cells [9, 10, 26]. Other OVs which have been studied include the adenoviruses ONYX-015 and ZD55-IL-24 [15].

Mathematical modelling of cancer treatment has seen widespread use in the last few decades. These models frequently take the form of ODE, PDE, and delay models in the continuous setting. By studying the effect of disease treatment from a quantitative perspective, based on biological and physical mechanistic modelling, new insights may be obtained to guide future treatment direction. This type of modelling has also been used to study the treatment of cancer via oncolytic virotherapy [13, 24]. The recent work of Wang et al [38]. in mathematical modelling of virotherapy as a treatment modality for melanoma, the models were able to provide insights concerning virus treatment thresholds as well as how immunosupperssive drugs may work in tandem with OVs. The work by Urenda-Cazares et al. examined the use of OVs in combination with chemotherapy to treat glioma. As a result of these types of models, some results were obtained on how to optimize treatment in a clinical setting [37].

In this chapter, we model the effect of hypoxic environments on oncolytic virotherapy treatment through the use of ordinary differential equation (ODE) modelling. Hypoxic refers to oxygen-poor environments. Typically, viruses which are more efficient at infecting cells in oxygen-rich environments tend to lose their infectivity under hypoxic conditions [11]. This is

particularly true of adenoviruses such as ONYX-015 [31]. Hypoxia has a negative effect on the efficacy of OVs as well as any adjuvant radiotherapy which may be administered [3, 4]. In the context of melanoma treatment, hypoxic environments can inhibit the action of OVs, such as their ability to infect cancer cells and their ability to induce the death of cancer cells. Due to the lack of mathematical modelling of this phenomenon, we explore the relationship between tumour microenvironment oxygen concentration and the efficacy of the OV. In our model, we study the effect of oxygen concentration when the OV is applied directly to the primary lesion. More specifically, we study the impact which parameters such as the infectiousness of the OV on the efficacy of the treatment under different oxygen conditions.

The structure of this chapter is organized as follows. In Section 3.2, we formulate an ODE model and give the assumptions on our functions. We refer to this as our local model, since we are studying the effect of OV directly on the primary tumour. We also perform non-dimensionalization of the model for the purposes of mathematical analysis. We explain the meaning of our model in terms of the biological context. In Section 3.3, we perform an analysis of the local model. This includes proofs on the well-posedness results. In Subsection 3.3.1, we first look at the case where we do not take into account the oxygen concentration dependence. In Subsection 3.3.2, we look at the case of oxygen concentration dependence. We perform an analysis of the stability of the relevant steady states of our system. In Section 3.4, we perform numerical simulations and give biological interpretations of these results. In Section 3.5, we extend our model to a regional model, where we take into account the movement of tumour cells into the surrounding lymph nodes. In Section 3.6, we perform numerical simulations on the regional model. We complete this chapter with some conclusions and discuss possible directions for future work in Section 3.7.

3.2 Local Oncolytic Virotherapy Model

We begin by considering a melanoma tumour, initially consisting of some initial quantity of proliferating tumour cells. At this initial point in time, a localized treatment of oncolytic virotherapy begins at the tumour site, by introducing the OV via direct injection into the lesion. We consider the use of an adenovirus such as ONYX-015. The OV then proceeds to infect the tumour cells. The model consists of three variables, the density of uninfected tumour cells, the density of infected tumour cells, and oxygen concentration, at time t, respectively represented by $u(t), n(t)$, and $c(t)$. Then, we have the following model:

$$\frac{\mathrm{d}u}{\mathrm{d}t} = r_1 u\left(1 - \frac{u+n}{K}\right) - \frac{\theta(c)nu}{\alpha+n}, \tag{3.1}$$

$$\frac{\mathrm{d}n}{\mathrm{d}t} = r_2 n\left(1 - \frac{u+n}{K}\right) + \frac{\theta(c)nu}{\alpha+n} - \gamma(c)n, \tag{3.2}$$

$$\frac{\mathrm{d}c}{\mathrm{d}t} = \phi - \beta c - q_1 uc - q_2 nc. \tag{3.3}$$

Note that we are considering cell-to-cell infections, which have been observed as a mode of infection used by oncolytic viruses [14]. Previous mathematical models of cell-to-cell viral infection made use of a mass-action-like terms to represent infection [6, 21] and we adopt a similar approach in our model, but with the infection mechanism of a Holling type II functional response function.

We prescribe the initial conditions $u(0) = u_0, n(0) = n_0$ and $c(0) = c_0$ to be non-negative quantities. We assume that both classes of tumour cells exhibit logistic growth. The carrying capacity of the tumour cells is given by K and the growth rates of the uninfected tumour cells and the infected tumour cells are given by r_1 and r_2, respectively. We further assume that $r_1 > r_2$ to reflect that the infected tumour cells are less effective at proliferating due their cell machinery being hijacked by the OV. Following the approach of [2], we use mass-action terms to express the oxygen consumption by the tumour cells. To that end, the parameters q_1 and q_2 give the oxygen consumption rate by the uninfected tumour cells and the infected tumour

cells, respectively. The rate of oxygenation, assumed constant (due to having some control over this parameter, i.e., through certain therapies [34]), is given by ϕ and the rate of oxygen consumption by surrounding *non-cancerous cells (or healthy cells)* is given by β.

We use a Hill function to represent the transition of a tumour cell from uninfected by an OV to infected by an OV. The parameter $\theta(c) \in \mathrm{C}^1(\mathbb{R}_+)$ represents the virus infection rate, which is dependent on available oxygen concentration. The other oxygen dependent parameter $\gamma(c) \in \mathrm{C}^1(\mathbb{R}_+)$ is the virus-induced death rate of the infected tumour cells. Note that the terms *virus-induced death rate* and *oncolysis rate* are used interchangeably in Chapters 3 and 4. The adenovirus is inhibited by a hypoxic environment and hence we assume that as oxygen concentration is locally decreased, the OV will become less effective, both in infecting the tumour cells and inducing tumour cell death [31]. Hence, we have the following conditions on $\theta(c)$ and $\gamma(c)$:

$$\begin{cases} \theta'(c) \geq 0, \quad \gamma'(c) \geq 0, \quad \text{for} \quad c \in (0, \infty), \\ \theta(0) = \theta_0 \geq 0, \quad \gamma(0) = \gamma_0 \geq 0, \\ \lim\limits_{c\to\infty} \theta(c) = \theta_\infty > \theta_0, \quad \lim\limits_{c\to\infty} \gamma(c) = \gamma_\infty > \gamma_0, \end{cases} \tag{3.4}$$

where θ_∞ and γ_∞ give the OV efficacy in response to high oxygen environments. Note that in hypoxic environments, oncolytic virotherapy will not be as efficient as an adenovirus is being used.

We non-dimensionalize the model by making the following substitutions:

$$x := \frac{u}{K}, \quad y := \frac{n}{K}, \quad z := \frac{\beta c}{\phi}, \quad \tau := r_1 t.$$

Then we obtain the system,

$$\frac{\mathrm{d}x}{\mathrm{d}\tau} = x(1 - x - y) - \frac{\hat{\theta}(z)xy}{\hat{\alpha} + y}, \tag{3.5}$$

$$\frac{\mathrm{d}y}{\mathrm{d}\tau} = ry(1 - x - y) + \frac{\hat{\theta}(z)xy}{\hat{\alpha} + y} - \hat{\gamma}(z)y, \tag{3.6}$$

$$\frac{\mathrm{d}z}{\mathrm{d}\tau} = \hat{\beta}(1-z) - \hat{q}_1 xz - \hat{q}_2 yz, \tag{3.7}$$

where we define

$$\hat{\theta}(z) := \frac{1}{r_1}\theta\left(\frac{\phi z}{\beta}\right), \quad \hat{\gamma}(z) := \frac{1}{r_1}\gamma\left(\frac{\phi z}{\beta}\right),$$

$$\hat{r} := \frac{r_2}{r_1}, \quad \hat{\alpha} := \frac{\alpha}{K}, \quad \hat{\beta} := \frac{\beta}{r_1}, \quad \hat{q}_1 := \frac{q_1 K}{r_1}, \quad \hat{q}_2 := \frac{q_2 K}{r_1}.$$

Note that the properties of $\theta(c)$ and $\gamma(c)$ given in (3.4) are preserved by $\hat{\theta}(z)$ and $\hat{\gamma}(z)$, respectively, up to some scaling. The most notable change is in the long-term behavior: $\hat{\theta}$ will approach $\hat{\theta}_\infty := \theta_\infty/r_1$ and $\hat{\gamma}$ will approach $\hat{\gamma}_\infty := \gamma_\infty/r_1$ as $z \to \infty$. We now drop the tilde and replace τ with t for notational convenience and hence, for the subsequent analysis, we consider the following model:

$$\frac{\mathrm{d}x}{\mathrm{d}t} = x(1-x-y) - \frac{\theta(z)xy}{\alpha+y}, \tag{3.8}$$

$$\frac{\mathrm{d}y}{\mathrm{d}t} = ry(1-x-y) + \frac{\theta(z)xy}{\alpha+y} - \gamma(z)y, \tag{3.9}$$

$$\frac{\mathrm{d}z}{\mathrm{d}t} = \beta(1-z) - q_1 xz - q_2 yz, \tag{3.10}$$

with non-negative initial conditions:

$$x(0) = x_0 \geq 0, \quad y(0) = y_0 \geq 0, \quad z(0) = z_0 \geq 0. \tag{3.11}$$

The functions θ and γ once again have the properties given in (3.4). In Section 3.3, we perform a mathematical analysis of the rescaled model (3.8) - (3.10) to explore some predictions related to the effect of available oxygen concentration on the OV treatment.

3.3 Analysis of the Local Model

We begin by considering the well-posedness of the model. Existence and uniqueness of the solution of (3.8) - (3.10), subject to initial conditions (3.11), follow from the elementary theory of ODEs. We consider the solution of this initial value problem, $(x(t), y(t), z(t)) \in \mathbb{R}^3$. Since the variables represent densities and concentration of physical quantities, the system must remain non-negative for all $t \geq 0$. We begin with equation (3.8). From this equation, it follows that

$$x(t) = x_0 \cdot \exp\left[\int_0^t \left(1 - x(s) - y(s) - \frac{\theta(z(s))y(s)}{\alpha + y(s)}\right) \mathrm{d}s\right],$$

and so, $x(t) \geq 0$ for all $t \geq 0$. Similarly, it follows from equation (3.9) that

$$y(t) = y_0 \cdot \exp\left[\int_0^t \left(r(1 - x - y) + \frac{\theta(z(s))x(s)}{\alpha + y(s)} - \gamma(z(s))y(s)\right) \mathrm{d}s\right].$$

Therefore, $y(t) \geq 0$ for all $t \geq 0$. Finally, equation (3.10) gives

$$z(t) = z_0 \cdot \exp\left(-\int_0^t (\beta + q_1 x(s) + q_2 y(s))\mathrm{d}s\right) + \beta \int_0^t \exp\left(-\int_s^t (\beta + q_1 x(\xi) + q_2 y(\xi))\mathrm{d}\xi\right) \mathrm{d}s.$$

This shows that $z(t) \geq 0$ for all $t \geq 0$. In fact, if $t > 0$, then z is strictly positive.

Next, we address the boundedness of the solution. To this end, we apply a comparison argument. From equations (3.8) and (3.10), a solution of the system satisfies the inequalities

$$\frac{\mathrm{d}x}{\mathrm{d}t} \leq x(1 - x), \quad \frac{\mathrm{d}z}{\mathrm{d}t} \leq \beta(1 - z).$$

Then, it follows that

$$\limsup_{t\to\infty} x(t) \leq 1, \quad \limsup_{t\to\infty} z(t) \leq 1.$$

Hence, $x(t)$ and $z(t)$ are bounded functions. Let $\bar{x}$ be an upper bound for $x(t)$, i.e., $x(t) \leq \bar{x}$ for

all $t \geq 0$. It then follows from equation (3.9) that

$$\frac{\mathrm{d}y}{\mathrm{d}t} \leq ry(1-y) + \frac{\theta_\infty \bar{x} y}{\alpha + y} \implies \frac{\mathrm{d}y}{\mathrm{d}t} \leq ry(1-y) + \theta_\infty \bar{x}.$$

Therefore, by a comparison argument,

$$\limsup_{t\to\infty} y(t) \leq \frac{r + \sqrt{r^2 + 4r\theta_\infty \bar{x}}}{2r},$$

which shows that $y(t)$ is a bounded function.

Summarizing these results, we have the following theorem:

Theorem 3.3.1 *The solution of the initial value problem (3.8) - (3.10), satisfying initial conditions (3.11), is non-negative and bounded.*

3.3.1 Dynamics of the Local Model – Case I: No Oxygen Dependence

We consider first the case with no oxygen dependence. That is, we set $\theta(z) = \theta$ and $\gamma(z) = \gamma$, where θ and γ are positive constants. In this case, system (3.8) - (3.10) reduces to the following two-variable system:

$$\frac{\mathrm{d}x}{\mathrm{d}t} = x(1-x-y) - \frac{\theta x y}{\alpha + y}, \tag{3.12}$$

$$\frac{\mathrm{d}y}{\mathrm{d}t} = ry(1-x-y) + \frac{\theta x y}{\alpha + y} - \gamma y. \tag{3.13}$$

If we consider system (3.12) - (3.13) over the region $(x, y) \in \mathbb{R}^2_+$, we can rule out the existence of non-constant periodic orbits.

Proposition 3.3.1 *Consider system (3.12) - (3.13) over the region $\mathbb{R}^2_+$. There are no closed orbits contained entirely $\mathbb{R}^2_+$.*

Proof Let $S(x,y) = 1/(xy)$ for $x, y > 0$. Then,

$$\frac{\partial}{\partial x}\left[S(x,y)\left(x(1-x-y) - \frac{\theta xy}{\alpha+y}\right)\right] + \frac{\partial}{\partial y}\left[S(x,y)\left(ry(1-x-y) + \frac{\theta xy}{\alpha+y} - \gamma y\right)\right]$$

may be computed to give

$$-\frac{1}{y} - \frac{r}{x} - \frac{\theta}{(\alpha+y)^2} < 0. \tag{3.14}$$

Since this function does not change sign on $\mathbb{R}^2_+$, we conclude by the Dulac-Bendixson Theorem that there are no closed orbits contained entirely in $\mathbb{R}^2_+$. ∎

Next, we determine the steady states of system (3.12) - (3.13) by solving the algebraic system

$$x(1-x-y) - \frac{\theta xy}{\alpha+y} = 0, \tag{3.15}$$

$$ry(1-x-y) + \frac{\theta xy}{\alpha+y} - \gamma y = 0. \tag{3.16}$$

It can be readily seen that $(x,y) = (0,0)$ and $(x,y) = (1,0)$ are solutions of this system for all parameter values. Another solution which may be easily seen is $(x,y) = (0,(r-\gamma)/r)$, which only exists if $r > \gamma$. It can be shown that the remaining steady states (if any exist) are determined by solving the system

$$(\theta - r\theta + \gamma)y^2 + (\theta^2 + \alpha\theta + 2\alpha\gamma - r\alpha\theta - \theta)y + \alpha(\alpha\gamma - \theta) = 0, \tag{3.17}$$

$$x = 1 - y - \frac{\theta y}{\alpha+y}. \tag{3.18}$$

We linearize the system at its steady states by first computing the Jacobian matrix

$$J(x,y) = \begin{pmatrix} 1 - 2x - y - \dfrac{\theta y}{\alpha+y} & -x - \dfrac{\theta\alpha x}{(\alpha+y)^2} \\ \\ -ry + \dfrac{\theta y}{\alpha+y} & r - rx - 2ry + \dfrac{\alpha\theta x}{(\alpha+y)^2} - \gamma \end{pmatrix}.$$

We begin with the assumption $r < \gamma$ in order to discount the steady state $(0, (r-\gamma)/r)$. Linearizing at the steady state $(0, 0)$ gives

$$J(0,0) = \begin{pmatrix} 1 & 0 \\ 0 & r-\gamma \end{pmatrix}.$$

By our assumption that $r < \gamma$, this steady state is a saddle. Linearizing the system at the steady state $(1, 0)$ gives

$$J(1,0) = \begin{pmatrix} -1 & -1-\dfrac{\theta}{\alpha} \\ 0 & \dfrac{\theta}{\alpha}-\gamma \end{pmatrix}.$$

From $J(1, 0)$, we then conclude that $(1, 0)$ is locally asymptotically stable if $\theta < \alpha\gamma$ and it is unstable if $\theta > \alpha\gamma$.

If we now impose the additional assumption $\theta < \alpha\gamma$, then the system only contains two non-negative steady states: $(0, 0)$ and $(1, 0)$. To see this, we note that the left-hand side of equation (3.17), as a function of y, is a convex parabola (since $r < 1$) with a positive constant term. The coefficient of the y term is also positive, as

$$\theta^2 + \alpha\theta + 2\alpha\gamma - r\alpha\theta - \theta = \theta^2 + \alpha\gamma + \alpha\theta(1-r) + (\alpha\gamma - \theta) > \theta^2 + \alpha\gamma > 0.$$

Therefore, the parabola has non-negative roots and system (3.17) - (3.18) has no non-negative solutions. This shows that the only non-negative steady states are $(0, 0)$ and $(1, 0)$.

Next, we consider the case $\theta > \alpha\gamma$. In this case, an additional co-existence steady state, (x_*, y_*), where $x_*, y_* > 0$ may be introduced if system (3.17) - (3.18) has positive solutions. It is clear to see that the parabola on the left-hand side of equation (3.17) is still convex but the constant term is now negative. Hence, this parabola has exactly one positive real root, y_*. Then x^* may be obtained from equation (3.18). In order for the steady state to be meaningful, we set x must be positive, which is not the case for all values of the model parameters. We impose the

following condition to ensure that x_* is positive:

$$y_*^2 + (\alpha + \theta)y_* < 1, \tag{3.19}$$

where

$$y_* = \frac{A + \sqrt{A^2 - 4\alpha(\theta - r\theta + \gamma)(\alpha\gamma - \theta)}}{2(\theta - r\theta + \gamma)},$$

and

$$A = r\alpha\theta + \theta - \theta^2 - \alpha\theta - 2\alpha\gamma.$$

We assume these conditions are satisfied so that the steady state (x_*, y_*) exists and has positive coordinates. In fact, since $r < \gamma$, these conditions are satisfied as the existence of a stable (unique) positive steady state is ensured as a corollary of non-negativity of solutions, boundedness of solutions, and Proposition 3.3.1.

As we will now show, the assumption $r < \gamma$ is not necessary for the local stability of the steady state (x_*, y_*) – only its existence is necessary. If it exists, linearizing at this steady state gives the matrix

$$J(x_*, y_*) = \begin{pmatrix} -x_* & -x_* - \dfrac{\theta\alpha x_*}{(\alpha + y_*)^2} \\ -ry_* + \dfrac{\theta y_*}{\alpha + y_*} & -ry_* - \dfrac{\theta x_* y_*}{(\alpha + y_*)^2} \end{pmatrix}.$$

We compute the determinant of this matrix:

$$\det J(x_*, y_*) = \left(rx_*y_* + \frac{\theta x_*^2 y_*}{(\alpha + y_*)^2}\right) - \left(rx_*y_* + \frac{\theta\alpha r x_* y_*}{(\alpha + y_*)^2} - \frac{\theta x_* y_*}{\alpha + y_*} - \frac{\theta^2\alpha x_* y_*}{(\alpha + y_*)^3}\right)$$

$$= \frac{\theta x_* y_*}{\alpha + y_*} + \frac{\theta x_* y_*}{(\alpha + y_*)^2}\left(x_* - ar + \frac{\alpha\theta}{\alpha + y_*}\right)$$

$$= \theta x_* y_* (\alpha + y_*)^2 \left(\alpha + y_* + x_* - \alpha r + \frac{\alpha\theta}{\alpha + y_*}\right) > 0,$$

where the last inequality follows since $r < 1$.

The trace of $J(x_*, y_*)$ is

$$\text{tr } J(x_*, y_*) = -x_* - ry_* - \frac{\theta x_* y_*}{(\alpha + y_*)^2} < 0.$$

Therefore, the steady state (x_*, y_*) is locally asymptotically stable whenever it exists. It is therefore also globally asymptotically stable.

By Theorem 3.3.1, Proposition 3.3.1, and the Poincaré-Bendixson Theorem, the local asymptotic stability of the steady state $(1, 0)$ implies the global asymptotic stability if $\theta < \alpha\gamma$. Similarly, if $\theta > \alpha\gamma$, then (x_*, y_*) is globally asymptotically stable.

We summarize these results as follows.

Theorem 3.3.2 *Consider system (3.12) - (3.13) over the region* $\mathbb{R}^2_+$.

1. *If* $\gamma > \max\{r, \theta/\alpha\}$*, then the only two non-negative steady states of the system are* $(x, y) = (0, 0)$ *and* $(x, y) = (1, 0)$*. The steady state* $(0, 0)$ *is a saddle and the steady state* $(1, 0)$ *is a stable node. Furthermore, the steady state* $(1, 0)$ *is globally asymptotically stable on* $\mathbb{R}^2_+$.

2. *If* $r < \gamma < \theta/\alpha$*, then there exists an additional, positive, steady state,* (x_*, y_*)*. The steady states* $(0, 0)$ *and* $(1, 0)$ *are unstable (saddles) and* (x_*, y_*) *is globally asymptotically stable on* $\mathbb{R}^2_+$.

We numerically illustrate Theorem 3.3.2 in Figure 3.1.

The phase portraits in Figure 3.1 are produced with all parameters, except for α, being assigned (after non-dimensionalization) based on the values in Table 3.2. Doing so gives the parameter values $\theta = 2.52908, r = 0.531107, \gamma = 1.29362$. In Figure 3.1(a), we set $\alpha = 10.0$ and in Figure 3.1(b), we set $\alpha = 1.0$.

Clinically, the stability of $(1, 0)$ is not a favourable result, representing a failure of the OV treatment. From Proposition 3.3.2, we see that one condition which leads to this occurrence is the virus-induced death rate, γ, being made sufficiently large. This leads to an idea which will come up again in the case of oxygen dependence: Having a virus-induced death rate which

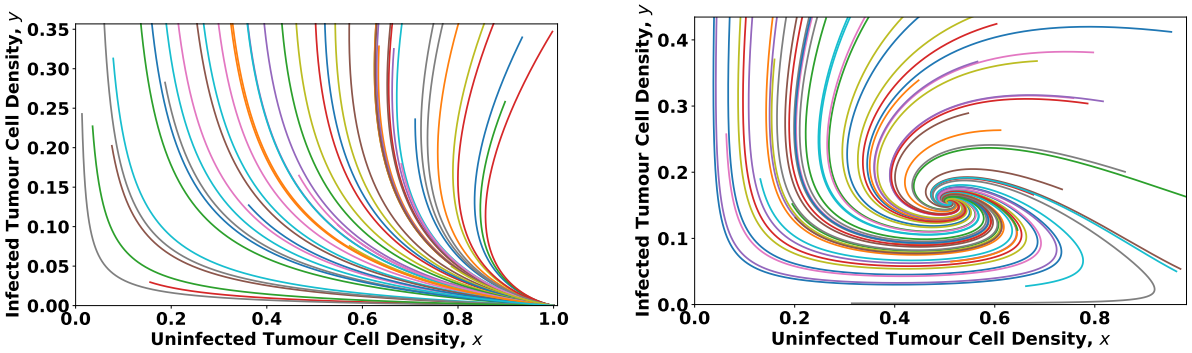

(a) (b)

Figure 3.1: The phase portrait of system (3.12) - (3.13) when $r < \gamma$. (a) When $\gamma > \max\{r, \theta/\alpha\}$, the trajectories approach the steady state $(1, 0)$ as $t \to \infty$. (b) When $r < \gamma < \theta/\alpha$, the trajectories approach the steady state (x_*, y_*) as $t \to \infty$.

is too large relative to the infection rate will decrease the efficacy of the OV. Instead, it is important to make sure that the tumour cells are not being killed faster than they are able to infect adjacent tumour cells. This suggests that when engineering an OV, it is important to achieve an appropriate balance between the infection rate and oncolysis rate of the virus.

Note that the condition $\gamma > \theta/\alpha$ in Proposition (3.3.2) follows directly from setting $\mathcal{R}_0 < 1$ where $\mathcal{R}_0$ is the basic reproduction number. Following the approach of [8], the basic reproduction number may be computed by using the next generation method. We omit the details here.

So far, we have considered the case where $r < \gamma$, i.e., when the growth rate of the infected tumour cells is bounded by their death rate. We have seen that total extinction of the uninfected tumour cells is not possible in this case. We now consider the case $r > \gamma$. In this case, we have an additional non-negative steady state, $(0, (r - \gamma)/r)$. This steady state may represent a semi-successful treatment outcome in the case $\gamma \approx r$. Hence, stability of this steady state is clinically preferable.

We note first that if $r > \gamma$, the matrix $J(0, 0)$ has two positive eigenvalues and hence, $(0, 0)$ is an unstable node. We assume that $\theta < \alpha\gamma$ in order to rule out the existence of a non-negative co-existence steady state. In this case, the eigenvalues of $J(1, 0)$ remain negative and so $(1, 0)$

remains a stable node. Linearizing system (3.12) - (3.13) at the steady state $(0, (r-\gamma)/r)$:

$$J\left(0, \frac{r-\gamma}{r}\right) = \begin{pmatrix} \dfrac{r\gamma(\alpha+\theta+1) - (r^2\theta+\gamma^2)}{r(\alpha r + r - \gamma)} & 0 \\ \dfrac{(r-\gamma)(\theta+\alpha+\alpha r - r)}{\alpha r + r - \gamma} & \gamma - r \end{pmatrix}.$$

Since this is a lower triangular matrix, the eigenvalues are the elements of the main diagonal. The eigenvalue $\gamma - r$ is negative since $r > \gamma$. The remaining eigenvalue is positive since

$$r\gamma(\alpha+\theta+1) = r(\alpha\gamma) + r\gamma\theta + r\gamma > (r^2)(\theta) + r\gamma\theta + (\gamma)(\gamma) > r^2\theta + \gamma^2.$$

Therefore, $(0, (r-\gamma)/r)$ is a saddle and hence unstable. Therefore, even in the case where $r > \gamma$, the only locally stable steady state is $(1, 0)$. This also remains true if $r = \gamma$, as can be seen via direct substitution.

The steady state $(1, 0)$ is unstable if $\theta > \alpha\gamma$ and $(0, 0)$ is always unstable. If $r > \gamma$, then the steady state $(0, (r-\gamma)/r)$ is locally asymptotically stable if and only if

$$\theta > \gamma\left(\frac{\alpha}{r-\gamma} + \frac{1}{r}\right). \tag{3.20}$$

This condition is obtained by requiring all the eigenvalues of $J(0, (r-\gamma)/r)$ to be negative. Note that since $r < 1$, condition (3.20) implies that $\theta > \alpha\gamma$. Since all solutions are non-negative and bounded, and closed orbits may not exist, it follows that violating condition (3.20) implies the existence and stability of the positive steady state (x_*, y_*).

We summarize the results of the case $r > \gamma$ in the following theorem.

Theorem 3.3.3 *Consider system (3.12) - (3.13) over the region $\mathbb{R}^2_+$. If $r > \gamma$, then:*

1. *The steady state $(x, y) = (1, 0)$ is globally asymptotically stable on $\mathbb{R}^2_+$ if*

$$\theta < \alpha\gamma.$$

2. *The positive steady state* $(x, y) = (x_*, y_*)$ *is globally asymptotically stable on* $\mathbb{R}^2_+$ *if*

$$\alpha\gamma < \theta < \gamma\left(\frac{\alpha}{r-\gamma} + \frac{1}{r}\right).$$

3. *The steady state* $(x, y) = (0, (r-\gamma)/r)$ *is globally asymptotically stable on* $\mathbb{R}^2_+$ *if*

$$\theta > \gamma\left(\frac{\alpha}{r-\gamma} + \frac{1}{r}\right).$$

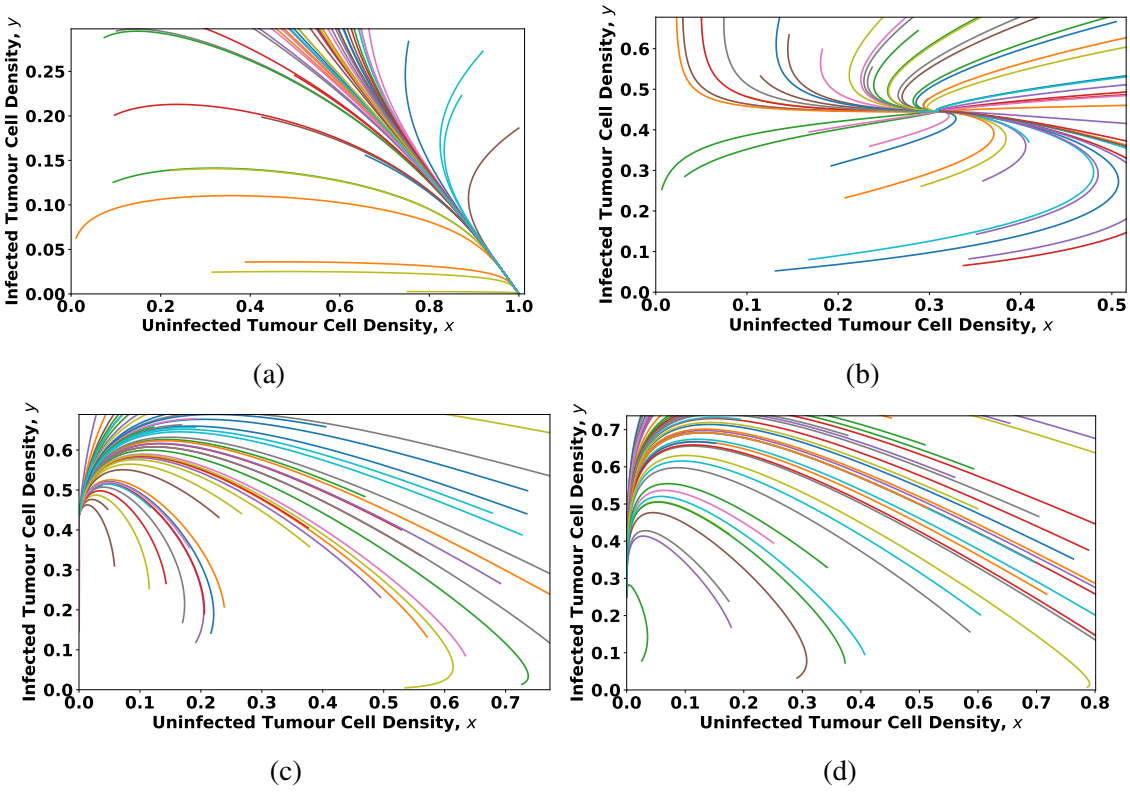

Figure 3.2: The phase portrait of system (3.12) - (3.13) when $r > \gamma$. (a) When $\theta < \alpha\gamma$, the trajectories approach the steady state $(1, 0)$ as $t \to \infty$. (b) When $\alpha\gamma < \theta < \gamma(\alpha/(r-\gamma)+1/r)$, the trajectories approach the steady state (x_*, y_*) as $t \to \infty$. (c) & (d) When $\theta > \gamma(\alpha/(r-\gamma)+1/r)$, the trajectories approach the steady state $(0, (r-\gamma)/r)$ as $t \to \infty$. In (d), the value of the parameter r is taken closer to γ than in (c), resulting in decreased density of infected tumour cells.

We numerically illustrate Theorem 3.3.3 in Figure 3.2. The phase portraits in this figure are produced by using the parameter values given in the code in Appendix A, except for the

parameters r, θ, and γ. We set $\gamma = 0.3$. In Figure 3.2 (a), we set $r = 0.5311$ and $\theta = 0.01$. In Figure 3.2 (b), we set $r = 0.5311$ and $\theta = 0.3$. In Figure 3.2 (c), we set $r = 0.5311$ and $\theta = 0.9$. In Figure 3.2 (d), we set $r = 0.4$ and $\theta = 1.4$.

Biologically, the case $\theta > \alpha\gamma$ corresponds to a low virus-induced death rate relative to the infection rate (since in practice, α is typically less than 1). This condition leads to a more clinically favourable outcome compared to the condition $\theta < \alpha\gamma$, as the uninfected tumour cell-dominant steady state becomes unstable. If we then consider the additional condition $r > \gamma$, then there exists an infected tumour cell-dominant steady, $(0, (r - \gamma)/\gamma)$, which corresponds to complete eradication of uninfected tumour cells. Biologically, this clinically favourable steady state exists when infected tumour cells can proliferate at a greater rate than they are destroyed by the virus. This (perhaps rather unintuitively) suggests that an OV should not be engineered to hinder the proliferation capability of the cancer cells and, in fact, a greater growth rate of the infected cancer cells can lead to improved clinical outcomes. The key is to minimize $(r - \gamma)/r$ while also ensuring that the infected tumour cell-dominant steady state is stable, i.e., inequality (3.20) holds. The modelling suggests that the most potent OV is one with a high infection rate, low oncolysis rate, and that minimally inhibits the proliferation rate of the cancer cells. By taking $\gamma \to r^-$, we have $y \to 0$ as $t \to \infty$ as long as θ still satisfies condition (3.20). While this might lead to the naive assumption of simply engineering a virus which has a very large infection rate compared to the proliferate rate of tumour cells, this type of OV may also be associated with increased toxicity [32], adding another layer of complexity.

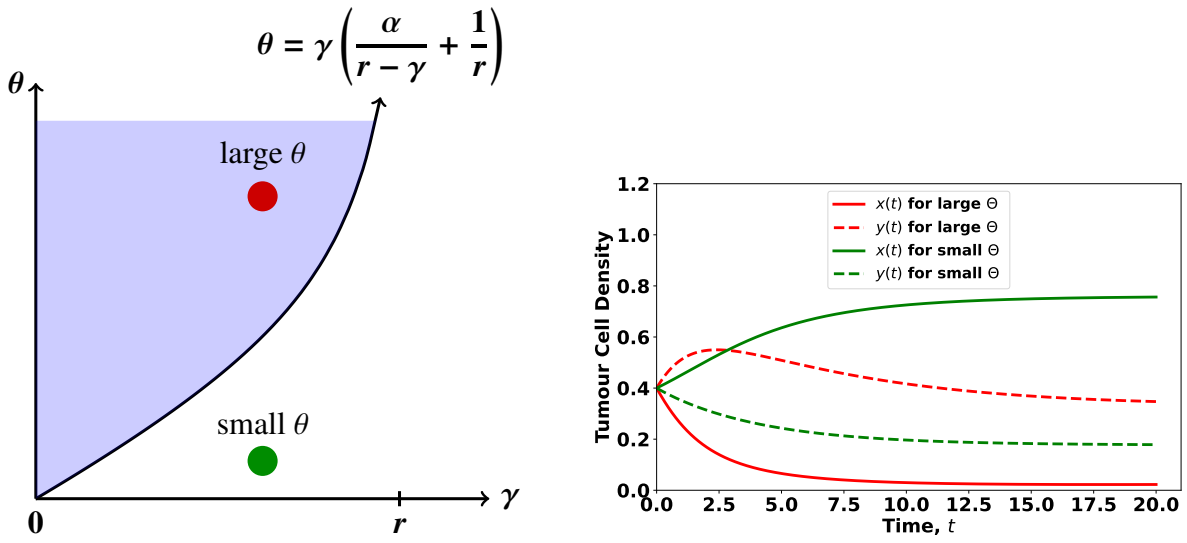

(a) (b)

Figure 3.3: (a) If the pair (γ_*, θ_*) belongs to the blue region of the $\gamma\theta$-plane, then the infected tumour cell-dominant steady state is stable. (b) The red curves are the solution curves when inequality (3.20) is satisfied. The green curves are the solution curves when the condition is not satisfied. In the latter case, the solutions converge to the positive steady state.

Figure 3.3 (a) gives guidance on how to choose the infection rate, θ, given the oncolysis rate, γ. It can be seen in Figure 3.3 (b) that if the infection rate is too small, the tumour cell densities will converge to the positive steady state. On the other hand, if θ is large enough, then all of the tumour cells are eventually infected by the virus.

We summarize the existence and stability results of this section in Table 3.1.

Table 3.1: Conditions for Existence and Stability of Steady States of System (3.12) - (3.13)

Steady State	**Existence Condition(s)**	**Global Asymptotic Stability Condition**
$(0,0)$	Always	Unstable
$(1,0)$	Always	$\theta < \alpha\gamma$
$\left(0, \frac{r-\gamma}{r}\right)$	$r > \gamma$	$\theta > \gamma\left(\frac{\alpha}{r-\gamma} + \frac{1}{r}\right)$
(x_*, y_*)	$\alpha\gamma < \theta < \gamma\left(\frac{\alpha}{r-\gamma} + \frac{1}{r}\right)$	Existence

3.3.2 Dynamics of the Local Model – Case II: Oxygen Dependence

We now perform a local stability analysis of the relevant steady states of system (3.8) - (3.10). We begin by computing the Jacobian matrix of this system,

$$J(x,y,z) = \begin{pmatrix} 1-2x-y-\dfrac{\theta(z)y}{\alpha+y} & -x-\dfrac{\alpha\theta(z)x}{(\alpha+y)^2} & -\dfrac{\theta'(z)xy}{\alpha+y} \\ -ry-\dfrac{\theta(z)y}{\alpha+y} & r-rx-2ry+\dfrac{\alpha\theta(z)x}{(\alpha+y)^2}-\gamma(z) & \dfrac{\theta'(z)xy}{\alpha+y}-\gamma'(z)y \\ -q_1z & -q_2z & -\beta-q_1x-q_2y \end{pmatrix}. \quad (3.21)$$

We first consider the simplest steady state, the *tumour-free* steady state, $(x,y,z) = (0,0,1)$. Linearizing the system about this point gives

$$J(0,0,1) = \begin{pmatrix} 1 & 0 & 0 \\ 0 & r-\gamma(1) & 0 \\ -q_1 & -q_2 & -\beta \end{pmatrix}, \quad (3.22)$$

which is a lower triangular matrix with eigenvalues $1, r-\gamma(1), -\beta$. Since this matrix will always have a positive eigenvalue, the tumour-free steady state is unstable. The maximum dimension of its stable manifold is 2, which occurs if and only if $r < \gamma(1)$. This corresponds to the fact that if the virus-induced death rate of tumour cells, γ, is sufficiently large, then there will be larger domain of initial conditions for which the solution will converge to the tumour-free steady state. Next, we consider the case where the uninfected tumour cells dominate, i.e., $x = 1$ and $y = 0$. In this case, we have the following steady state, which corresponds to the failure of OV treatment:

$$(x,y,z) = (1,0,z^*), \quad \text{where} \quad z^* := \frac{\beta}{\beta+q_1}. \quad (3.23)$$

Linearizing the system at this steady state gives

$$J(1,0,z^*) = \begin{pmatrix} -1 & -1-\dfrac{\gamma(z^*)}{\alpha} & 0 \\ 0 & \dfrac{\theta(z^*)}{\alpha}-\gamma(z^*) & 0 \\ -q_1 z^* & -q_2 z^* & -\beta-q_1 \end{pmatrix}, \tag{3.24}$$

which has eigenvalues

$$\lambda_1^u = -1, \quad \lambda_2^u = \frac{\theta(z^*)}{\alpha} - \gamma(z^*), \quad \lambda_3^u = -\beta - q_1. \tag{3.25}$$

Considering the conditions for which these eigenvalues are all negative gives the following proposition.

Proposition 3.3.2 *The tumour-dominant steady-state,* $(x, y, z) = (1, 0, z^*)$*, is locally asymptotically stable if* $\theta(z^*) < \alpha\gamma(z^*)$.

From a clinical perspective, the local asymptotic stability of the tumour-dominant steady-state is an unfavourable result. Biologically, this occurs when the infection rate of tumour cells by the OV is too low compared to the virus-induced death rate. This leads to an important insight: engineering a virus which can destroy tumour cells at a fast rate is not useful if the infection rate is too low. It is important to have a virus which is sufficiently effective at infecting cancer cells - not just destroying them. The inequality in Proposition 3.3.2 can give an estimate on how large these rates should be for a useful OV.

We are also interested in the existence of an uninfected tumour cell-free steady, i.e., one of the form $(0, y_*, z_*)$. From system (3.8) - (3.10), it can been seen that such a solution may be determined by solving the system

$$r(1-y) - \gamma(z) = 0, \tag{3.26}$$

$$\beta(1-z) - q_2 yz = 0. \tag{3.27}$$

This system may have no solutions, one solution, or multiple solutions depending on the properties of the oncolysis function, $\gamma(z)$. Stability of this steady state is favourable and hence, we impose the additional condition $\gamma_\infty < r$ so as to ensure the existence of a positive solution of system (3.26) - (3.27). Notice that this condition is similar to the existence of the uninfected tumour cell-free steady state condition in Subsection 3.3.1. Moreover, it should also be noted that $0 \leq y_*, z_* \leq 1$.

Linearizing at $(0, y_*, z_*)$ gives the matrix

$$J(0, y_*, z_*) = \begin{pmatrix} 1 - y_* - \dfrac{\theta(z_*)y_*}{\alpha + y_*} & 0 & 0 \\ -ry_* - \dfrac{\theta(z_*)y_*}{\alpha + y_*} & -ry_* & -\gamma'(z_*)y_* \\ -q_1 z_* & -q_2 z_* & -\dfrac{\beta}{z_*} \end{pmatrix}. \tag{3.28}$$

The eigenvalues of this matrix are

$$\lambda_1^n = 1 - y_* - \frac{\theta(z_*)y_*}{\alpha + y_*}, \quad \lambda_{2,3}^n = \frac{-(\beta + y_* z_*) \pm \sqrt{(\beta + r y_* z_*)^2 - 4z_*(\beta r y_* - \gamma'(z_*) q_2 y_* z_*^2)}}{2z_*}.$$

It is clear that all of these eigenvalues have no imaginary part. Hence, $(0, y_*, z_*)$ is either a stable node or a three-dimensional saddle. The former case is preferable, as all tumour cells will eventually be infected as $t \to \infty$. This occurs when the eigenvalues are all negative, leading to the following proposition.

Proposition 3.3.3 *Consider the steady state* $(0, y_*, z_*)$*, where* y_* *and* z_* *satisfy the equations*

$$\gamma(z_*) = r\left(1 + \frac{\beta}{q_2} - \frac{\beta}{q_2 z_*}\right), \quad y_* = \frac{\beta}{q_2} \cdot \frac{1 - z_*}{z_*}. \tag{3.29}$$

If $\gamma_\infty < r$*, then such* y_* *and* z_* *exist and* $0 \leq y_* \leq 1$*,* $\beta/(\beta + q_2) \leq z_* \leq 1$*. Moreover, the steady*

state $(0, y_*, z_*)$ *is locally asymptotically stable if and only if*

$$\theta(z_*) > \frac{(1-y_*)(\alpha+y_*)}{y_*} \quad \textit{and} \quad \gamma'(z_*) < \frac{\beta r}{q_2 z_*^2}. \tag{3.30}$$

Remark 3.3.1 *The condition* $\gamma_\infty < r$ *is a sufficient condition for the existence of the steady state* $(0, y_*, z_*)$*. A necessary and sufficient condition for the existence of this steady state is* $\gamma_\infty < r(1+\beta/q_2)$*. The latter condition, however, does not guarantee that* $z_* \leq 1$*.*

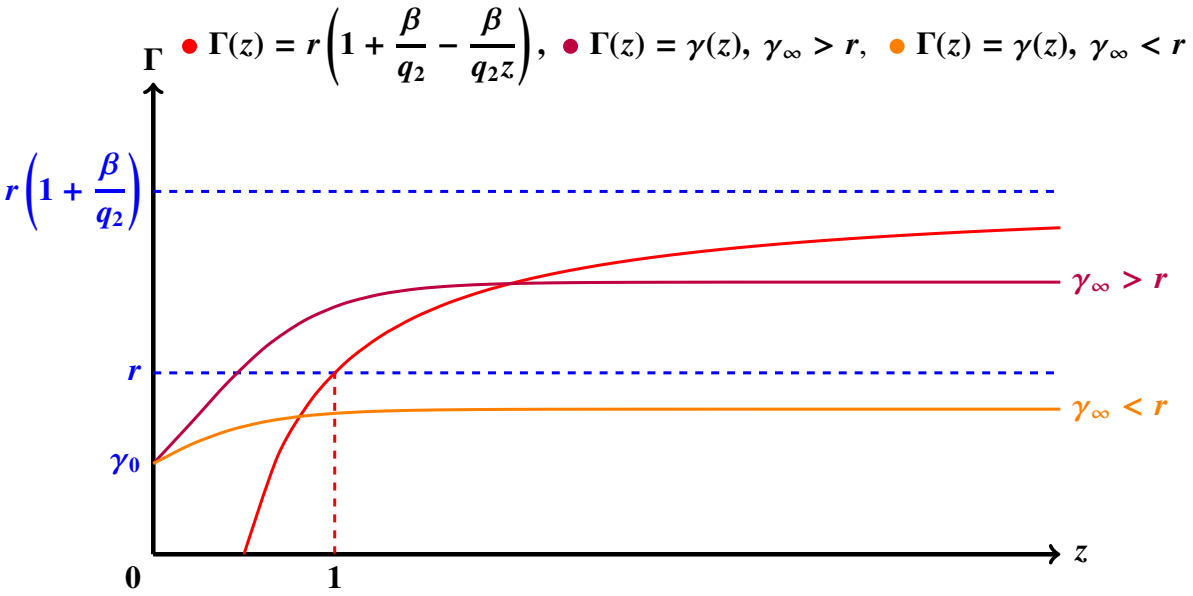

Figure 3.4: The z-coordinate of the intersection of the red curve with the purple curve gives the oxygen concentration at the steady state, z_*, if $r < \gamma_\infty < r(1+\beta/q_2)$. The intersection of the red curve with the orange curve gives this steady state if $\gamma_\infty < r$. This latter case guarantees $z_* < 1$. Note that the equation of the red curves comes from (3.29) in Proposition 3.3.3.

Proposition 3.3.3 gives some important conditions for constructing an effective OV. The condition $\gamma_\infty < r$, similarly to Subsection 3.3.1, gives a sufficient existence condition. The first stability condition is consistent with our previous results: namely, a sufficiently large infection rate is an important factor of OV efficacy. The second stability condition is perhaps

more interesting: an oncolysis rate which grows *slowly* in response to increases in oxygen concentration of the tumour microenvironment.

We now consider system (3.8) - (3.10) under certain parameter conditions and establish a global stability result concerning the tumour-dominant steady state, $(1, 0, z^*)$. In particular, we consider the case $q_1 = 0$ for the sake of mathematical tractability. Biologically, this corresponds to tumour cells which are unable to consume oxygen. While this condition does not typically represent a biologically realistic situation, it may be considered a *best-case scenario*, as less oxygen is consumed and therefore, more oxygen is available to increase the efficacy of the OV.

We begin by proving an auxiliary result for which we do not need the assumption $q_1 = 0$. Consider the following region in the positive octant in $\mathbb{R}^3$:

$$\mathcal{U} := \left\{(x, y, z) \in \mathbb{R}^3 : x \geq 0,\ y \geq 0,\ x + y \leq 1,\ 0 \leq z \leq 1\right\} \tag{3.31}$$

The idea is to show that this region defines a so-called *trapping region* from which no solution trajectories of system (3.8) - (3.10) may exit. We state this in the following lemma.

Lemma 3.3.1 *The region $\mathcal{U} \subset \mathbb{R}^3_+$ is a positively invariant set for system (3.8) - (3.10).*

Proof Let $(x(t), y(t), z(t))$ denote a solution of system (3.8) - (3.10) with initial condition in $\mathcal{U}$. Proving this lemma is equivalent to showing that $\mathcal{U}$ defines a trapping region for all $t \geq 0$. First note that by Theorem 3.3.1, $x(t), y(t), z(t) \geq 0$ for all $t \geq 0$. If the trajectory were to exit the region, then by continuity, it would cross either the $z = 1$ boundary or the plane $x + y = 1$ at some time t^*. Assume that the trajectory crosses $z = 1$ at time t^*. Then from equation (3.10), $z'(t^*) = -q_1 x - q_2 y \leq 0$. Therefore, the vector field at this boundary point does not point in the positive z direction, contradicting the assumption since the trajectory may not exit through the $z = 1$ plane. Hence, we have shown that $z \leq 1$.

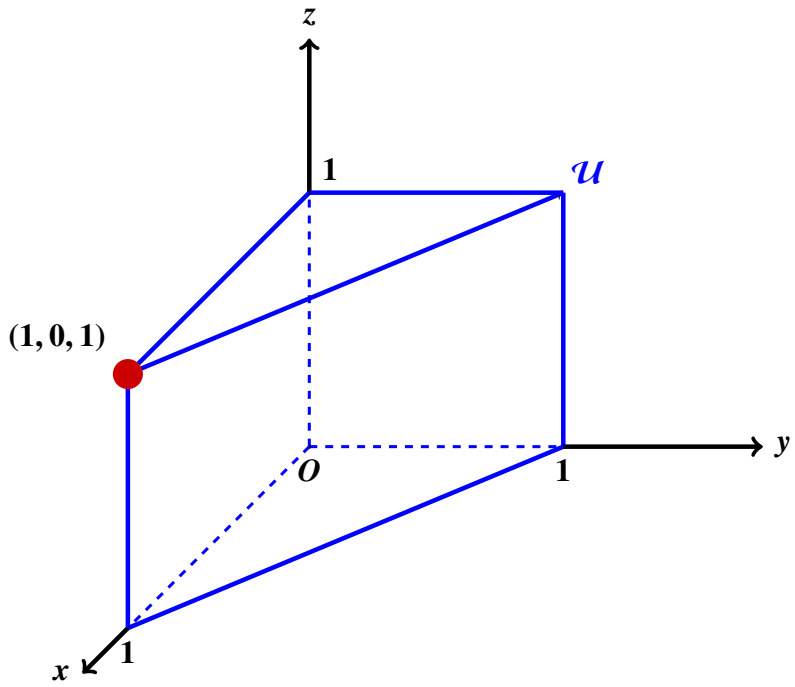

Figure 3.5: The trapping region $\mathcal{U}$. When $q_1 = 0$, all solutions of system (3.8) - (3.10) with initial conditions in this region converge to the steady state $(x, y, z) = (1, 0, 1)$ as $t \to \infty$.

Now we need only establish that no trajectory may exit the region through the plane $x + y = 1$. We do this by showing that the vector field on this plane points into the region $\mathcal{U}$. On the plane $x + y = 1$, the sum of equations (3.8) and (3.9) is

$$\begin{aligned}\frac{\mathrm{d}}{\mathrm{d}t}[x(t) + y(t)] &= (x + ry)(1 - x - y) - \gamma(z)y \\ &= (x + ry)(0) - \gamma(z)y < 0.\end{aligned}$$

Hence, $y'(t) < -x'(t)$ which implies that, by the chain rule, $\mathrm{d}y/\mathrm{d}x < -1$. Therefore, the vector field on the plane $x + y = 1$ points into the region and no trajectory may exit through this plane. We conclude that no trajectory contained in the region $\mathcal{U}$ may exit this region, completing the proof. ∎

We are now in a position to give the theorem on global stability of the steady state $(1, 0, z^*)$. Since we consider the case $q_1 = 0$, we have $z^* = \beta/(\beta + q_1) = 1$. Hence, the steady state

becomes $(1, 0, 1)$. We then have the following theorem:

Theorem 3.3.4 *Consider system (3.8) - (3.10) when $q_1 = 0$ and $q_2 > 0$. If $\theta(z) < \alpha\gamma(z)$ for $z \in [0, 1]$, then $(x, y, z) = (1, 0, 1)$ is globally asymptotically stable on $\mathcal{U}$.*

Proof Since $[0, 1]$ is a compact interval, we can choose $\varepsilon \in (0, 1)$ such that $\theta(z) < \varepsilon\alpha\gamma(z)$ for all $z \in [0, 1]$. Define the function $V : \text{Int}\,\mathcal{U} \cup \{(1, 0, 1)\} \to \mathbb{R}$ as

$$V(x, y, z) := x - \ln(x) - 1 + y + \frac{(1-\varepsilon)\gamma_0}{2q_2}\left[z - \ln(z) - 1\right]. \tag{3.32}$$

We can show that V defines a Lyapunov function. V is positive definite as $V(1, 0, 1) = 0$ and $V(x, y, z) > 0$ for all $(x, y, z) \in \text{Int}\,\mathcal{U}$. Taking the time derivative of V gives

$$\begin{aligned}
\frac{\mathrm{d}V}{\mathrm{d}t} &= \left(\frac{x-1}{x}\right)\left[x(1-x-y) - \frac{\theta(z)xy}{\alpha+y}\right] + ry(1-x-y) + \frac{\theta(z)xy}{\alpha+y} - \gamma(z)y + \left(\frac{z-1}{z}\right)[\beta(1-z) - q_2yz] \\
&= -(1-x-ry)(1-x-y) - \frac{\theta(z)y(x-1)}{\alpha+y} + \frac{\theta(z)xy}{\alpha+y} - \gamma(z)y + \frac{(1-\varepsilon)\gamma_0}{2q_2}\left[-\frac{\beta}{z}(1-z)^2 - q_2y(z-1)\right] \\
&= -(1-x-ry)(1-x-y) + \frac{\theta(z)y}{\alpha+y} - \varepsilon\gamma(z)y - (1-\varepsilon)\gamma(z)y + \frac{(1-\varepsilon)\gamma_0}{2q_2}\left[-\frac{\beta}{z}(1-z)^2 - q_2y(z-1)\right] \\
&\leq -(1-x-ry)(1-x-y) + \frac{[\theta(z) - \varepsilon\alpha\gamma(z)]y}{\alpha+y} - (1-\varepsilon)\gamma(z)y + \frac{(1-\varepsilon)\gamma_0 y}{2}.
\end{aligned}$$

Note that $\dot{V}(1, 0, 1) = 0$. Next, since $r < 1$ and $x+y \leq 1$ by Lemma 3.3.1, we have $1-x-ry \geq 0$. Hence, $-(1-x-ry)(1-x-y) \leq 0$. By our assumption, it follows that $\theta(z) - \varepsilon\alpha\gamma(z) < 0$ since z remains in $[0, 1]$ by Lemma 3.3.1. Finally, since $\gamma(z) \geq \gamma_0$, it holds that

$$-(1-\varepsilon)\gamma(z)y + \frac{(1-\varepsilon)\gamma_0 y}{2} < 0.$$

Therefore, $\dot{V} < 0$ on $\text{Int}\,\mathcal{U}$. By LaSalle's invariance principle, we conclude that the tumour-dominant steady state $(x, y, z) = (1, 0, 1)$ is globally asymptotically stable. ∎

Remark 3.3.2 *Theorem 3.3.4 assumes that q_2 is a positive constant. If $q_2 = 0$, establishing global stability is trivial as equations (3.8) and (3.9) are decoupled from equation (3.10) and global asymptotic stability of the tumour-dominant steady state of the resulting two-variable system follows from Theorem 3.3.2.*

As previously stated, the condition $q_1 = 0$ in Theorem 3.3.4 biologically represents a best-case scenario in which the uninfected tumour cells are unable to consume oxygen, leading to a more effective adenovirus due to increased oxygen concentration in the tumour microenvironment. In practice $\alpha < 1$ and so the condition $\theta(z) < \alpha\gamma(z)$ reflects a virus which has a significantly larger oncolysis rate compared to its infection rate. This is analogous to the condition required in Theorem 3.3.2, providing further evidence that a very high oncolysis rate is not a favourable characteristic of an oncolytic adenovirus.

While we do not analytically consider the case $q_1 > 0$, the numerical simulations in Section 3.4 lead us to conjecture that the steady state $(1, 0, z^*)$ remains globally asymptotically stable in this case, under the condition $\theta(z) < \alpha\gamma(z)$.

It is clear that the relationship between the functions $\theta(z)$ and $\gamma(z)$ is an important factor in the dynamics of the system. Biologically, if the infection rate is too low relative to the virus-induced death rate, infected tumour cells may die faster than they are able to infect a sufficient number of uninfected cells, hence leading to an uninfected tumour cell-dominant steady state. On the other hand, if the virus-induced death rate is too low, not enough tumour cells will die for the OV to be an effective therapeutic agent. The interplay between these functions and their effect on the OV efficacy is one of the topics of the next section.

3.4 Numerical Simulations: Local Model

In this section, we perform numerical simulations of the local model. We perform the simulations using system (3.1) - (3.3). The units of u and n are cells/mm^3 and the units of c are millimolars (mM). Unless otherwise stated, we set the initial conditions to be $u_0 = 10000$ and $n_0 = 100$, as in [22]. Similarly to [35], we set $c_0 = 4.3751$.

Table 3.2: Local Model Parameters

Parameter	Parameter Name	Value	Reference
r_1	Growth Rate of Uninfected Tumour Cells	0.3954 day^{-1}	[7]
r_2	Growth Rate of Infected Tumour Cells	0.21 day^{-1}	Estimated ($r_2 < r_1$)
K	Tumour Carrying Capacity	1.0×10^6 cells/mm^3	[22]
α	Hill Constant	1.0×10^5 cells/mm^3	[22]
ϕ	Oxygenation Rate	1.0×10^4 mM day^{-1}	[35]
β	Oxygen Consumption Rate of Healthy Surrounding Cells	5.0976 day^{-1}	[19]
q_1	Oxygen Consumption Rate of Uninfected Tumour Cells	5.47×10^{-5} mm^3 cells^{-1} day^{-1}	[23]
q_2	Oxygen Consumption Rate of Infected Tumour Cell	2.735×10^{-5} mm^3 cells^{-1} day^{-1}	[23]
γ	Virus-Induced Death Rate	0.5115 day^{-1}	[22]
θ	Infection Rate	1.0 day^{-1}	[22]

Table 3.2 gives the parameters value which we use in the case where γ and θ are constants, rather than functions of oxygen concentration. In this case, plotting the tumour cell densities gives Figure 3.6. If we consider this to be the standard case, we can test the effect of including oxygen dependence of the functions θ and γ.

In our simulations, we set θ and γ to be sigmoid functions of c. In particular, we have

$$\theta(c) = \frac{\theta_\infty \theta_0}{\theta_0 + (\theta_\infty - \theta_0)e^{-k_\theta c}}, \quad \gamma(c) = \frac{\gamma_\infty \gamma_0}{\gamma_0 + (\gamma_\infty - \gamma_0)e^{-k_\gamma c}}. \tag{3.33}$$

We consider how different parameter values $\theta_0, \theta_\infty, \gamma_0, \gamma_\infty, k_\theta, k_\gamma$ impact the efficacy of the OV. Guided by Proposition 3.3.2, we choose these parameters such that we consider $\theta(c) < (\alpha/K)\gamma(c)$, $\theta(c) > (\alpha/K)\gamma(c)$, etc. We plot these results in Figures 3.6 - 3.11.

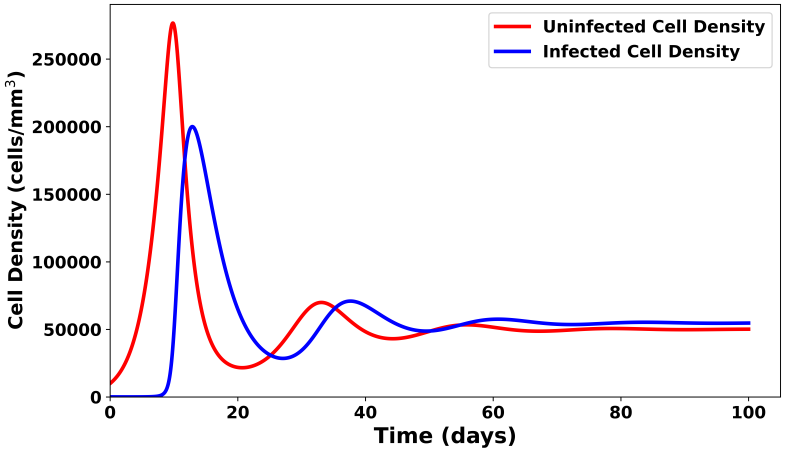

Figure 3.6: Tumour cell density dynamics: constant θ and γ

In Figure 3.6, we consider the case in which θ and γ are the constants given in Table 3.2 rather than functions of the oxygen concentration. This is our first numerical exposure to a result which will be echoed throughout this subsection: higher infection rates relative to virus-induced death rates tend to lead to more favourable clinical results. In this case, the tumour cell densities both settle to a steady state well below the carrying capacity, suggesting some inhibition of the growth of the tumour cells.

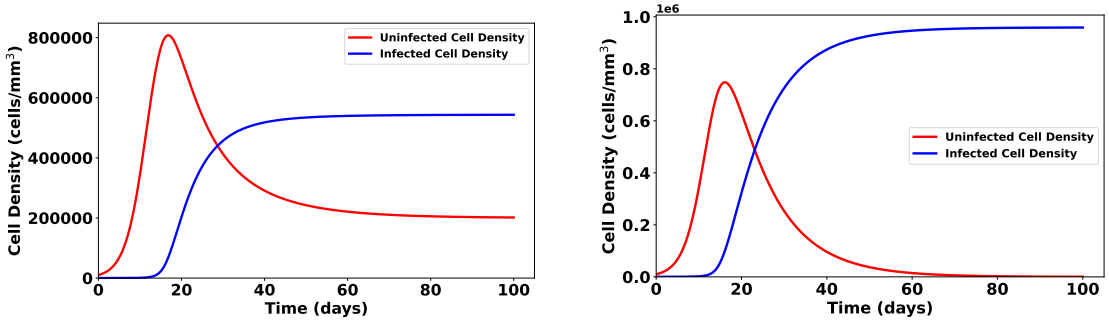

(a) (b)

Figure 3.7: Tumour cell density dynamics in the case where $\theta(c) > (\alpha/K)\gamma(c)$ for all $c \geq 0$. (a) In this case, we have $\theta_0 = 0.1, \theta_\infty = 0.12, k_\theta = 0.08, \gamma_0 = 0.05115, \gamma_\infty = 0.09115, k_\gamma = 0.08$. The infected tumour cells dominate in the long run. This represents a relatively favourable response to the oncolytic virotherapy. (b) In this case, we have $\theta_0 = 0.1, \theta_\infty = 0.12, k_\theta = 0.08, \gamma_0 = 0.005115, \gamma_\infty = 0.009115, k_\gamma = 0.008$. When the virus-induced death rate is too low, infected cells still dominate but will ultimately approach a larger value at the steady state compared to the previous case.

In Figure 3.7, we have the case of a high infection rate relative to the virus-induced death rate. The assumption of Proposition 3.3.2 is not satisfied and, unsurprisingly, the uninfected cell density is driven below the infected cell density, asymptotically. This case potentially represents a favourable result since in Figure 3.7 (a), as the tumour cell density approaches a positive stable steady state value below the carrying capacity. In particular, the uninfected tumour cell density remains significantly lower than the infected tumour cell density. This illustrates the importance of the infection rate being sufficiently large. On other hand, as in Figure 3.7 (b), having the virus-induced death rate be *too low* leads to an unfavourable result in which all the tumour cells are infected but they nevertheless approach a value *near* the carrying capacity – note that they do not approach the carrying capacity in the case depicted by the figure. This illustrates the delicate balance between viral infection and virus-induced mortality. Furthermore, we note the differences between Figure 3.7 and Figure 3.6: In both cases, $\theta > (\alpha/K)\gamma$, yet the dynamics are qualitatively different. This difference is a result of Figure 3.7 depending on oxygen concentration; a consideration not made in Figure 3.6.

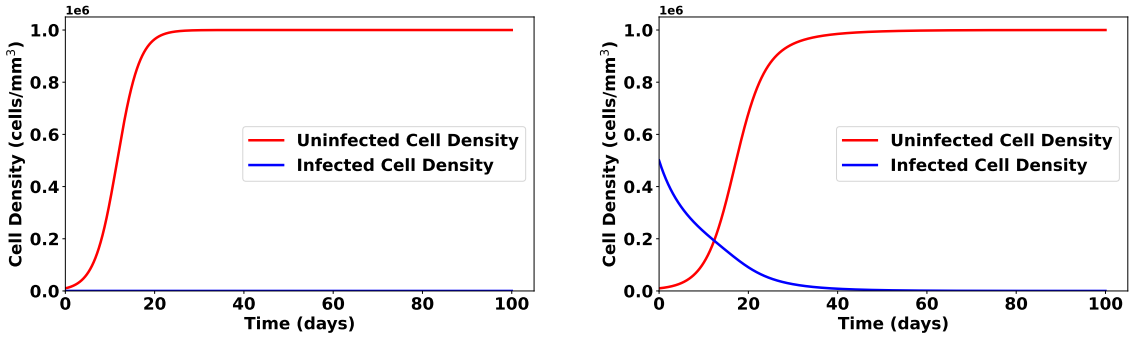

(a) (b)

Figure 3.8: Tumour cell density dynamics in the case where $\theta(c) > (\alpha/K)\gamma(c)$ for $0 \leq c < c^*$ and $\theta(c) < (\alpha/K)\gamma(c)$ for $c > c^*$. In this case, we have $\theta_0 = 0.01, \theta_\infty = 0.012, k_\theta = 0.008, \gamma_0 = 0.05115, \gamma_\infty = 0.2115, k_\gamma = 0.08$. (a) $n_0 = 100$. (b) $n_0 = 0.5 \times 10^6$.

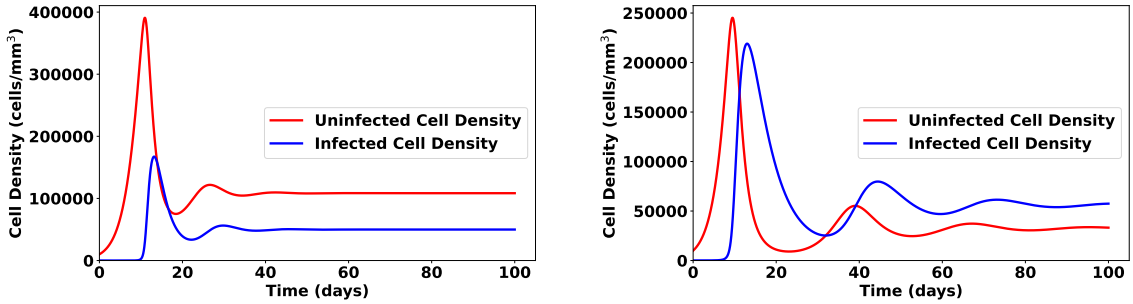

(a) (b)

Figure 3.9: Tumour cell density dynamics in the case where $\theta(c) < (\alpha/K)\gamma(c)$ for $0 \leq c < c^*$ and $\theta(c) > (\alpha/K)\gamma(c)$ for $c > c^*$. In this case, we have $\theta_0 = 5.115 \times 10^{-3}, \theta_\infty = 1.0, k_\theta = 0.08$ (a) $\gamma_0 = 0.7, \gamma_\infty = 0.9, k_\gamma = 0.08$. (b) $\gamma_0 = 0.2, \gamma_\infty = 0.4, k_\gamma = 0.08$.

On the other hand, Figure 3.8 shows a clinically unfavourable result. Namely, the uninfected tumour cell density approaches the carrying capacity value while the infected tumour cells die out. In this case, treatment via OV has failed. This occurs when the θ and $(\alpha/K)\gamma$ curves intersect at some oxygen value, c^*. The outcome of the numerics, in this case, directly follows from Proposition 3.3.2. Regardless of the initial density of OV injection, n_0, (i.e., Figure 3.8 (a) vs. Figure 3.8 (b)) the asymptotic behaviour is the same. Biologically, this gives the following insight: in hypoxic environments, having very low lysis capabilites of the OV yields failure of the treatment regardless of initial density of the OV injection. It is worthwhile to note that the z^* from the steady state considered in Proposition 3.3.2 is **NOT** related to the quantity c^*, the c-coordinate of the intersection point of θ and γ.

Figure 3.9 represents the reverse case of Figure 3.8, in which the inequalities are reversed are the results are clinically more favourable. This once again illustrates the importance of the virus-induced death rate in hypoxic environments and also shows the importance of the infection rate in oxygen-rich environments. Moving from Figure 3.9 (a) to Figure 3.9 (b), the virus-induced death rate is decreased, while still maintaining a high viral infection rate in oxygen-rich conditions. Once again, this reflects that an oncolysis rate that is too large can lead to clinically unfavourable outcomes as tumour cells are killed faster than the virus may use them to replicate. This further supports the idea of achieving a balance between infection

rates and oncolysis capacity as an OV engineering consideration.

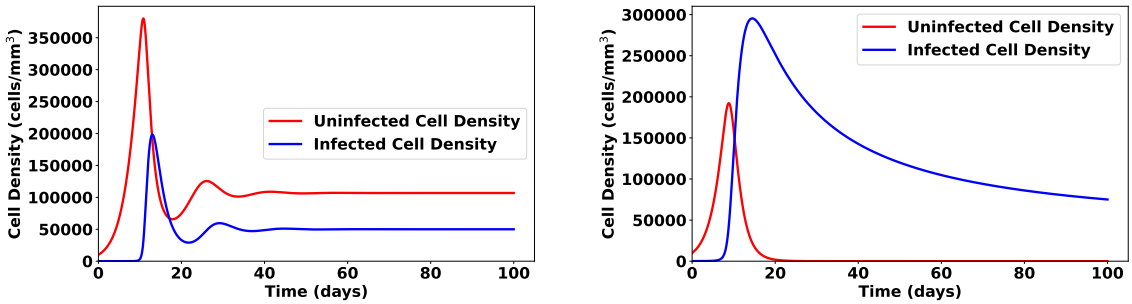

Figure 3.10: Tumour cell density dynamics in the case where $\theta(c) < (\alpha/K)\gamma(c)$ for $0 \leq c < c^*$ and $\theta(c) > (\alpha/K)\gamma(c)$ for $c > c^*$. In this case, we have $\gamma_0 = 0.1, \gamma_\infty = 0.9, \theta_0 = 5.115 \times 10^{-3}, \theta_\infty = 1.0, k_\theta = 0.08$. (a) $k_\gamma = 0.008$. (b) $\gamma_0 = 0.09, \gamma_\infty = 0.2, k_\gamma = 0.01$.

In Figure 3.10, for low values of oxygen concentration (i.e., hypoxic environments) the infection rate is significantly less than the virus-induced death rate, whereas for high values of oxygen concentration, the virus-induced death rate is reduced. The figure shows that this case also represents a favourable clinical outcome represented by the dampening oscillations in Figure 3.10 (a). Asymptotically, the tumour cell density approaches a positive steady state value well below the carrying capacity. This (once again) suggests the following insight: in hypoxic environments, it is important that the OV is more efficient at killing cancer cells than infecting them. However, if the oxygen concentration should be large, the OV must be more efficient at infecting tumour cells than inducing their death. In Figure 3.10 (b), we decrease the growth rate of the $\gamma(c)$ function, leading to near-extinction of all tumour cells. Biologically, this represents an OV which has greater tumour-destroying capabilities over a lesser range of lower oxygen concentrations. Another interpretation is that it would be favourable for the infection rate to surpass the virus-induced death rate at lesser oxygen concentrations as long as the virus-induced death rate does initially dominates under *extremely* hypoxic conditions. Such a virus must be engineered to initially be extremely potent at destroying tumour cells when there is almost no oxygen available in the tumour microenvironment but must quickly be able to adapt by having a much greater infection rate if the available oxygen concentration should increase.

These results are consistent with Proposition 3.3.3.

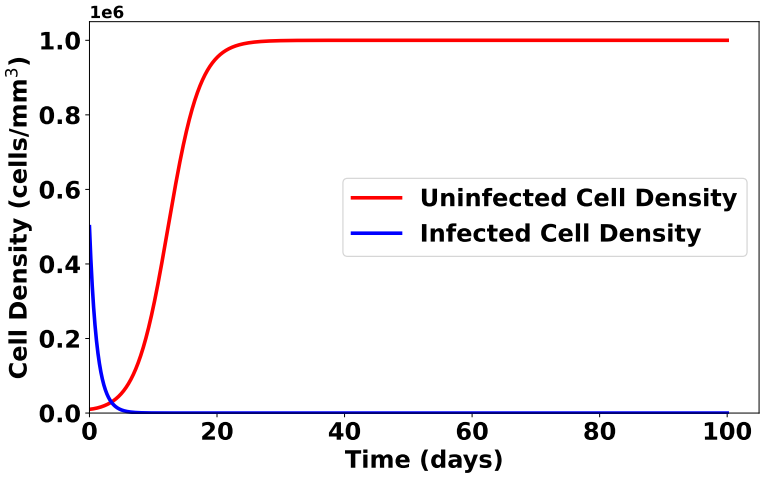

Figure 3.11: Tumour cell density dynamics in the case where $\theta(c) < (\alpha/K)\gamma(c)$ for all $c \geq 0$. In this case, we have $\gamma_0 = 0.3, \gamma_\infty = 1.0, k_\gamma = 0.8, \theta_0 = 0.005115, \theta_\infty = 0.02115, k_\theta = 0.8$. In this case, the virus-induced death rate is significantly greater than the infection rate. In this case, we set $n_0 = 0.5 \times 10^6$.

Figure 3.11 shows the case where the infection rate is very low compared to the virus-induced death rate. In this case, the uninfected tumour cell density dominates and approaches the carrying capacity. This result agrees with Proposition 3.3.2. This further supports the idea of a delicate balance between how effective the virus is at infected cancer cells and how potent the virus is at inducing death of tumour cells. In particular, we must ensure that the death rate is not too large compared to the infection rate.

These cases illustrate the following point which must be considered when engineering the OV: Having a virus too efficient at destroying and not efficient enough at infecting is not recommended. Perhaps equally importantly, we must also consider the oxygen conditions (i.e., hypoxia) when engineering the OV as the functionality of the virus also depends on whether or not the tumour microenvironment is hypoxic.

3.5 Regional Oncolytic Virotherapy Model

In this section, we extend our model to the regional setting by considering the case of lymph node invasion by the tumour cells. As the thickness of the melanoma tumour increases, there is an increased probability of the tumour spreading to nearest lymph nodes [5]. We model a network of lymph nodes as a one-dimensional lattice, where each node represents a lymph node and the edges represent lymphatic vessels.

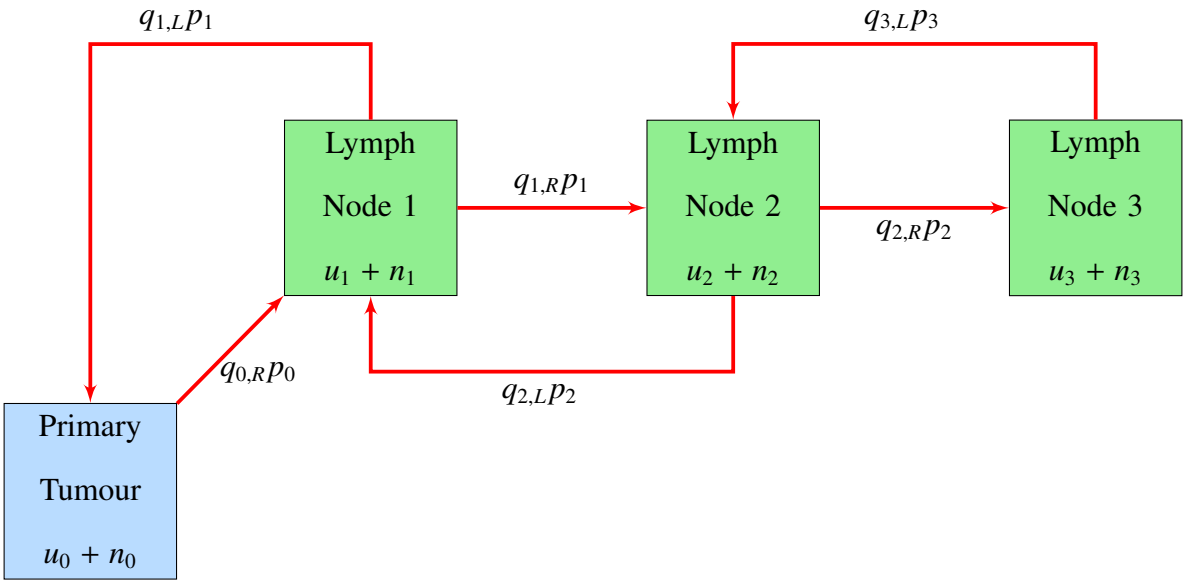

Figure 3.12: The first three lymph nodes in a network. Each lymph node represents a different node (green) in the lattice. The tumour cells begin in the primary tumour (blue) and can travel through the lymphatic network, with some rate of spreading which depends on the tumour cell density.

The initial concentration of tumour cells at each node is set to 0. Let i denote the i^{th} node from the primary tumour for $i = 1, 2, 3, \ldots, \ell$ and let $i = 0$ denote the primary tumour. That is, $i = 0$ corresponds to the local case presented in Section 3.2. Note that u_0, n_0 and c_0 no longer represent initial conditions, but rather the primary tumour. The tumour cells may either travel to the left or to the right of their current position. We assume that the probability of tumour cells spreading to the adjacent lymph nodes depends on the density of the tumour cells at the given node and, hence, on the sum $u_i(t) + n_i(t)$. Let $P_i(u_i + n_i)$ be the spreading rate of some fraction of tumour cells away from node i to an adjacent lymph node in the network. This

fraction of cells which leaves a given node is dependent on the tumour cell density at the given node i.e., $u_i(t) + n_i(t)$.

The probability of the cells travelling left is $q_{i,L}$ and the probability of travelling right is $q_{i,R}$, where $q_{i,L} + q_{i,R} = 1$ for $i = 1, 2, \ldots, \ell - 1$. Moreover, $q_{0,R} = 1$. While it has been observed that lymph typically flows only in one direction [40], we allow for the possibility of some tumour cells to travel in the reverse direction. We assume that the probability of tumour cells reversing direction is low and therefore, we consider $q_{i,R} >> q_{i,L}$ in the numerical simulations.

On each node in the network, we have a system of ODEs which describes the number of tumour cells and the oxygen concentration. We use system (3.8) - (3.10) to model the dynamics of the tumour cells at each individual node. To this end, we propose the following system:

$$\frac{\mathrm{d}u_0}{\mathrm{d}t} = r_1 u_0 \left(1 - \frac{u_0 + n_0}{K_0}\right) - \frac{\theta(c_0) n_0 u_0}{\alpha_0 + n_0} - q_{0,R} P_0 u_0 + q_{1,L} P_1 u_1, \tag{3.34}$$

$$\frac{\mathrm{d}n_0}{\mathrm{d}t} = r_2 n_0 \left(1 - \frac{u_0 + n_0}{K_0}\right) + \frac{\theta(c_0) n_0 u_0}{\alpha_0 + n_0} - \gamma(c_0) n_0 - q_{0,R} P_0 n_0 + q_{1,L} P_1 n_1, \tag{3.35}$$

$$\frac{\mathrm{d}u_i}{\mathrm{d}t} = r_1 u_i \left(1 - \frac{u_i + n_i}{K_i}\right) - \frac{\theta(c_i) n_i u_i}{\alpha_i + n_i} + q_{i-1,R} P_{i-1} u_{i-1} + q_{i+1,L} P_{i+1} u_{i+1} - P_i u_i, \tag{3.36}$$

$$\frac{\mathrm{d}n_i}{\mathrm{d}t} = r_2 n_i \left(1 - \frac{u_i + n_i}{K_i}\right) + \frac{\theta(c_i) n_i u_i}{\alpha_i + n_i} - \gamma(c_i) n_i + q_{i-1,R} P_{i-1} n_{i-1} + \ldots$$

$$\cdots + q_{i+1,L} P_{i+1} n_{i+1} - P_i n_i, \tag{3.37}$$

$$\frac{\mathrm{d}u_\ell}{\mathrm{d}t} = r_1 u_\ell \left(1 - \frac{u_\ell + n_\ell}{K_\ell}\right) - \frac{\theta(c_\ell) n_\ell u_\ell}{\alpha_\ell + n_\ell} + q_{\ell-1,R} P_{\ell-1} u_{\ell-1} - q_{\ell,L} P_\ell u_\ell, \tag{3.38}$$

$$\frac{\mathrm{d}n_\ell}{\mathrm{d}t} = r_2 n_\ell \left(1 - \frac{u_\ell + n_\ell}{K_\ell}\right) + \frac{\theta(c_\ell) n_\ell u_\ell}{\alpha_\ell + n_\ell} - \gamma(c_\ell) n_\ell + q_{\ell-1,R} P_{\ell-1} n_{\ell-1} - q_{\ell,L} P_\ell n_\ell, \tag{3.39}$$

$$\frac{\mathrm{d}c_k}{\mathrm{d}t} = \phi_k - \beta c_k - q_1 u_k c_k - q_2 n_k c_k, \tag{3.40}$$

where $i = 1, 2, 3, \ldots, \ell - 1$, $k = 0, 1, 2, 3, \ldots, \ell$, and $P_k := P_k(u_k + n_k)$. Note that ℓ is the number of lymph nodes in the network. We set $\phi_0 = \phi$ and $\phi_k = 0$ for $k = 1, 2, 3, \ldots, \ell$ for the purpose of following an individual over the course of treatment. The amount of time which tumour

cells spend in compartment i, in the case of a large density of tumour cells in the compartment, is $1/\eta_i$, in days. We may therefore consider η_i to give a per capita *spreading speed* of tumour cells *away* from compartment i. We assume that the speed with which tumour cells travel to the next node is equal to the speed with which they travel to the previous node. In practice, $q_{i,R} \approx 1$ and $q_{i,L} \approx 0$, so this assumption is not typically needed. It will be necessary for the purpose of tractability of the subsequent mathematical analysis. In this chapter, we only consider the case of a linear lymphatic network.

With all these considerations, the spreading rate of tumour cells leaving the lymph node and spreading to adjacent nodes is given by

$$P_i(x) = \eta_i \left[1 - e^{-\lambda_i x}\right], \quad \lambda_i > 0. \tag{3.41}$$

The rationale behind defining P_i in such a way is based on experimental results relating the size of a primary lesion to the probability of the cancer reaching the sentinel lymph nodes. See, for example, [5]. For the purpose of simulations, we assume that once the carrying capacity is reached, the probability of spreading is 0.7. Hence, we take $(1/\eta_i)P_i(K_i) = 0.7$ and solve this equation to determine the value λ_i to be $\lambda_i = -\ln(0.3)/(K_i)$.

We can show that the regional model is also well-posed in the sense of existence, uniqueness, non-negativity of the solution of the corresponding initial value problem with non-negative initial conditions, and boundedness of solutions. We summarize this result in the following theorem.

Theorem 3.5.1 *There exists a unique solution of the initial value problem (3.34) - (3.40), with non-negative initial conditions, which remains non-negative and bounded for all $t \geq 0$.*

Proof Existence and unqiueness of solutions follow directly from the fundamental theory of ODEs. To address the non-negativity of solutions, we apply Theorem 2.1 in Chapter 5 of [33].

Let $(u_0(t), n_0(t), u_1(t), n_1(t), \ldots u_\ell(t), n_\ell(t), c_0(t), c_1(t), \ldots, c_\ell(t)) \in \mathbb{R}^{3\ell+3}$ be the solution of the initial value problem consisting of system (3.34) - (3.40) with non-negative initial con-

ditions. We begin by showing that none of the components $u_0, u_1, \ldots, u_\ell$ become negative. Assume to the contrary that at some time, t^*, at least one of the components of the solution becomes negative. By continuity, these components must first cross 0. If u_0 is one of these components, then plugging in $u_0 = 0$ into equation (3.34) gives

$$\frac{\mathrm{d}u_0}{\mathrm{d}t} = q_{1,L} u_1 P_1(u_1 + n_1) \geq 0,$$

which implies that u_0 is non-decreasing at $t = t^*$. Therefore, u_0 cannot become negative, leading to a contradiction. The same argument can be used to show that none of the u_i components may become negative.

Similarly, this contradiction argument can be used to conclude the non-negativity of n_i for $i = 0, 1, 2, \ldots, \ell$.

Finally, it can be seen that for $k = 0, 1, 2, \ldots, \ell$, equation (3.40) gives

$$c_k(t) = c_k(0) \exp\left[- \int_0^t \beta + q_1 u_k(s) + q_2 n_k(s) \mathrm{d}s \right] + \phi_k \int_0^t \exp\left[- \int_s^t (\beta + q_1 u_k(\xi) + q_2 n_k(\xi)) \, \mathrm{d}\xi \right] \mathrm{d}s,$$

from which non-negativity of $c_k(t)$ follows.

Hence, for non-negative initial conditions, $u_i(0), n_i(0), c_i(0) \geq 0$, for $i = 0, 1, 2, \ldots, \ell$, it follows that the solution of the initial value problem remains non-negative for all $t \geq 0$.

Next, we show that solutions of the regional model remain bounded. Define $U(t) := u_0(t) + u_1(t) + \cdots + u_\ell(t)$. Then adding equations (3.34), (3.36), and (3.38) for $i = 1, 2, \ldots, \ell - 1$, gives

$$\frac{\mathrm{d}U}{\mathrm{d}t} \leq \sum_{i=0}^{\ell} r_1 u_i \left(1 - \frac{u_i}{K}\right),$$

where $K := \max_{i=0,1,\ldots,\ell}\{K_i\}$. Then,

$$\begin{aligned}\frac{\mathrm{d}U}{\mathrm{d}t} &\leq r_1\left[(u_0+u_1+\cdots+u_\ell)-\frac{u_0^2+u_1^2+\cdots+u_\ell^2}{K}\right]\\ &\leq r_1\left[(u_0+u_1+\cdots+u_\ell)-\frac{(u_0+u_1+\cdots+u_\ell)^2}{(\ell+1)K}\right].\end{aligned}$$

The last inequality follows from the Cauchy-Schwarz inequality, namely,

$$(\ell+1)(u_0^2+u_1^2+\cdots+u_\ell^2)\geq(u_0+u_1+\cdots+u_\ell)^2.$$

Hence, we have

$$\frac{\mathrm{d}U}{\mathrm{d}t}\leq r_1U\left[1-\frac{U}{(\ell+1)K}\right]\implies\limsup_{t\to\infty}U(t)\leq(\ell+1)K.$$

Therefore, the sum $U(t)$ is a bounded function. Since each component of the sum is non-negative, we conclude that each $u_i(t)$ is bounded for each $i=0,1,\ldots,\ell$.

We can similarly show that the infected tumour cells remain bounded at each node by defining $N(t) := n_0(t)+n_1(t)+\cdots+n_\ell(t)$. Adding equations (3.35), (3.37), and (3.39) for $i=1,2,\ldots,\ell-1$ gives

$$\begin{aligned}\frac{\mathrm{d}N}{\mathrm{d}t} &\leq \sum_{i=0}^{\ell}\left[r_2n_i\left(1-\frac{n_i}{K}\right)+\theta_\infty u_i\right]\\ &\leq r_2N\left[1-\frac{N}{(\ell+1)K}\right]+\theta_\infty\bar{U},\end{aligned}$$

where $\bar{U}$ is any upper bound for $U(t)$. The last inequality follows by applying the Cauchy-Schwarz inequality as in the previous case. Hence,

$$\limsup_{t\to\infty}N(t)\leq\frac{r_2(\ell+1)K+\sqrt{r_2^2(\ell+1)^2K^2+4r_2(\ell+1)K\theta_\infty\bar{U}}}{2r_2}.$$

Since the components of the sum $N(t)$ are non-negative, we conclude that $n_i(t)$ is bounded for each $i = 0, 1, \ldots, \ell$.

Next, it is clear to see by a comparison argument that

$$\limsup_{t\to\infty} c_i(t) \leq \frac{\phi_k}{\beta}, \quad i = 0, 1, 2, \ldots, \ell,$$

and so we may conclude that $c_i(t)$ are bounded.

We have successfully shown that solutions of the regional model with non-negative initial conditions are non-negative and bounded. ∎

While an analytic investigation of system (3.34) - (3.40) can be challenging to perform due to the potentially large number of equations, we may establish a result which is analogous to Proposition 3.3.2 of the local model. In particular, we may establish the a sufficiently large oncolysis rate leads to stability of a tumour-dominant steady state. We begin by showing the existence of this steady state.

Since we are also interested in obtaining results related to the spreading speed away from node i, i.e., η_i, we rewrite the function $P_i(x)$ from equation (3.41) by defining the dimensionless quantity $p_i(x) := 1 - e^{-\lambda_i x}$, hence allowing us to formulate $P_i(x)$ in terms of the spreading speed. That is,

$$P_i(x) = \eta_i p_i(x). \tag{3.42}$$

For the remainder of this subsection, we consider only the case where $\phi_k = 0$ for $k = 0, 1, 2, \ldots, \ell$. Biologically, this condition corresponds to the case with no external oxygen input. Furthermore, we consider the case where a tumour cell may only travel forward through the network (i.e., in the right, R, direction). Hence, we set $q_{j,R} = 1$ and $q_{j,L} = 0$ for $j = 0, 1, 2, \ldots, \ell$. This is biologically consistent with the unidirectional flow of tumour cells through the lymphatic system [40].

A virus-free or *uninfected tumour cell-dominant* steady state is of the form

$$E_u := (u_0, n_0, u_1, n_1, \ldots, u_\ell, n_\ell, c_0, c_1, \ldots, c_\ell) = (u_0^*, 0, u_1^*, 0, \ldots, u_\ell^*, 0, 0, 0, \ldots, 0), \tag{3.43}$$

for $i \in \{0, 1, \ldots, \ell\}$, where $u_i^* > 0$.

It follows from system (3.34) - (3.40) that the components of the tumour-dominant steady state satisfy the equations

$$\begin{cases} r_1\left(1 - \dfrac{u_0}{K_0}\right) & = \eta_0\left(1 - e^{-\lambda_0 u_0}\right), \\ r_1 u_i\left(1 - \dfrac{u_i}{K_i}\right) & = -\eta_{i-1}u_{i-1}\left(1 - e^{-\lambda_{i-1}u_{i-1}}\right) + \eta_i u_i\left(1 - e^{-\lambda_i u_i}\right), \quad i \in \{1, 2, \ldots, \ell - 1\}, \\ r_1 u_\ell\left(1 - \dfrac{u_\ell}{K_\ell}\right) & = -\eta_{\ell-1}u_{\ell-1}\left(1 - e^{-\lambda_{\ell-1}u_{\ell-1}}\right). \end{cases} \tag{3.44}$$

The existence of the solution $u_0^* < K_0$ of the first equation of system (3.44) is clear. The solutions of the remaining equations of this system may subsequently be obtained by solving for u_i^* recursively, given u_{i-1}^*.

Based on a numerical exploration of the system (see Section 3.6), we also require that $u_i^* > K_i$ for $i \in \{1, 2, \ldots, \ell\}$. It is trivial to see that this inequality holds for $i = \ell$. To ensure that this inequality is true for all other values of i, it is sufficient to consider the additional condition

$$K_i < \frac{10\eta_{i-1}}{7\eta_i}u_{i-1}^*\left(1 - e^{-\lambda_{i-1}u_{i-1}^*}\right), \quad i \in \{1, 2, \ldots, \ell - 1\}. \tag{3.45}$$

These upper bounds on K_i come from system (3.44) and from $p_i(K_i) = 7/10$. They may be obtained recursively given u_{i-1}^*.

Let $J = [J_{ij}] \in \mathbb{R}^{(3\ell+3)\times(3\ell+3)}$ be the Jacobian matrix of system (3.34) - (3.40).

We are now in a position to establish the stability of E_u. To do so, we make use of the Gershgorin Disc Theorem [39] which is stated as follows.

Lemma 3.5.1 (Gershgorin Disc Theorem [39]) *Consider an $n \times n$ matrix $A = [A_{ij}]$ in $\mathbb{C}^{n\times n}$. Define*

$$R_i := \sum_{\substack{j=1 \\ j\neq i}}^{n} \left|A_{ij}\right|, \quad |z| \text{ is the modulus of } z \in \mathbb{C}.$$

If $\lambda \in \mathbb{C}$ is an eigenvalue of A, then

$$\lambda \in \bigcup_{i=1}^{n} \{z \in \mathbb{C} : |z - A_{ii}| \leq R_i\}.$$

The circles of the form $\{z \in \mathbb{C} : |z - A_{ii}| \leq R_i\} \subset \mathbb{C}$ in Lemma 3.5.1 are also called *Gershgorin discs*. Since all eigenvalues of A are contained in these discs, we may bound the real part of these eigenvalues above by 0 by ensuring that all of the Gershgorin discs lie in the left half of the complex plane.

We use the following approach in order to find sufficient conditions for the local asymptotic stability of E_u:

1. Linearize system (3.34) - (3.40) at the steady state E_u. Let $J(E_u) = [J_{ij}(E_u)]$ denote this matrix.

2. For all i, compute R_i by adding the absolute value of all of the off-diagonal elements in row i of $J(E_u)$, as in Lemma 3.5.1.

3. Find conditions (if any) such that $\forall i \in \{1, 2, \ldots, 3\ell + 3\} : J_{ii}(E_u) + R_i < 0$. If this is possible, then all of the eigenvalues of $J(E_u)$ have negative real part and hence, E_u is locally asymptotically stable.

For notational convenience, note that system (3.34) - (3.40) may be written in the form

$$\frac{\mathrm{d}u_i}{\mathrm{d}t} = \mathcal{U}_i(u_0, n_0, u_1, n_1, \ldots, u_\ell, n_\ell, c_0, c_1, \ldots, c_\ell),$$

$$\frac{\mathrm{d}n_i}{\mathrm{d}t} = \mathcal{N}_i(u_0, n_0, u_1, n_1, \ldots, u_\ell, n_\ell, c_0, c_1, \ldots, c_\ell),$$

$$\frac{\mathrm{d}c_i}{\mathrm{d}t} = C_i(u_0, n_0, u_1, n_1, \ldots, u_\ell, n_\ell, c_0, c_1, \ldots, c_\ell),$$

where $i = 0, 1, 2, \ldots, \ell$, for appropriately defined functions $\mathcal{U}_i$, $\mathcal{N}_i$, and C_i.

We begin by noting that the diagonal elements of $J(E_u)$ are

$$J_{jj}(E_u) = \begin{cases} \left.\dfrac{\partial \mathcal{U}_i}{\partial u_i}\right|_{E_u} = r_1 - \dfrac{2r_1}{K_i}u_i^* - \eta_i\left[p_i(u_i^*) + \lambda_i u_i^* e^{-\lambda_i u_i^*}\right], & j = 2i+1, \quad i \in \{0, 1, \ldots, \ell-1\}, \\ \left.\dfrac{\partial \mathcal{N}_i}{\partial n_i}\right|_{E_u} = r_2 - \dfrac{r_2}{K_i}u_i^* + \dfrac{\theta_0 u_i^*}{\alpha_i} - \gamma_0 - \eta_i p_i(u_i^*), & j = 2i+2, \quad i \in \{0, 1, \ldots, \ell-1\}, \\ \left.\dfrac{\partial \mathcal{U}_\ell}{\partial u_\ell}\right|_{E_u} = r_1 - \dfrac{2r_1}{K_\ell}u_\ell^*, & j = 2\ell+1, \\ \left.\dfrac{\partial \mathcal{N}_\ell}{\partial n_\ell}\right|_{E_u} = r_2 - \dfrac{r_2}{K_\ell}u_\ell^* + \dfrac{\theta_0 u_\ell^*}{\alpha_\ell} - \gamma_0, & j = 2\ell+2, \\ \left.\dfrac{\partial C_i}{\partial c_i}\right|_{E_u} = -\beta - q_1 u_i^*, & j = 2\ell+3+i, \quad i \in \{0, 1, \ldots \ell\}, \end{cases}$$

To ensure that the eigenvalues lie in the left half of the complex plane, it is sufficient to find conditions such that $J_{ii}(E_u) + R_i < 0$ for all i.

We begin by computing $J_{11}(E_u) + R_1$ which yields

$$\begin{aligned} J_{11}(E_u) + R_1 &= \left.\frac{\partial \mathcal{U}_0}{\partial u_0}\right|_{E_u} + \left|\left.\frac{\partial \mathcal{U}_0}{\partial n_0}\right|_{E_u}\right| + \left|\left.\frac{\partial \mathcal{U}_0}{\partial c_0}\right|_{E_u}\right| + \sum_{j=1}^{\ell}\left(\left|\left.\frac{\partial \mathcal{U}_0}{\partial u_j}\right|_{E_u}\right| + \left|\left.\frac{\partial \mathcal{U}_0}{\partial n_j}\right|_{E_u}\right| + \left|\left.\frac{\partial \mathcal{U}_0}{\partial c_j}\right|_{E_u}\right|\right) \\ &= r_1 - \frac{2r_1}{K_0}u_0^* - \eta_0\left[p_0(u_0^*) + \lambda_0 u_0^* e^{-\lambda_j u_0^*}\right] + \frac{r_1}{K_0}u_0^* + \frac{\theta_0 u_0^*}{\alpha_0} + \eta_0\lambda_0 u_0^* e^{-\lambda_0 u_0^*} \\ &= r_1\left(1 - \frac{u_0^*}{K_0}\right) + \frac{\theta_0 u_0^*}{\alpha_0} - \eta_0 p_0(u_0^*). \end{aligned}$$

This quantity is negative for a sufficiently large spreading speed away from the primary tumour

site, η_0. In particular, this is true if

$$\eta_0 > \frac{1}{p_0(u_0^*)}\left[r_1\left(1-\frac{u_0^*}{K_0}\right)+\frac{\theta_0 u_0^*}{\alpha_0}\right]. \tag{3.46}$$

Next, computing $J_{22}(E_u)+R_2$ yields

$$\begin{aligned} J_{22}(E_u)+R_2 &= \left.\frac{\partial \mathcal{N}_0}{\partial n_0}\right|_{E_u} + \left|\left.\frac{\partial \mathcal{N}_0}{\partial u_0}\right|_{E_u}\right| + \left|\left.\frac{\partial \mathcal{N}_0}{\partial c_0}\right|_{E_u}\right| + \sum_{j=1}^{\ell}\left(\left|\left.\frac{\partial \mathcal{N}_0}{\partial u_j}\right|_{E_u}\right| + \left|\left.\frac{\partial \mathcal{N}_0}{\partial n_j}\right|_{E_u}\right| + \left|\left.\frac{\partial \mathcal{N}_0}{\partial c_j}\right|_{E_u}\right|\right) \\ &= r_2 - \frac{r_2}{K_0}u_0^* + \frac{\theta_0 u_0^*}{\alpha_0} - \gamma_0 - \eta_0 p_0(u_0^*). \end{aligned}$$

Condition (3.46) is sufficient for the negativity of this quantity since $r_1 > r_2$ and hence, no additional conditions are necessary.

We now consider the case $\ell > 1$, i.e., there are at least two lymph nodes in the network. Let $\mathcal{I} := \{1, 2, \ldots, \ell-1\}$. For $i \in \mathcal{I}$, we define $k := 2i+1$. Then we have

$$\begin{aligned} J_{kk}(E_u)+R_k &= \left.\frac{\partial \mathcal{U}_i}{\partial u_i}\right|_{E_u} + \left|\left.\frac{\partial \mathcal{U}_i}{\partial n_i}\right|_{E_u}\right| + \left|\left.\frac{\partial \mathcal{U}_i}{\partial c_i}\right|_{E_u}\right| + \sum_{j\in\mathcal{I}\setminus\{i\}}\left(\left|\left.\frac{\partial \mathcal{U}_i}{\partial u_j}\right|_{E_u}\right| + \left|\left.\frac{\partial \mathcal{U}_i}{\partial n_j}\right|_{E_u}\right| + \left|\left.\frac{\partial \mathcal{U}_i}{\partial c_j}\right|_{E_u}\right|\right) \\ &= r_1 - \frac{2r_1}{K_i}u_i^* - \eta_i\left[p_i(u_i^*) + \lambda_i u_i^* e^{-\lambda_i u_i^*}\right] + \frac{r_1}{K_i}u_i^* + \frac{\theta_0 u_i^*}{\alpha_i} + \ldots \\ &\qquad \cdots + \eta_i\lambda_i u_i^* e^{-\lambda_i u_i^*} + \eta_{i-1}\left[p_{i-1}(u_{i-1}^*) + 2\lambda_{i-1}u_{i-1}^* e^{-\lambda_{i-1}u_{i-1}^*}\right] \\ &= r_1\left(1-\frac{u_i^*}{K_i}\right) + \frac{\theta_0 u_i^*}{\alpha_i} - \eta_i p_i(u_i^*) + \eta_{i-1}\left[p_{i-1}(u_{i-1}^*) + 2\lambda_{i-1}u_{i-1}^* e^{-\lambda_{i-1}u_{i-1}^*}\right]. \end{aligned}$$

Since $u_i^* > K_i$, the negativity of the above quantity follows given the following condition:

$$r_1\left(1-\frac{u_i^*}{K_i}\right) < -\frac{\theta_0 u_i^*}{\alpha_i} - \eta_{i-1}\left[p_{i-1}(u_{i-1}^*) + 2\lambda_{i-1}u_{i-1}^* e^{-\lambda i-1 u_{i-1}^*}\right] \tag{3.47}$$

$$\iff K_i < \frac{r_1 u_i^*}{r_1 + \left[\frac{\theta_0 u_i^*}{\alpha_i} + \eta_{i-1}\left[p_{i-1}(u_{i-1}^*) + 2\lambda_{i-1}u_{i-1}^* e^{-\lambda i-1 u_{i-1}^*}\right]\right]}. \tag{3.48}$$

Biologically, this condition corresponds a sufficiently small carrying capacity of the lymph nodes.

Next, for $i \in \mathcal{I}$, let $k = 2i + 2$. We have

$$J_{kk}(E_u) + R_k = \left.\frac{\partial \mathcal{N}_i}{\partial n_i}\right|_{E_u} + \left|\left.\frac{\partial \mathcal{N}_i}{\partial u_i}\right|_{E_u}\right| + \left|\left.\frac{\partial \mathcal{N}_i}{\partial c_i}\right|_{E_u}\right| + \sum_{j\in\mathcal{I}\setminus\{i\}}\left(\left|\left.\frac{\partial \mathcal{N}_i}{\partial u_j}\right|_{E_u}\right| + \left|\left.\frac{\partial \mathcal{N}_i}{\partial n_j}\right|_{E_u}\right| + \left|\left.\frac{\partial \mathcal{N}_i}{\partial c_j}\right|_{E_u}\right|\right)$$

$$= r_2 - \frac{r_2}{K_i}u_i^* + \frac{\theta_0 u_i^*}{\alpha_i} - \gamma_0 - \eta_i p_i(u_i^*) + \eta_{i-1}p_{i-1}(u_{i-1}^*).$$

In order to ensure negativity of this quantity, it suffices to impose the condition

$$\gamma_0 > \frac{\theta_0 u_i^*}{\alpha_i} + \eta_{i-1}p_{i-1}(u_{i-1}^*), \tag{3.49}$$

which is a condition for the local asymptotic stability of the tumour-dominant steady state which is similar to that of the local model in Section 3.3.

Finally, we consider the final node in the network, lymph node ℓ. We have

$$J_{(2\ell+1)(2\ell+1)}(E_u) + R_{2\ell+1} = \left.\frac{\partial \mathcal{U}_\ell}{\partial u_\ell}\right|_{E_u} + \left|\left.\frac{\partial \mathcal{U}_\ell}{\partial n_\ell}\right|_{E_u}\right| + \left|\left.\frac{\partial \mathcal{U}_\ell}{\partial c_\ell}\right|_{E_u}\right| + \sum_{j=0}^{\ell-1}\left(\left|\left.\frac{\partial \mathcal{U}_\ell}{\partial u_j}\right|_{E_u}\right| + \left|\left.\frac{\partial \mathcal{U}_\ell}{\partial n_j}\right|_{E_u}\right| + \left|\left.\frac{\partial \mathcal{U}_\ell}{\partial c_j}\right|_{E_u}\right|\right)$$

$$= r_1 - \frac{2r_1}{K_\ell}u_\ell^* + \frac{r_1}{K_\ell}u_\ell^* + \frac{\theta_0 u_\ell^*}{\alpha_\ell} + \eta_{\ell-1}\left[p_{\ell-1}(u_{\ell-1}^*) + 2\lambda_{\ell-1}u_{\ell-1}^* e^{-\lambda_{\ell-1}u_{\ell-1}^*}\right]$$

$$= r_1\left(1-\frac{u_\ell^*}{K_\ell}\right) + \frac{\theta_0 u_\ell^*}{\alpha_\ell} + \eta_{\ell-1}\left[p_{\ell-1}(u_{\ell-1}^*) + 2\lambda_{\ell-1}u_{\ell-1}^* e^{-\lambda_{\ell-1}u_{\ell-1}^*}\right].$$

It is clear that this quantity is negative if condition (3.48) is satisfied for $i = \ell$. Next,

$$J_{(2\ell+2)(2\ell+2)}(E_u) + R_{2\ell+2} = \left.\frac{\partial \mathcal{N}_\ell}{\partial n_\ell}\right|_{E_u} + \left|\left.\frac{\partial \mathcal{N}_\ell}{\partial u_\ell}\right|_{E_u}\right| + \left|\left.\frac{\partial \mathcal{N}_\ell}{\partial c_\ell}\right|_{E_u}\right| + \sum_{j=0}^{\ell-1}\left(\left|\left.\frac{\partial \mathcal{N}_\ell}{\partial u_j}\right|_{E_u}\right| + \left|\left.\frac{\partial \mathcal{N}_\ell}{\partial n_j}\right|_{E_u}\right| + \left|\left.\frac{\partial \mathcal{N}_\ell}{\partial c_j}\right|_{E_u}\right|\right)$$

$$= r_2 - \frac{r_2}{K_\ell}u_\ell^* + \frac{\theta_0 u_\ell^*}{\alpha_\ell} - \gamma_0 + \eta_{\ell-1}p_{\ell-1}(u_{\ell-1}^*).$$

It is again clear that this quantity is negative if condition (3.49) is satisfied for $i = \ell$.

Finally, define $\tilde{\mathcal{I}} := \{0, 1, 2, \ldots, \ell\}$. For $i \in \tilde{\mathcal{I}}$, we define $k := 2\ell + 3 + i$. It follows that

$$J_{kk}(E_u) + R_K = \left.\frac{\partial C_i}{\partial c_i}\right|_{E_u} + \left|\left.\frac{\partial C_i}{\partial u_i}\right|_{E_u}\right| + \left|\left.\frac{\partial C_i}{\partial n_i}\right|_{E_u}\right| + \sum_{j\in\tilde{\mathcal{I}}\setminus\{i\}}\left(\left|\left.\frac{\partial C_i}{\partial u_j}\right|_{E_u}\right| + \left|\left.\frac{\partial C_i}{\partial n_j}\right|_{E_u}\right| + \left|\left.\frac{\partial C_i}{\partial c_j}\right|_{E_u}\right|\right)$$

$$= -\beta - q_1 u_i^*.$$

Hence, $J_{kk}(E_u) + R_K < 0$. By Lemma 3.5.1, we conclude that if all of the above conditions are satisfied, then E_u is locally asymptotically stable. We state this result in the following proposition.

Proposition 3.5.1 *Consider system (3.34) - (3.40) when $\phi_k = 0$, $q_{k,R} = 1$, and $q_{k,L} = 0$ for $k = 0, 1, 2, \ldots, \ell$. The tumour-dominant steady state E_u is locally asymptotically stable if the following conditions are satisfied:*

1. $$\eta_0 > \frac{1}{p_0(u_0^*)}\left[r_1\left(1 - \frac{u_0^*}{K_0}\right) + \frac{\theta_0 u_o^*}{\alpha_0}\right].$$

2. *For $i = 1, 2, \ldots, \ell$,*

$$K_i < \min\left\{\frac{10\eta_{i-1}}{7\eta_i}u_{i-1}^*\left(1 - e^{-\lambda_{i-1}u_{i-1}^*}\right), \frac{r_1 u_i^*}{r_1 + \left[\frac{\theta_0 u_i^*}{\alpha_i} + \eta_{i-1}\left[p_{i-1}(u_{i-1}^*) + 2\lambda_{i-1}u_{i-1}^* e^{-\lambda i-1 u_{i-1}^*}\right]\right]}\right\}.$$

3. *For* $i = 1, 2, \ldots, \ell$,

$$\gamma_0 > \frac{\theta_0 u_i^*}{\alpha_i} + \eta_{i-1} p_{i-1}(u_{i-1}^*).$$

Proposition 3.5.1 has some significant biological implications. Since this proposition gives conditions for the stability of the tumour-dominant steady state, the conditions being satisfied represents a clinically unfavourable outcome. The condition $\phi_k = 0$ represents no external oxygenation. Similarly to the local model, we see that hypoxic environments are beneficial to the tumour cells and reduce the efficacy of the adenovirus. Condition 1 of the proposition represents a sufficiently large rate of spreading of tumour cells away from the primary tumour. Condition 2 represents smaller carrying capacities of the lymph nodes – this is not surprising, as tumour cells will more easily spread away from lymph nodes with lesser carrying capacities, i.e., due to less available resources. Condition 3 once again mirrors an important insight from the local model – the oncolysis rate must not be too large in relation to the infection rate for an OV to be effective. However, this condition now comes with the additional consideration of incoming tumour cells from the previous lymph node in the network. In general, in a clinical setting, the model suggests effective treatment with an OV requires the engineering of a virus with a sufficiently large infection rate under hypoxic environments, which takes into account the spreading speed of the tumour cells as well as the carrying capacities of the lymph nodes. We further explore the implications of the regional model in the next section.

3.6 Numerical Simulations: Regional Model

Due to the lack of analytic tractability of system (3.34) - (3.40), we perform simulations to investigate the dynamics of this system. The primary tumour parameters (except for θ and γ) are pulled directly from Table 3.2. The parameters K_i and α_i are estimated by taking into account the corresponding tumour parameters, K_0 and α_0. In particular, for all i, we take $\eta_i = 0.0002$ days^{-1}, $K_i = K_0/10$ and $\alpha_i = \alpha_0/10$. Note that these parameters are the same

for all lymph nodes. We make the biologically reasonable assumption that cells have a higher probability of migrating away from the primary tumour, i.e., in the direction of increasing node index. Hence, we set $q_{1,L} = q_{2,L} = q_{3,L} = 0.05$ and $q_{1,R} = q_{2,R} = 0.95$.

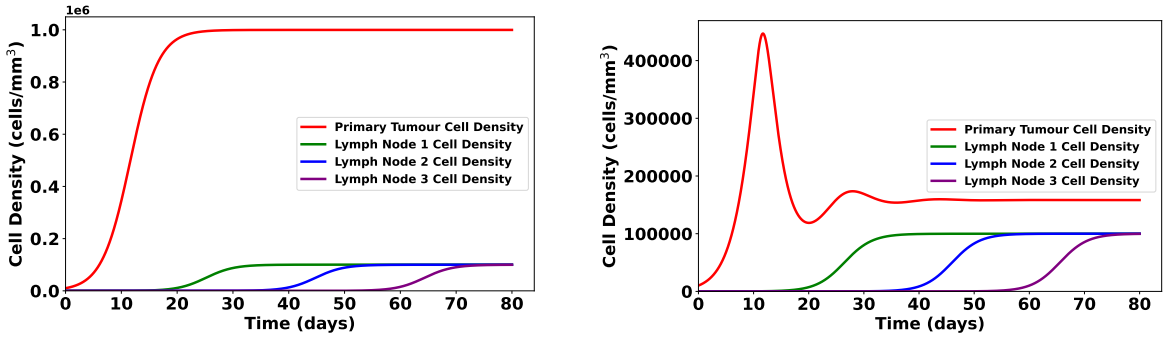

(a) (b)

Figure 3.13: The impact of oxygenation rate of the primary tumour, ϕ_0, on the tumour cell density at the primary site and the first three lymph nodes in a network. (a) The case of no external oxygenation, $\phi_0 = 0$. (b) The case where $\phi_0 = 10^4$ mM day^{-1}. There is a marked reduction in long-term tumour cell density when oxygenation is increased.

In Figure 3.13, we compare the case of no external oxygen input, $\phi_0 = 0$, to the case of some external oxygen input, $\phi_0 = 10^4$ mM day^{-1}. We graph the total number of tumour cells, $u_i(t) + n_i(t)$ over the course of 80 days. The functions $\theta(c)$ and $\gamma(c)$ are given by equations (3.33), where $\theta_0 = 0.005115, \theta_\infty = 1.0, k_\theta = 0.08, \gamma_0 = 0.1, \gamma_\infty = 0.9$, and $k_\gamma = 0.08$. These parameter values are similar to the ones used in Figure 3.10 – they yield a favourable clinical outcome in the local model. The model assumes that external oxygenation may only be performed on the primary tumour site – not at the lymph nodes. From Figure 3.13 (a), we see that in the case where no external oxygen is provided, the tumour cells ultimately dominate at the primary tumour site and also approach a value near the carrying capacity at the lymph nodes. This unfavourable result is in stark contrast to the results of Figure 3.10, in which the tumour cells are either eradicated or kept under control. On the other hand, in the case of external oxygenation seen in Figure 3.13 (b), there is a sharp drop in the total tumour cell density. Namely, from a peak value approaching the carrying capacity at the primary site to approximately 4.47×10^5 cells/mm^3. This is a result of the benefit which the OV acquires as

a result of an oxygen-rich environment. This is consistent with the benefit consistently seen when treating cancer in oxygen-sufficient tumour microenvironments compared to hypoxic microenvironments. Even though the oxygenation occurs only at the primary tumour sites, the model allows for the proliferation of infected tumour cells through the lymphatic vessels into the lymph nodes, and hence the oxygenation also confers an increase in the efficacy of the OV treatment at the lymph nodes.

To this end, we turn our attention to the behaviour at the lymph nodes. In Figure 3.13 (a), the total tumour cell density across all three lymph nodes in the long-term is approximately given by the sum of their carrying capacities. In Figure 3.13 (b), as a result of external oxygenation, it takes a longer period of time for the tumour cell densities at the lymph nodes to reach their carrying capacities. This is because the benefit of the oxygenation here is less direct – the oxygenation is only occurring at the primary site. There is still an indirect benefit, however, as a marked decrease of tumour cells at the primary site will result in slower spreading rates.

In summary, Figure 3.13 further illustrates the importance of the oxygen concentration in treatment with adenoviruses, a result which is consistent with the existing oncology literature [31]. It may also be worth noting that in contrast to Figure 3.13 (a), the tumour cell density at lymph node 3 eventually dominates the tumour cell density at lymph node 1 in Figure 3.13 (b). This may be explained by the fact that oxygenation occurs at the primary tumour site and, therefore, the infected cells are initially closer to the lymph nodes closer to the primary site rather than the subsequent lymph nodes in the network. Hence, lymph node 1 has a slightly greater benefit from the OV treatment than do lymph nodes 2 and 3.

From the local model, we found that having a lower virus-induced death rate compared to the infection rate tends to yield more favourable clinical outcomes. To this end, we investigate the dynamics of the regional model in the case where $\theta(c) \geq (\alpha/K)\gamma(c)$ for all $c \geq 0$. We set $\theta_0 = 0.05115, \theta_\infty = 2.115, k_\theta = 0.016$ and $\gamma(c) = 0.5115$ for all $c \geq 0$. We once again plot the cases $\phi_0 = 0$ and $\phi_0 = 10^4$ mm day^{-1}.

Figure 3.14 shows that the impact of having a sufficiently low virus oncolysis rate in the

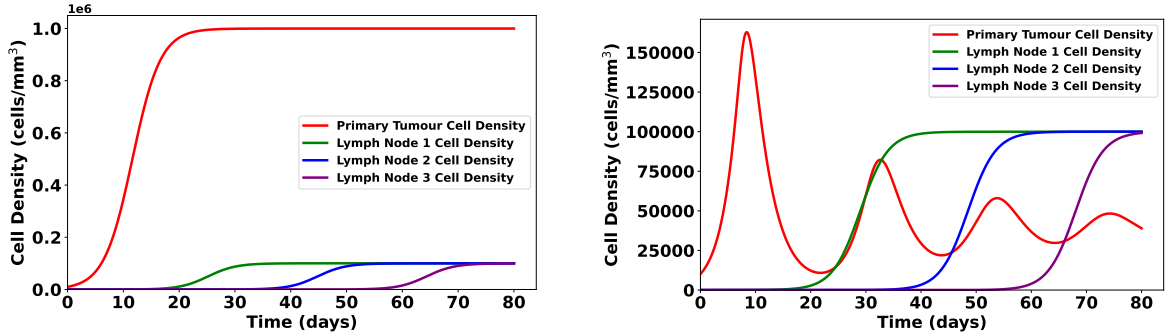

(a) (b)

Figure 3.14: Dynamics of the regional model in the case where $\theta(c) \geq (\alpha/K)\gamma(c)$. (a) The case of no external oxygenation, $\phi_0 = 0$. (b) The case where $\phi_0 = 10^4$ mM day^{-1}. There is a very sharp reduction in long-term tumour cell density at the site of the primary tumour but the impact on the lymph nodes is much less pronounced.

regional model is consistent with the local model. Once again, the effect of an increased external oxygenation rate is much more pronounced at the primary tumour compared to the lymph nodes.

Motivated by Figure 3.14, we now consider the impact of the infection rate, θ, and the virus-induced death rate, γ, on the regional model. These parameters were considered extensively in the the numerical simulations of the local model in Section 3.4. In this case, we consider keeping θ and γ constant rather than as functions of oxygen concentration. The results of the simulations are plotted in Figure 3.15.

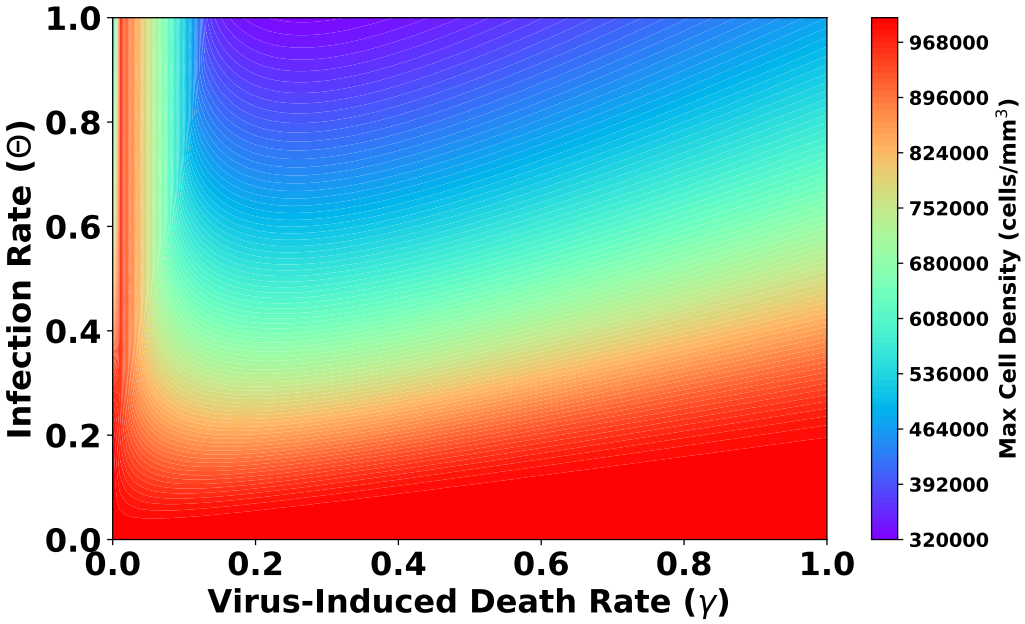

Figure 3.15: Maximum tumour cell density at the location of the primary tumor over the course of 80 days after treatment for various values of θ and γ.

In Figure 3.15, we plot the maximum value of the tumour cell density at the primary tumour site over the course of 80 days after OV treatment. That is, we plot $\max\{u_0(t) + n_0(t)\}$ for different values of θ and γ. Consistent with our prior results, we can again visualize the relationship between infection and oncolysis. We see that increasing the virus-induced death rate to a much greater value relative to the infection rate leads to an unfavourable outcome (red region). This also occurs if the virus-induced death rate is too small, regardless of the value of the infection rate. Therefore, this provides further evidence of the importance of a high infection rate and a oncolysis rate that is *not too low* in oder to obtain favourable results (blue region).

Finally, we return to the case where θ and γ depend on the oxygen concentration. In particular, we assume that we have some mechanism through which to administer external oxygen to the lymph nodes and set $\phi_k = 10^4$ mM day^{-1} for $k = 1, 2, \ldots, \ell$. The functions $\theta(c)$ and $\gamma(c)$ are once again given by equations (3.33), where $\theta_0 = 0.05115, \theta_\infty = 2.115, k_\theta = 0.016, \gamma_0 = 0.5115, \gamma_\infty = 0.9115$, and $k_\gamma = 0.016$. This corresponds to the case where the oncolysis rate dominates under hypoxic conditions while the infection rate dominates in oxygen-rich microenvironments.

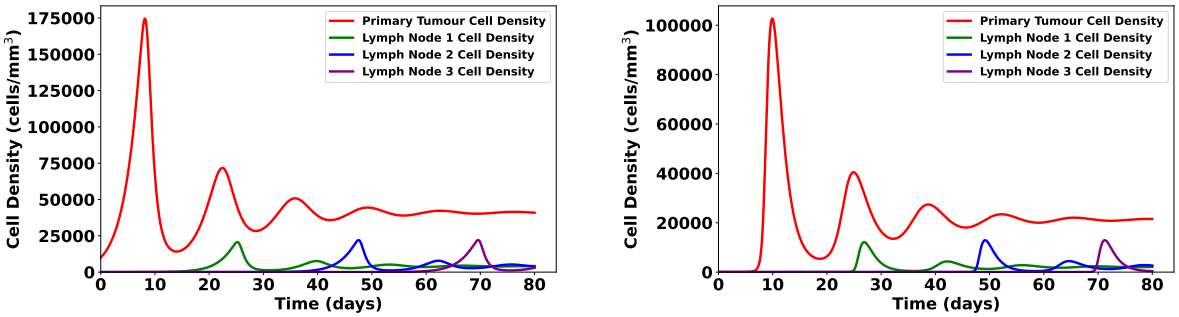

(a) (b)

Figure 3.16: The impact of oxygenation rate at the primary tumour site and the first three lymph nodes in the network. (a) Uninfected tumour cell density at the primary tumour and at each node. (b) Infected tumour cell density at the primary tumour and at each node

Figure 3.16 shows the case of oxygen dependence of the infection rate and the oncolysis rate. In this case, there is a marked reduction in the total tumour cell density in all compartments. Figure 3.16 (a) shows the uninfected tumour cell density, u_i and Figure 3.16 (b) shows the infected tumour cell density, n_i. In contrast to the case of no oxygen input at the lymph nodes, the infected tumour cell density at each lymph node asymptotically approaches a value below the carrying capacity of its corresponding node. This provides further evidence which supports the lack of efficacy of oncolytic adenoviruses in hypoxic environments and the increased efficacy of these OVs when external oxygenation is provided.

3.7 Conclusion and Discussion

From the mathematical results of this work, as well as the simulations, the importance of the functions θ and γ are emphasized. Biologically, this refers to the interplay between viral infection rate and the virus-induced death rate of the cancer cells. If the virus-induced cancer cell death rate is too large compared to the infection rate, the cancer cells end-up dominating in the long-run. This is a reflection of the virus not being able to infect cells faster than the infected cells are destroyed. On the other-hand, if the infection rate of the OV is significantly large compared to the virus-induced death rate in *all* oxygen environments, the infected tumour

cells will dominate in the long-run and will reach some steady state. This steady state may represent the case where we avoid uncontrollable cancer cell growth as the number of cells will not approach the carrying capacity. This translates to a favourable clinical result. On the other hand, it may also represent a state in which the infected tumour cells dominate *at* the carrying capacity if the OV tumour-destroying capabilities are *too* low. For this reason, we suggest that when engineering OVs, it is important to make sure that these viruses have greater infection capabilities than they have oncolytic capabilities while ensuring that the virus-induced death rate is not too low. In particular, our results suggest that maintaining high viral infection rates tends to lead to clinically favourable results regardless of oxygen concentration of the tumour microenvironment. Our findings on the importance of the infection rate are consistent with [16, 18] and contribute to a growing body of literature regarding efficacy of engineered viruses [16, 18, 20].

Another important component of this chapter is the modelling of the impact of hypoxic conditions on OV treatment efficacy. As previously stated, the modelling suggests that significantly high infection rates are preferable under any oxygen conditions. However, another layer of complexity is added when considering the threat of toxicity which the OV poses toward healthy cells [32]. Furthermore, having a virus-induced death rate which is *too low* will lead to a decreased mortality of cancer cells. Hence, it is not sufficient to simply conclude that engineering extremely infectious viruses is the solution. Instead, we proposed taking into account the effect of different oxygen conditions and hypoxia when constructing the OVs. To address this, we considered the case in which which function dominates, θ or γ, depends on the oxygen concentration. A favourable result occurs when γ dominates for low oxygen concentrations but θ dominates for high oxygen concentrations. Hence, we conjecture that another consideration of engineering OVs is whether or not the tumour microenvironment is hypoxic. The preferential virus characteristic would be to have greater oncolytic capabilities in hypoxic environments and greater infectious capabilities in more oxygen-rich environments. According to the modelling, this may lead to stability of a steady tumour load rather than uncontrollable

growth. However, we also found that making the virus-induced death rate *too* great under hypoxic conditions also leads to a reduction in the efficacy of the treatment, as the infected tumour cells die faster than they may infect the remaining susceptible tumour cells.

We extended the model to a regional model which incorporated spatial structure through considering the axillary lymph nodes. This was done by considering ODEs on a one-dimensional lattice. This natural extension captures the invasive nature of melanoma (and many other invasive cancers). Once again, the importance of considering oxygen cannot be understated. When considering a system with three lymph nodes, we found that providing oxygenation at the site of the primary lesion (through an external oxygen source) yields an approximately 72% decrease in tumour cell density at the site of the primary lesion. Lymph nodes closer to the site of oxygenation similarly obtained benefit from more hyperoxic conditions. This benefit of external oxygenation in (various forms of) the treatment of cancer has also been observed clinically, such as in the use of hyperbaric-oxygen therapy [34]. Our simulations further support these experimental findings. We also found that the impact of the infection rate, θ, is also present in the regional model and the findings were consistent with those of the local model. This leads us to further stress the importance of oxygen-rich microenvironments being used in tandem with highly infectious OVs.

This model may be further enhanced by the addition of a variable which accounts for the free virus particles. Although this would increase the complexity of system in terms of mathematical analysis, it would lead to more interesting dynamics, biologically. In terms of the parameters, the growth rate of tumour cells also depends on the available oxygen of the tumour microenvironment [1]. Hence an important next step is the use of growth rates which depend on the oxygen concentration, i.e., $r_1(c), r_2(c)$. Future work also includes adding a *continuous* spatial structure to the model, i.e., through the use of PDE modelling. This can take into account the spatial properties of the tumour as well as the efficacy of OV treatment in the context of metastatic disease by modelling cancer cell spreading at the site of the primary lesion. Extending the types of geometry of the lattice representing the lymphatic network is also an important

next step. For example, this involves allowing certain lymph nodes in the network to have connections with multiple neighbouring lymph nodes. From a clinical perspective, incorporating the use of conventional chemotherapy along with the virotherapy is also likely to provide potentially useful insights. Finally, the toxic effects of an increased tumour cell infection rate may also be worth considering in order to model a more comprehensive treatment approach.

Bibliography

[1] Bedogni, B., & Powell, M. B. (2009). Hypoxia, melanocytes and melanoma–survival and tumor development in the permissive microenvironment of the skin. *Pigment Cell & Melanoma Research*, 22(2), 166-174.

[2] Billy, F., Ribba, B., Saut, O., Morre-Trouilhet, H., Colin, T., Bresch, D., ... & Flandrois, J. P. (2009). A pharmacologically based multiscale mathematical model of angiogenesis and its use in investigating the efficacy of a new cancer treatment strategy. *Journal of Theoretical Biology*, 260(4), 545-562.

[3] Bommareddy, P. K., Patel, A., Hossain, S., & Kaufman, H. L. (2017). Talimogene laherparepvec (T-VEC) and other oncolytic viruses for the treatment of melanoma. *American Journal of Clinical Dermatology*, 18(1), 1-15.

[4] Busk, M., Overgaard, J., & Horsman, M. R. (2020, November). Imaging of tumor hypoxia for radiotherapy: Current status and future directions. In *Seminars in Nuclear Medicine* (Vol. 50, No. 6, pp. 562-583). WB Saunders.

[5] Chen, L. L., Nolan, M. E., Silverstein, M. J., Mihm Jr, M. C., Sober, A. J., Tanabe, K. K., ... & Michaelson, J. S. (2009). The impact of primary tumor size, lymph node status, and other prognostic factors on the risk of cancer death. *Cancer: Interdisciplinary International Journal of the American Cancer Society*, 115(21), 5071-5083.

[6] Culshaw, R. V., Ruan, S., & Webb, G. (2003). A mathematical model of cell-to-cell spread of HIV-1 that includes a time delay. *Journal of Mathematical Biology*, 46(5), 425-444.

[7] DePillis, L., Gallegos, A., & Radunskaya, A. (2013). A model of dendritic cell therapy for melanoma. *Frontiers in Oncology*, 3, 56.

[8] Van den Driessche, P. (2017). Reproduction numbers of infectious disease models. *Infectious Disease Modelling*, 2(3), 288-303.

[9] Filley, A. C., & Dey, M. (2017). Immune system, friend or foe of oncolytic virotherapy?. *Frontiers in Oncology*, 7, 106.

[10] Fountzilas, C., Patel, S., & Mahalingam, D. (2017). Oncolytic virotherapy, updates and future directions. *Oncotarget*, 8(60), 102617.

[11] Gan, E. S., & Ooi, E. E. (2020). Oxygen: viral friend or foe?. *Virology Journal*, 17(1), 1-12.

[12] Harrington, K. J., Puzanov, I., Hecht, J. R., Hodi, F. S., Szabo, Z., Murugappan, S., & Kaufman, H. L. (2015). Clinical development of talimogene laherparepvec (T-VEC): A modified herpes simplex virus type-1–derived oncolytic immunotherapy. *Expert Review of Anticancer Therapy*, 15(12), 1389-1403.

[13] Heidbuechel, J. P., Abate-Daga, D., Engeland, C. E., & Enderling, H. (2020). Mathematical modeling of oncolytic virotherapy. In *Oncolytic Viruses* (pp. 307-320). Humana, New York, NY.

[14] Hill, C., & Carlisle, R. (2019). Achieving systemic delivery of oncolytic viruses. *Expert Opinion on Drug Delivery*, 16(6), 607-620.

[15] Hu, H. J., Liang, X., Li, H. L., Du, C. M., Hao, J. L., Wang, H. Y., ... & Liu, X. Y. (2020). The armed oncolytic adenovirus ZD55-IL-24 eradicates melanoma by turning the tumor cells from the self-state into the nonself-state besides direct killing. *Cell Death & Disease*, 11(11), 1-21.

[16] Jenner, A. L., Yun, C. O., Kim, P. S., & Coster, A. C. (2018). Mathematical modelling of the interaction between cancer cells and an oncolytic virus: insights into the effects of treatment protocols. *Bulletin of Mathematical Biology*, 80(6), 1615-1629.

[17] Johnson, D. B., Puzanov, I., & Kelley, M. C. (2015). Talimogene laherparepvec (T-VEC) for the treatment of advanced melanoma. *Immunotherapy*, 7(6), 611-619.

[18] Kim, D., Kim, H., Wu, H., & Shin, D. H. (2020). The Effect of the Infection Rate on Oncolytic Virotherapy. *Computational Biology and Bioinformatics*, 8(1).

[19] Kumar, A., Parthasarathy, V., Sridhar, K., & Tan, W. K. J. Modeling Oxygen Diffusion and Consumption in a Skin Graft.

[20] Kurozumi, K., Hardcastle, J., Thakur, R., Yang, M., Christoforidis, G., Fulci, G., ... & Kaur, B. (2007). Effect of tumor microenvironment modulation on the efficacy of oncolytic virus therapy. *Journal of the National Cancer Institute*, 99(23), 1768-1781.

[21] Lai, X., & Zou, X. (2014). Modeling HIV-1 virus dynamics with both virus-to-cell infection and cell-to-cell transmission. *SIAM Journal on Applied Mathematics*, 74(3), 898-917.

[22] Malinzi, J., Ouifki, R., Eladdadi, A., Torres, D. F., & White, K. A. (2018). Enhancement of chemotherapy using oncolytic virotherapy: mathematical and optimal control analysis. *Mathematical Biosciences & Engineering*, 15(6), 1435-1463.

[23] Menon, C., Polin, G. M., Prabakaran, I., Hsi, A., Cheung, C., Culver, J. P., ... & Fraker, D. L. (2003). An integrated approach to measuring tumor oxygen status using human melanoma xenografts as a model. *Cancer Research*, 63(21), 7232-7240.

[24] Paiva, L. R., Binny, C., Ferreira Jr, S. C., & Martins, M. L. (2009). A multiscale mathematical model for oncolytic virotherapy. *Cancer Research*, 69(3), 1205-1211.

[25] Puzanov, I., Milhem, M. M., Minor, D., Hamid, O., Li, A., Chen, L., ... & Andtbacka, R. H. (2016). Talimogene laherparepvec in combination with ipilimumab in previously

untreated, unresectable stage IIIB-IV melanoma. *Journal of Clinical Oncology*, 34(22), 2619.

[26] Russell, S. J., Peng, K. W., & Bell, J. C. (2012). Oncolytic virotherapy. *Nature Biotechnology*, 30(7), 658-670.

[27] Saginala, K., Barsouk, A., Aluru, J. S., Rawla, P., & Barsouk, A. (2021). Epidemiology of melanoma. *Medical sciences*, 9(4), 63.

[28] Shain, A., Bastian, B. From melanocytes to melanomas. *Nat Rev Cancer* 16, 345–358 (2016). https://doi.org/10.1038/nrc.2016.37

[29] Schadendorf, D., van Akkooi, A. C., Berking, C., Griewank, K. G., Gutzmer, R., Hauschild, A., ... & Ugurel, S. (2018). Melanoma. *The Lancet*, 392(10151), 971-984.

[30] Schadendorf, D., Fisher, D. E., Garbe, C., Gershenwald, J. E., Grob, J. J., Halpern, A., ... & Hauschild, A. (2015). Melanoma. *Nature Reviews Disease Primers*, 1(1), 1-20.

[31] Sheng Guo, Z. (2011). The impact of hypoxia on oncolytic virotherapy. *Virus Adaptation and Treatment*, 3(1), 71-82.

[32] Simpson, G. R., Relph, K., Harrington, K., Melcher, A., & Pandha, H. (2016). Cancer immunotherapy via combining oncolytic virotherapy with chemotherapy: recent advances. *Oncolytic virotherapy*, 5, 1.

[33] Smith, H. L. (2008). *Monotone dynamical systems: an introduction to the theory of competitive and cooperative systems: an introduction to the theory of competitive and cooperative systems* (No. 41). American Mathematical Soc.

[34] Tibbles, P. M., & Edelsberg, J. S. (1996). Hyperbaric-oxygen therapy. *New England Journal of Medicine*, 334(25), 1642-1648.

[35] Unsal, S., Aybar, A. C. A. R., Mehmet, I. T. İ. K., Kabatas, A., Gedikli, O., Ozdemir, F., & Turhan, K. (2020). Personalized Tumour Growth Prediction Using Multiscale Modeling. *Journal of Basic and Clinical Health Sciences*, 4(3), 347-363.

[36] Uong, A., & Zon, L. I. (2010). Melanocytes in development and cancer. *Journal of Cellular Physiology*, 222(1), 38–41. https://doi.org/10.1002/jcp.21935.

[37] Urenda-Cázares, E., Gallegos, A., & Macías-Díaz, J. E. (2020). A mathematical model that combines chemotherapy and oncolytic virotherapy as an alternative treatment against a glioma. *Journal of Mathematical Chemistry*, 58(3), 544-554.

[38] Wang, Z., Guo, Z., & Smith, H. (2019). A mathematical model of oncolytic virotherapy with time delay. *Mathematical Biosciences and Engineering*, 16(4), 1836-1860.

[39] Weisstein, Eric W. "Gershgorin Circle Theorem." From MathWorld–A Wolfram Web Resource. http://mathworld.wolfram.com/GershgorinCircleTheorem.html

[40] Zimmermann, K. A. (2016). Lymphatic System: Facts, Functions & Diseases. *Live Science*.

Chapter 4

A Continuous Spatial Model of Melanoma Treatment via Oncolytic Virotherapy

4.1 Introduction

In this chapter, we develop and analyze a continuous spatial model of oncolytic virotherapy. In the previous chapter, we developed both a local model and a discrete spatial model in order to simulate the regional spread of melanoma through the adjacent lymph nodes, in the presence of an oncolytic virus (OV). In contrast, we now focus on the spreading of the melanoma tumour cells locally on the surface of the skin, in a continuous spatial domain, by modelling the growth of the primary lesion over the surface of the skin. As in the previous chapter, we consider the effect of an OV which is introduced into the system directly via injection into the primary site. Furthermore, as in the previous chapter, we consider only the effect of cell-to-cell viral infections of the cancer cells.

We make use of a partial differential equation (PDE) model and, as in Chapter 2, consider the existence of travelling wave (TWS) solutions. In the context of melanoma spreading, these solutions represent invasion waves. Such models have seen extensive use in the modelling of melanoma [5, 6, 11, 14]. One of the key features of many of these models is the use of a

diffusion term in the PDE which represents the spreading of the cancer cells.

In their work, El-Hachem et al. [11] considered the spread of melanoma through the skin by using the following system of PDEs

$$\frac{\partial u}{\partial t} = D\frac{\partial}{\partial x}\left[\left(1-\frac{v}{K}\right)\frac{\partial u}{\partial x}\right] + ru\left(1-\frac{u+v}{K}\right), \tag{4.1}$$

$$\frac{\partial v}{\partial t} = -\phi uv, \tag{4.2}$$

where $u(x,t)$ is the density of melanoma cells at time t and position x. $v(x,t)$ gives the density healthy skin cells. D is the diffusivity of the melanoma cells and K is the carrying capacity of the skin cell density. The authors use logistic growth to represent growth of the melanoma cells, with growth rate r. From the second equation, it can be seen that ϕ is the rate at which the melanoma cells degrade the skin cells. The authors use a degenerative diffusion term to represent the dampening effect which healthy skin cells have on the melanoma spreading rate. Indeed, if v is very close to K, then the diffusion rate of the melanoma cells is decreased. Such a mechanism reflects the property of cancer cells favouring spreading in the direction of lower healthy cell densities, toward more nutrient rich environments. In their paper, El-Hachem et al. use a variety of analytical and numerical techniques to investigate the existence of TWS of their model. A similar system is also considered in [6].

The novelty of the current chapter is that we introduce the presence of an OV, (i.e., T-Vec) much in the same vein as in Chapter 3. Once again, we consider the modelling of cell-to-cell infection of melanoma cells by previously infected melanoma cells. The virus is once again considered to be introduced via direct injection into the lesion. In this case, we introduce a new variable, $n(x,t)$, the density of melanoma cells which have been infected by the virus at time t and position x. Furthermore, we note that $u(x,t)$ will now represent density of uninfected melanoma cells at time t and position x. We are considering $x \in \mathbb{R}$, i.e., spreading on a line, as in [6, 11, 13]. We use a mass-action term to model the infection of melanoma cells, with mass-action coefficient θ. We assume that the infected melanoma cells are killed by the virus

at a per-capita rate γ. If we consider that infected cells and uninfected cells may have different rates of degrading the healthy skin, we consider ϕ_1 and ϕ_2 in place of ϕ. These parameters give the degradation of the healthy skin cell density due to uninfected tumour cells and infected tumour cells, respectively. Therefore, we consider the following model:

$$\frac{\partial u}{\partial t} = D_1 \frac{\partial}{\partial x}\left[\left(1 - \frac{v}{K}\right)\frac{\partial u}{\partial x}\right] + r_1 u\left(1 - \frac{u+n+v}{K}\right) - \theta un, \tag{4.3}$$

$$\frac{\partial n}{\partial t} = D_2 \frac{\partial}{\partial x}\left[\left(1 - \frac{v}{K}\right)\frac{\partial n}{\partial x}\right] + r_2 n\left(1 - \frac{u+n+v}{K}\right) + \theta un - \gamma n, \tag{4.4}$$

$$\frac{\partial v}{\partial t} = -\phi_1 uv - \phi_2 nv + r_3 v\left(1 - \frac{u+n+v}{K}\right). \tag{4.5}$$

The parameters D_1 and D_2 give the diffusivity of uninfected tumour cells and infected tumour cells, respectively. The parameters r_1, r_2, and r_3 give the (logistic) growth rates of the uninfected tumour cells, infected tumour cells, and healthy skin cells, respectively. Hence, we are assuming that if the cancer should be eradicated entirely, ($u = n = 0$), then the healthy skin cells should be able to recover back to their carrying capacity. The parameter K represents the carrying capacity of the skin cell density.

In contrast to Chapter 3, we have now dropped the dependence of viral infection and virus-induced death rate (oncolysis) on oxygen concentration in order to reduce the analytic complexity of the model. Furthermore, for the sake of mathematical tractability, we have replaced the Holling type II functional response used in Chapter 3 to represent infection, choosing to instead use a Holling type I functional response. The parameter θ acts as the mass-action coefficient. Such a functional response has seen use in the modelling of OV infection, such as in [17, 19, 21].

We note that the term $(1 - v/K)$ appears as the flux in equations (4.3) and (4.4). This accounts for a kind of resource driven property of the tumour cells' movement. In particular, the cancer cells have a lesser affinity for spreading in locations rich with healthy cells (i.e., healthy cell densities near the carrying capacity) as such locations may be considered unfavourable due

to a lesser availability of resources. This assumption is consistent with the assumptions made in [6, 11].

In Section 4.2, we perform a mathematical analysis and consider the existence TWS. In Section 4.3, we perform some numerical simulations on the PDE model in order to obtain some insights on the various parameters. In particular, as in chapter 3, we explore the impact of the infection rate and the oncolysis rate on the efficacy of the treatment. We conclude with a discussion of the results and directions for future work in Section 4.4.

4.2 Mathematical Analysis

We non-dimensionalize system (4.3) - (4.5) by making the following substitutions:

$$\tilde{u} := \frac{u}{K}, \quad \tilde{n} := \frac{n}{K}, \quad \tilde{v} := \frac{v}{K}, \quad \tilde{t} := r_1 t, \quad \tilde{x} := \sqrt{\frac{r_1}{D_1}}x, \quad D := \frac{D_2}{D_1},$$

$$\tilde{\theta} := \frac{\theta K}{r_1}, \quad \tilde{\gamma} := \frac{\gamma}{r_1}, \quad \tilde{\phi_1} := \frac{\phi_1 K}{r_1}, \quad \tilde{\phi_2} := \frac{\phi_2 K}{r_1}, \quad r := \frac{r_2}{r_1}, \quad \psi := \frac{r_3}{r_1}.$$

After dropping all of the tildes for notational convenience, this yields the following system of PDEs:

$$\frac{\partial u}{\partial t} = \frac{\partial}{\partial x}\left[(1-v)\frac{\partial u}{\partial x}\right] + u(1-u-n-v) - \theta un, \tag{4.6}$$

$$\frac{\partial n}{\partial t} = D\frac{\partial}{\partial x}\left[(1-v)\frac{\partial n}{\partial x}\right] + rn(1-u-n-v) + \theta un - \gamma n, \tag{4.7}$$

$$\frac{\partial v}{\partial t} = -\phi_1 uv - \phi_2 nv + \psi v(1-u-n-v). \tag{4.8}$$

We seek to show the existence of a TWS of the above system. In particular, we are interested in the existence of a right-travelling TWS, with wave speed c. Such a solution has the form

$$u(x,t) = U(\xi), \quad n(x,t) = N(\xi), \quad v(x,t) = V(\xi), \tag{4.9}$$

where $\xi := x - ct$ and $c > 0$. Note that ξ is also known as the travelling wave variable. Substituting (4.9) into system (4.6) - (4.8) yields the travelling wave system:

$$\frac{\mathrm{d}}{\mathrm{d}\xi}\left[(1-V)\frac{\mathrm{d}U}{\mathrm{d}\xi}\right] + c\frac{\mathrm{d}U}{\mathrm{d}\xi} + U(1-U-N-V) - \theta UN = 0, \tag{4.10}$$

$$D\frac{\mathrm{d}}{\mathrm{d}\xi}\left[(1-V)\frac{\mathrm{d}N}{\mathrm{d}\xi}\right] + c\frac{\mathrm{d}N}{\mathrm{d}\xi} + rN(1-U-N-V) + \theta UN - \gamma N = 0, \tag{4.11}$$

$$c\frac{\mathrm{d}V}{\mathrm{d}\xi} - \phi_1 UV - \phi_2 NV + \psi V(1-U-N-V) = 0. \tag{4.12}$$

The steady states of this system are $(U, N, V) = E_i$, $i = 0, 1, 2, \ldots, 6$, where

$$E_0 = (0,0,0), \quad E_1 = (1,0,0), \quad E_2 = (0,0,1), \quad E_3 = \left(0, 1-\frac{\gamma}{r}, 0\right),$$

$$E_4 = \left(0, \frac{\gamma\psi}{r\phi_2}, 1-\frac{\gamma}{r}-\frac{\psi\gamma}{r\phi_2}\right), \quad E_5 = (U_1^*, N_1^*, V_1^*), \quad E_6 = (U_2^*, N_2^*, V_2^*),$$

where

$$\begin{cases} N_1^* &= \dfrac{\theta-\gamma}{\theta^2-\theta r+\theta} \\ U_1^* &= \dfrac{\gamma - r\theta N_1^*}{\theta} \\ V_1^* &= 0, \end{cases} \qquad \begin{cases} N_2^* &= \dfrac{\phi_1\gamma}{\theta(r\phi_1+\psi\theta-\phi_2)} \\ U_2^* &= \dfrac{\gamma - r\theta N_2^*}{\theta} \\ V_2^* &= 1 - U_2^* - (\theta+1)N_2^*. \end{cases}$$

We summarize the biological meaning and conditions for existence of the above steady states in Table 4.1. Since we are considering only biologically meaningful steady states, the condition for existence is non-negativity (and in some cases, positivity) of the coordinates.

Table 4.1: Positive Steady States: Conditions for Existence

Steady State	Biological Meaning	Existence
E_0	extinction of tumour cells and healthy cells	Always
E_1	uninfected tumour cells dominate – treatment unsuccessful	Always
E_2	extinction of tumour cells – treatment successful	Always
E_3	infected tumour cells dominate – treatment semi-successful	$r > \gamma$
E_4	extinction of uninfected tumour cells – treatment semi-successful	$r\phi_2 > \gamma\phi_2 + \gamma\psi$
E_5	degradation of healthy tissue – treatment potentially successful	A
E_6	coexistence of tumour cells and healthy cells – treatment potentially successful	B

Note that the conditions A and B in Table 4.1. are given by

$$A: \quad \theta > \gamma \quad \text{AND} \quad r\theta < \gamma(\theta + 1),$$

$$B: \quad \phi_2 < \psi\theta \quad \text{AND} \quad \theta\gamma(\psi + \phi_1) + \gamma\phi_1 + \theta\phi_2 < r\theta\phi_1 + \psi\theta^2 + \gamma\phi_2.$$

In order to investigate the existence of TWS, we prescribe appropriate boundary conditions. The existence of some TWS are trivial. For example, consider a solution connecting the steady states E_1 to E_0. That is,

$$\lim_{\xi\to-\infty}[U, N, V]^T = [1, 0, 0]^T, \quad \lim_{\xi\to\infty}[U, N, V]^T = [0, 0, 0]^T.$$

A solution with these boundary conditions exists on the line $N = V = 0$. Indeed, setting $N = V = 0$ transforms equation (4.6) into the classic Fisher-KPP reaction-diffusion equation [12]. It is well known [12] that for all $c \geq 2$, there exists a solution of system (4.10) - (4.12) connecting the steady states E_1 and E_0. Biologically, this represents a solution which approaches E_1 as $t \to \infty$. Hence, this is an example of an invasion wave, in which the uninfected tumour cells dominate in the long term. This is not surprising, as we are dealing with the case of no treatment *and* no healthy surrounding tissue. Indeed, in reverse time, we have a system which

approaches an extinction equilibrium (the origin) which is biologically meaningless. Hence, we are not interested in such TWS involving the origin as a boundary condition.

In the following subsections, we will specify relevant biological boundary conditions on the TWS. Note that system (4.10) - (4.12) is singular at $V = 1$ as a result of the cross-dependent diffusion. Following the approach outlined in [6, 11, 13, 15], we remove the singularity by introducing the variable $\zeta := G(\xi)$, defined as a solution of the differential equation

$$\frac{\mathrm{d}\zeta}{\mathrm{d}\xi} = \frac{1}{1 - V(\xi)} = G'(\xi) \tag{4.13}$$

for all $\xi \in (-\infty, \infty)$. We define the new dependent variables as

$$\mathcal{U}(\zeta) := U(G^{-1}(\xi)), \quad \mathcal{N}(\zeta) := N(G^{-1}(\xi)), \quad \mathcal{V}(\zeta) := V(G^{-1}(\xi)). \tag{4.14}$$

From the chain rule, it follows that system (4.10) - (4.12) may be re-written, in terms of the new independent variable, as

$$\frac{\mathrm{d}^2\mathcal{U}}{\mathrm{d}\zeta^2} + c\frac{\mathrm{d}\mathcal{U}}{\mathrm{d}\zeta} + (1 - \mathcal{V})\left[\mathcal{U}(1 - \mathcal{U} - \mathcal{N} - \mathcal{V}) - \theta\mathcal{U}\mathcal{N}\right] = 0, \tag{4.15}$$

$$D\frac{\mathrm{d}^2\mathcal{N}}{\mathrm{d}\zeta^2} + c\frac{\mathrm{d}\mathcal{N}}{\mathrm{d}\zeta} + (1 - \mathcal{V})\left[r\mathcal{N}(1 - \mathcal{U} - \mathcal{N} - \mathcal{V}) + \theta\mathcal{U}\mathcal{N} - \gamma\mathcal{N}\right] = 0, \tag{4.16}$$

$$c\frac{\mathrm{d}\mathcal{V}}{\mathrm{d}\zeta} + (1 - V)V\left[-\phi_1\mathcal{U} - \phi_2\mathcal{N} + \psi(1 - \mathcal{U} - \mathcal{N} - \mathcal{V})\right] = 0. \tag{4.17}$$

Note that all of the steady states of the original travelling wave ODE system are also steady states of system (4.15) - (4.17). Since $0 \leq V < 1$ for initial conditions in the region $0 \leq V < 1$ (this can be seen using a comparison argument, similar to the one employed in Chapter 3), then it follows from equation (4.13) that $\zeta'(\xi) > 0$. That is, ζ is a monotonically increasing function of ξ. Therefore, the transformations in (4.14) preserve the orientations of the trajectories of (4.10) - (4.12). This means that a solution of system (4.10) - (4.12) that connects steady states

E_i and E_j is topologically equivalent to a solution of system (4.15) - (4.17) that connects steady states E_i and E_j.

It is worthwhile to note that system (4.15) - (4.17), due to the transformation, also contains an additional plane of steady states, $\{(\bar{u}, \bar{n}, 1) : \bar{u}, \bar{n} \in \mathbb{R}\}$. These steady states are not biologically relevant and will not be considered.

In the following subsections, we consider two separate cases. First, we consider the case in which the tumour cells are allowed to proliferate in the absence of any treatment by setting $\mathcal{N} = 0$ in Subsection 4.2.1. This reduces our system to a two-variable system. In contrast to previous papers [6, 11, 13], we account for the impact of the competition between melanoma cells and the healthy tissue on the growth and spread of the tumour. In Subsection 4.2.2, we consider the case with OV treatment. In performing a travelling wave analysis, we need to specify relevant boundary conditions. That is, we choose two steady states E_i and E_j such that a solution of system (4.10) - (4.12) satisfies

$$\lim_{\xi \to -\infty} (U(\xi), N(\xi), V(\xi) = E_i, \quad \lim_{\xi \to \infty} (U(\xi), N(\xi), V(\xi)) = E_j, \tag{4.18}$$

or, equivalently, a solution of system (4.15) - (4.17) satisfies

$$\lim_{\zeta \to -\infty} (\mathcal{U}(\zeta), \mathcal{N}(\zeta), \mathcal{V}(\zeta)) = E_i, \quad \lim_{\zeta \to \infty} (\mathcal{U}(\zeta), \mathcal{N}(\zeta), \mathcal{V}(\zeta)) = E_j. \tag{4.19}$$

We may write system (4.15) - (4.17) as a system of first-order ODEs by setting $\mathcal{W}(\zeta) := \mathcal{U}'(\zeta)$ and $\mathcal{M}(\zeta) := D\mathcal{N}'(\zeta)$. This yields

$$\frac{\mathrm{d}\mathcal{U}}{\mathrm{d}\zeta} = \mathcal{W}, \tag{4.20}$$

$$\frac{\mathrm{d}\mathcal{W}}{\mathrm{d}\zeta} = -c\mathcal{W} + (\mathcal{V} - 1)\left[\mathcal{U}(1 - \mathcal{U} - \mathcal{N} - \mathcal{V}) - \theta\mathcal{U}\mathcal{N}\right], \tag{4.21}$$

$$\frac{\mathrm{d}\mathcal{N}}{\mathrm{d}\zeta} = \frac{1}{D}\mathcal{M}, \tag{4.22}$$

$$\frac{\mathrm{d}\mathcal{M}}{\mathrm{d}\zeta} = -c\mathcal{M} + (\mathcal{V}-1)\left[r\mathcal{N}(1-\mathcal{U}-\mathcal{N}-\mathcal{V}) + \theta\mathcal{U}\mathcal{N} - \gamma\mathcal{N}\right], \tag{4.23}$$

$$\frac{\mathrm{d}\mathcal{V}}{\mathrm{d}\zeta} = \frac{1}{c}\mathcal{V}(\mathcal{V}-1)\left[-\phi_1\mathcal{U} - \phi_2\mathcal{N} + \psi(1-\mathcal{U}-\mathcal{N}-\mathcal{V})\right]. \tag{4.24}$$

Computing the Jacobian of this system gives the matrix

$$J(\mathcal{U},\mathcal{W},\mathcal{N},\mathcal{M},\mathcal{V}) = \begin{pmatrix} 0 & 1 & 0 & 0 & 0 \\ J_{21} & -c & J_{23} & 0 & J_{25} \\ 0 & 0 & 0 & 1/D & 0 \\ J_{41} & 0 & J_{43} & -c & J_{45} \\ J_{51} & 0 & J_{53} & 0 & J_{55} \end{pmatrix}, \tag{4.25}$$

where

$$\begin{aligned}
J_{21} &= (\mathcal{V}-1)(1-2\mathcal{U}-\mathcal{N}-\mathcal{V}-\theta\mathcal{N}),\\
J_{23} &= -(\theta+1)(\mathcal{V}-1)\mathcal{U},\\
J_{25} &= 2\mathcal{U} - \mathcal{U}^2 - (\theta+1)\mathcal{U}\mathcal{N} - 2\mathcal{U}\mathcal{V},\\
J_{41} &= (\theta-r)(\mathcal{V}-1)\mathcal{N},\\
J_{43} &= (\mathcal{V}-1)(r - r\mathcal{U} - 2r\mathcal{N} - r\mathcal{V} + \theta\mathcal{U} - \gamma),\\
J_{45} &= 2r\mathcal{N} - (r-\theta)\mathcal{U}\mathcal{N} - r\mathcal{N}^2 - \gamma\mathcal{N} - 2r\mathcal{N}\mathcal{V},\\
J_{51} &= \frac{1}{c}(\phi_1+\psi)\mathcal{V}(1-\mathcal{V}),\\
J_{53} &= \frac{1}{c}(\phi_2+\psi)\mathcal{V}(1-\mathcal{V}),\\
J_{55} &= \frac{1}{c}(2\mathcal{V}-1)(-\phi_1\mathcal{U} - \phi_2\mathcal{N} + \psi - \psi\mathcal{U} - \psi\mathcal{N}) - \frac{\psi}{c}(3\mathcal{V}^2 - 2\mathcal{V}).
\end{aligned}$$

We are now in a position to investigate the existence of TWS under different conditions. These solutions represent the transition of the biological system from one state to another. While total eradication of the cancer is not generally possible, the general goal is to find conditions on the

model parameters which can optimize the treatment outcomes.

4.2.1 Dynamics of the Travelling Wave ODE System – Case I: No OV

We first consider the case in which there is no OV treatment, i.e., $\mathcal{N} = 0$. Then system (4.20) - (4.24) is reduced to

$$\mathcal{U}'(\zeta) = \mathcal{W}, \tag{4.26}$$

$$\mathcal{W}'(\zeta) = -c\mathcal{W} + \mathcal{U}(\mathcal{V} - 1)(1 - \mathcal{U} - \mathcal{V}), \tag{4.27}$$

$$\mathcal{V}'(\zeta) = \frac{1}{c}\mathcal{V}(\mathcal{V} - 1)[-\phi_1\mathcal{U} + \psi(1 - \mathcal{U} - \mathcal{V})]. \tag{4.28}$$

Similar models of tumour growth were investigated in [6, 13]. However, we have the additional consideration ψ, which reflects the regeneration of the healthy skin cells. Unlike those previous papers, we analyze this system by applying LaSalle's invariance principle to show that TWS of system (4.26) - (4.28) asymptotically approach a tumour-extinction steady state as $\zeta \to \infty$.

We seek solutions satisfying the boundary conditions

$$\begin{cases} \lim\limits_{\zeta\to-\infty}[\mathcal{U}, \mathcal{W}, \mathcal{V}]^T = [1, 0, 0]^T, \quad (E_1), \\ \lim\limits_{\zeta\to\infty}[\mathcal{U}, \mathcal{W}, \mathcal{V}]^T = [0, 0, 1]^T, \quad (E_2). \end{cases} \tag{4.29}$$

From the Jacobian matrix (4.25), linearizing the system about E_1 gives

$$J(1, 0, 0) = \begin{pmatrix} 0 & 1 & 0 \\ 1 & -c & 1 \\ 0 & 0 & \phi_1/c \end{pmatrix}, \tag{4.30}$$

which has eigenvalues

$$\lambda_1^{E_1} = \frac{-c + \sqrt{c^2+4}}{2}, \quad \lambda_2^{E_1} = \frac{-c - \sqrt{c^2+4}}{2}, \quad \lambda_3^{E_1} = \phi_1/c. \tag{4.31}$$

Hence, E_1 has an unstable manifold of dimension 2. These eigenvalues do not impose any conditions on the wave speed c and we are led to conjecture that, as in [6, 13], there is no minimal wave speed in the no treatment case. It can be shown through standard linearization at this steady state that E_2 is a degenerate stable node (eigenvalues $0, 0, -c$).

By following the techniques of Lemmas 2.5 and 2.6 of [13], with some modifications, it can be shown that there exists a solution of system (4.26) - (4.28) on the unstable manifold of E_1 as $\zeta \to -\infty$. Furthermore, the components $\mathcal{U}$ and $\mathcal{V}$ of this solution remain positive for all $\zeta \in \mathbb{R}$.

We state the existence of a TWS in the special case $\psi = 0$ in the following theorem. Note that this case was previously considered in [11], however the authors did not analytically explore global stability results. In this case, while E_2 remains a steady state, a line of steady states of the form $(\mathcal{U}, \mathcal{W}, \mathcal{V}) = (0, 0, \bar{\mathcal{V}})$ are introduced, where $\bar{\mathcal{V}} \in (0, 1)$. We have the following theorem.

Theorem 4.2.1 *If $\mathcal{N} = 0$, $\psi = 0$, $\phi_1 > 1$, then for all $c > 0$, there exists a TWS of system (4.6) - (4.8) satisfying the boundary condition*

$$\lim_{\zeta \to -\infty} (\mathcal{U}(\zeta), \mathcal{W}(\zeta), \mathcal{V}(\zeta)) = (1, 0, 0),$$

and approaches the set $E_\infty := \{(0, 0, \bar{\mathcal{V}}) : \bar{\mathcal{V}} \in [0, 1]\} \cup \{(\bar{\mathcal{U}}, 0, 1) : \bar{\mathcal{U}} \in [0, 1]\}$ as $\zeta \to \infty$.

Proof Consider the region where $\mathcal{W}$ remains negative, so that $\mathcal{U}$ is monotonically decreasing. We define the variable $\mathcal{Q} := -\mathcal{W}$ so we may consider the positive octant. Then system (4.26)

- (4.28) may be written as

$$\mathcal{U}'(\zeta) = -\mathcal{Q}, \tag{4.32}$$

$$\mathcal{Q}'(\zeta) = -c\mathcal{Q} - \mathcal{U}(\mathcal{V}-1)(1-\mathcal{U}-\mathcal{V}), \tag{4.33}$$

$$\mathcal{V}'(\zeta) = -\frac{\phi_1}{c}\mathcal{U}\mathcal{V}(\mathcal{V}-1). \tag{4.34}$$

Consider a positive solution of this system with initial condition on the unstable manifold in the first octant. Then it is clear that this solution trajectory approaches $(1,0,0)$ as $\zeta \to -\infty$. To complete the proof, we now need only show that the TWS approaches E_∞ as $\zeta \to \infty$.

Define the function $\mathcal{L} : \mathbb{R}^3_+ \to \mathbb{R}$ as

$$\mathcal{L}(\mathcal{U},\mathcal{Q},\mathcal{V}) := \mathcal{U} + \mathcal{Q} + c\left(\mathcal{V} - \ln\mathcal{V} - 1\right).$$

Note that if $\mathcal{V}(0) < 1$, then $\mathcal{V}$ remains bounded above by 1 for all $\zeta > 0$. Furthermore, it is also clear that $\mathcal{L}$ is positive definite. Differentiating the function $\mathcal{L}$ yields

$$\begin{aligned}\frac{\mathrm{d}\mathcal{L}}{\mathrm{d}\zeta} &= -\mathcal{Q} - c\mathcal{Q} - \mathcal{U}(\mathcal{V}-1)(1-\mathcal{U}-\mathcal{V}) + (\mathcal{V}-1)^2[-\phi_1\mathcal{U}] \\ &\leq -\mathcal{U}^2(1-\mathcal{V}) + \mathcal{U}(1-\mathcal{V})^2 - \phi_1\mathcal{U}(1-\mathcal{V})^2.\end{aligned}$$

Since $\mathcal{V} \leq 1$ and $\mathcal{U} \geq 0$, it follows that $-\mathcal{U}^2(1-\mathcal{V}) \leq 0$. Hence,

$$\frac{\mathrm{d}\mathcal{L}}{\mathrm{d}\zeta} \leq \mathcal{U}(1-\mathcal{V})^2(1-\phi_1) \leq 0,$$

since $\phi_1 > 1$. It is clear that on the set E_∞, $\dot{\mathcal{L}} = 0$ and that E_∞ is a positively invariant with respect to system (4.32) - (4.34). Hence, since E_∞ is the largest positively invariant subset of E_∞ with respect to this system, we conclude by LaSalle's invariance principle that all trajectories

must approach the set E_∞ as $\zeta \to \infty$. ∎

Remark 4.2.1 *Using a modified version of the function $\mathcal{L}$ in Theorem 4.2.1, it can be shown that the condition $\phi_1 > 1$ is not necessary for the existence of a TWS. Instead, we could impose the condition $c < \phi_1$.*

Biologically, the condition $\phi_1 > 1$ in Theorem 4.2.1 shows that with a sufficiently large degradation rate of the healthy tissue, there will exist some invasion wave, in which the tumour cells dominate in the long-term. Note that the set of steady states of the form $(\bar{\mathcal{U}}, 0, 1)$ do not correspond to steady states of the original travelling wave ODE system. The biological consequence of Theorem 4.2.1 is the long-term degradation of the healthy tissue, as solutions move away from steady states of the form $(0, 0, \bar{\mathcal{V}})$ as $t \to \infty$. The TWS guaranteed by Theorem 4.2.1 approaches the tumour-dominant steady state E_1 as $t \to \infty$, representing an invasion wave.

We now return to the case $\psi > 0$. We seek TWS satisfying the boundary conditions (4.29). We consider this case in the following numerical simulations. Figure 4.1 is obtained by solving the non-dimensionalized OV-free PDE model assuming no flux boundary conditions and initial conditions with compact support. More details on this are provided in Section 4.3.

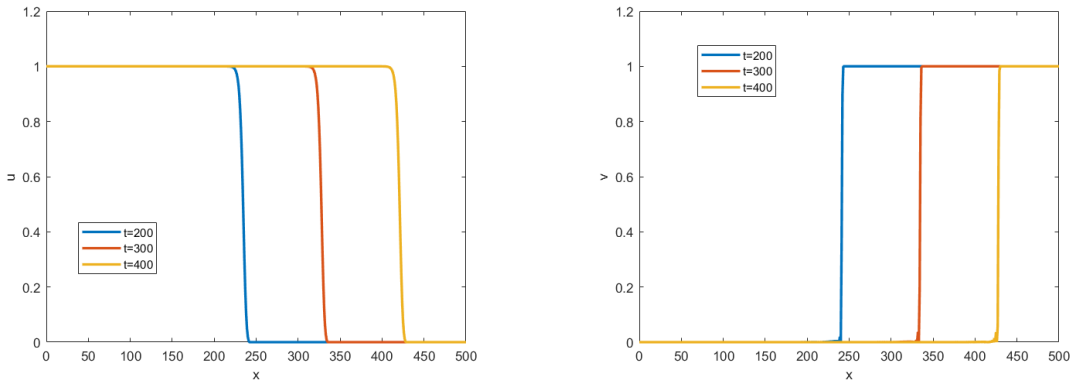

(a) Uninfected Tumour Cell Density. (b) Healthy Skin Cell Density.

Figure 4.1: TWS connecting E_1 and E_2 in the case of no OV treatment.

We have illustrated that even for a positive rate of regeneration of the healthy skin cells,

ψ, an invasion wave still exists. This further suggests the need for therapeutic intervention to potentially avoid a TWS representing complete invasion of the uninfected tumour cells.

4.2.2 Dynamics of the Travelling Wave ODE System – Case II: OV Treatment

We now consider the original system (4.10) - (4.12), the no OV treatment case. When referencing a steady state, E_j, for the remainder of this subsection, we add two additional zero components – the $\mathcal{W}$ and $\mathcal{M}$ components – to the steady state. For example, we now consider E_1 to mean $(1,0,0,0,0)$, E_2 to mean $(0,0,0,0,1)$, etc.

Since we are dealing with a five-variable system, analytically proving the existence of a TWS is a challenging task due to the difficulty of establishing global stability results. We approach this problem mainly by using a numerical approach while also analytically establishing some auxiliary local results about the steady states. In certain cases, we are able to analytically rule out the existence of TWS – doing this also has relevant biological significance. The local analysis can also provide guidance for performing numerical simulations.

An important outcome of treatment is the existence of a wave connecting E_1 to another steady state, which approaches E_1 as $\zeta \to \infty$. Such a TWS reflects a transition from full cancer cell dominance to a milder outcome. Finding conditions which rule out such a TWS can give guidance on how to avoid failure of the treatment. That is, we seek to rule out solutions which converge to the tumour-dominant steady state $(\mathcal{U},\mathcal{W},\mathcal{N},\mathcal{M},\mathcal{V}) = (1,0,0,0,0)$ as $\zeta \to \infty$. Linearizing the system about this point yields

$$J(1,0,0,0,0) = \begin{pmatrix} 0 & 1 & 0 & 0 & 0 \\ 1 & -c & \theta+1 & 0 & 1 \\ 0 & 0 & 0 & 1/D & 0 \\ 0 & 0 & \gamma-\theta & -c & 0 \\ 0 & 0 & 0 & 0 & \phi_1/c \end{pmatrix}, \tag{4.35}$$

which has characteristic polynomial

$$P_{E_1}(\lambda) = -\frac{1}{D}\left(\lambda - \frac{\phi_1}{c}\right)\left[D\lambda^4 + 2cD\lambda^3 + (c^2D - D - \gamma + \theta)\lambda^2 + c(\theta - \gamma - D)\lambda + \gamma - \theta\right]$$
$$= -\frac{1}{D}\left(\lambda - \frac{\phi_1}{c}\right)\left(\lambda^2 + c\lambda - 1\right)\left[\lambda^2 + c\lambda + \frac{1}{D}(\theta - \gamma)\right].$$

Hence, the eigenvalues of $J(1,0,0,0,0)$ are

$$\lambda_1^{\bar{E}_1} = \frac{\phi_1}{c}, \quad \lambda_{2,3}^{\bar{E}_1} = \frac{-c \pm \sqrt{c^2+4}}{2} \quad \lambda_{4,5}^{\bar{E}_1} = \frac{1}{2}\left(-c \pm \sqrt{c^2 + \frac{4}{D}(\gamma - \theta)}\right), \tag{4.36}$$

Since $(1,0,0,0,0)$ is an axial/boundary steady state, we rule out oscillations about this point so that the solution remains non-negative. Equivalently, we require that the eigenvalues have zero imaginary part. This is always the case for $\lambda_1^{\bar{E}_1}, \lambda_2^{\bar{E}_1}, \lambda_3^{\bar{E}_1}$. The eigenvalues $\lambda_4^{\bar{E}_1}$ and $\lambda_5^{\bar{E}_1}$ are non-real complex numbers if

$$c^2 + \frac{4}{D}(\gamma - \theta) < 0.$$

Since we consider $c > 0$, this inequality never holds if $\gamma \geq \theta$. On the other hand, if $\gamma < \theta$, then this inequality holds if

$$c < \frac{2}{\sqrt{D}}\sqrt{\theta - \gamma}.$$

In this case, we may rule out the existence of a TWS which converges to E_1 as $\zeta \to \infty$. We summarize this result in the following proposition.

Proposition 4.2.1 *System (4.6) - (4.8) has no non-negative invasion wave TWS connecting any steady state to E_1 if $\theta > \gamma$ and*

$$0 < c < \frac{2}{\sqrt{D}}\sqrt{\theta - \gamma}. \tag{4.37}$$

Remark 4.2.2 *Proposition 4.2.1 contains a very frequently occurring assumption: an infection rate which is greater than the oncolysis rate. The speed with which a transition away from*

the cancer-dominant steady state occurs is bounded below and this bound increases with an increasing gap between the infection rate and the oncolysis rate.

We can similarly rule out the existence of TWS when considering the steady state E_3. From Table 4.1, this steady state is biologically relevant when $r > \gamma$. In this case, the tumour cells dominate, but all of the tumour cells are infected by the OV. This treatment may be considered semi-successful if $\gamma \approx r$. Biologically, this represents a virus which is almost as potent in its oncolytic efficiency as the infected tumour cells are at proliferation.

We omit the details (as they are simply more tedious versions of the calculations performed for E_1) and summarize the result in the following proposition.

Proposition 4.2.2 *System (4.6) - (4.8) has no non-negative TWS satisfying* $\lim_{\zeta\to\infty}(\mathcal{U}, \mathcal{N}, \mathcal{V}) = E_3$ *if* $(\theta + 1)\gamma > r\theta$ *and*

$$0 < c < \frac{2}{\sqrt{r}}\sqrt{(\theta + 1)\gamma - r\theta}. \tag{4.38}$$

The steady state $(\mathcal{U}, \mathcal{W}, \mathcal{N}, \mathcal{M}, \mathcal{V}) = (0, 0, 0, 0, 1)$ is also of biological significance as it represents the healthy (cancer-free) state. Linearizing about this point yields the matrix $J(0, 0, 0, 0, 1)$ which has eigenvalues $-c$ (of algebraic multiplicity 2) and 0 (of algebraic multiplicity 3). Hence, this steady state is a degenerate stable node for all parameter values. As can be seen in the accompanying numerical simulations, we find that the TWS which we investigate converge to the healthy steady state. Therefore, the long-term behaviour of solutions is to tend away from the healthy state. This indicates that rather than seeking complete eradication of the cancer, we should optimize the treatment by minimizing the asymptotic tumour cell density.

When analyzing the existence of TWS of the OV treatment model, the primary difficulty arises from the fact that we are dealing with a system in $\mathbb{R}^5$. We will consider solutions which approach E_1 or E_3 as $\zeta \to -\infty$. Note again that $\mathcal{V}$ remains positive and bounded above by 1 if at any point $\mathcal{V}(\zeta_0) < 1$. Based on simulation results, we conjecture that there exists a solution trajectory on the unstable manifold of E_j, where $j = 1, 3$, for which the tumour

cell densities remain positive. We assume that this conjecture is true in order to prove the subsequent theorem.

Theorem 4.2.2 *Assume that there exists a solution trajectory on the unstable manifold of E_j, where $j = 1, 3$, for which the components $\mathcal{U}$ and $\mathcal{N}$ remain positive for all $\zeta \in \mathbb{R}$. If $\psi = 0$, $\phi_1 > 1$, and $\phi_2 > r$, then for all $c > 0$, there exists a TWS of system (4.6) - (4.8) satisfying the boundary condition*

$$\lim_{\zeta \to -\infty} (\mathcal{U}(\zeta), \mathcal{W}(\zeta), \mathcal{N}(\zeta), \mathcal{M}(\zeta), \mathcal{V}(\zeta)) = E_j, \quad j \in \{1, 3\}$$

and approaches the set $\tilde{E}_\infty := \{(0, 0, 0, 0, \bar{\mathcal{V}}) : \bar{\mathcal{V}} \in [0, 1]\} \cup \{(\bar{\mathcal{U}}, 0, \bar{\mathcal{N}}, 0, 1) : \bar{\mathcal{U}}, \bar{\mathcal{N}} \in [0, 1]\}$ as $\zeta \to \infty$.

Proof Consider the region where $\mathcal{W}$ and $\mathcal{M}$ remain negative, so that $\mathcal{U}$ and $\mathcal{N}$ are monotonically decreasing. We define the variables $\mathcal{Q} := -\mathcal{W}$ and $\mathcal{S} := -\mathcal{M}$ so we may instead consider solutions with non-negative components. Then system (4.20) - (4.24) may be written as

$$\mathcal{U}'(\zeta) = -\mathcal{Q}, \tag{4.39}$$

$$\mathcal{Q}'(\zeta) = -c\mathcal{Q} - (\mathcal{V} - 1)\left[\mathcal{U}(1 - \mathcal{U} - \mathcal{N} - \mathcal{V}) - \theta\mathcal{U}\mathcal{N}\right], \tag{4.40}$$

$$\mathcal{N}'(\zeta) = -\frac{1}{D}\mathcal{S}, \tag{4.41}$$

$$\mathcal{S}'(\zeta) = -c\mathcal{S} - (\mathcal{V} - 1)\left[r\mathcal{N}(1 - \mathcal{U} - \mathcal{N} - \mathcal{V}) + \theta\mathcal{U}\mathcal{N} - \gamma\mathcal{N}\right], \tag{4.42}$$

$$\mathcal{V}'(\zeta) = \frac{1}{c}\mathcal{V}(\mathcal{V} - 1)\left[-\phi_1\mathcal{U} - \phi_2\mathcal{N}\right]. \tag{4.43}$$

We assume our conjecture on the positivity of a solution with initial condition on the unstable manifold of E_j holds. To show that such a solution converges approaches $\tilde{E}_\infty$ as $\zeta \to \infty$, we

define the function $\mathcal{L} : \mathbb{R}^5_+ \to \mathbb{R}$ as

$$\mathcal{L}(\mathcal{U}, \mathcal{Q}, \mathcal{N}, \mathcal{S}, \mathcal{V}) := \mathcal{U} + \mathcal{Q} + \mathcal{N} + \mathcal{S} + c\,(\mathcal{V} - \ln \mathcal{V} - 1)\,.$$

It is clear that this function is positive definite and satisfies $\mathcal{L}(E_2) = 0$. Differentiating this function yields

$$\frac{\mathrm{d}\mathcal{L}}{\mathrm{d}\zeta} = -(1+c)\mathcal{Q} - [\mathcal{U}^2 + (1+r)\mathcal{U}\mathcal{N} + r\mathcal{N}^2 - \gamma\mathcal{N}](1-\mathcal{V}) - \left(\frac{1}{D} + c\right)\mathcal{S} + \ldots$$

$$\cdots + (\mathcal{U} + r\mathcal{N})(1-\mathcal{V})^2 - (\phi_1 U + \phi_2 \mathcal{N})(1-\mathcal{V})^2$$

$$\leq (1-\phi_1)\mathcal{U}(1-\mathcal{V})^2 + (r-\phi_2)\mathcal{N}(1-\mathcal{V})^2.$$

Since $\phi_1 > 1$ and $\phi_2 > r$, it follows that $\mathcal{L}'(\zeta) \leq 0$. It is clear that on the set $\tilde{E}_\infty$, $\dot{\mathcal{L}} = 0$ and that $\tilde{E}_\infty$ is positively invariant with respect to system (4.39) - (4.43), making it the largest positively invariant subset of $\tilde{E}_\infty$. Hence, by LaSalle's invariance principle, we conclude that all trajectories must approach the set $\tilde{E}_\infty$ as $\zeta \to \infty$. ∎

Remark 4.2.3 *An important corollary of Theorem 4.2.2 is that any positive TWS will necessarily approach to $\tilde{E}_\infty$ as $\zeta \to \infty$, i.e., as $t \to -\infty$. Hence, for sufficiently large degradation rates, ϕ_1 and ϕ_2, any TWS will result (at least) in partial degradation of the healthy tissue. This is even true in the case of OV treatment. As a consequence, the modelling suggests that we should consider treatment as a method of reducing the extent of spread rather than a method of completely eradicating the tumour cells.*

We now investigate the existence of a TWS satisfying the conditions

$$\begin{cases} \lim\limits_{\zeta \to -\infty} [\mathcal{U}, \mathcal{W}, \mathcal{N}, \mathcal{M}, \mathcal{V}]^T = [U_1^*, 0, N_1^*, 0, 0]^T, \\ \lim\limits_{\zeta \to \infty} [\mathcal{U}, \mathcal{W}, \mathcal{N}, \mathcal{M}, \mathcal{V}]^T = [0, 0, 0, 0, 1]^T. \end{cases} \tag{4.44}$$

where U_1^* and N_1^* come from E_5. A TWS satisfying these boundary conditions is also an invasion wave, but may represent a favourable treatment outcome if the tumour cells density at the steady state, $U_1^* + N_1^*$, is significantly low. To maintain the existence of this steady state, we require that the conditions given by A in Table 4.1 be satisfied, i.e., $r\theta/(\theta + 1) < \gamma < \theta$. Consistent with all of our prior results, these inequalities reflect the importance of a virus-induced death rate that is not too large nor too small. We numerically verify the existence of a TWS in Figure 4.2.

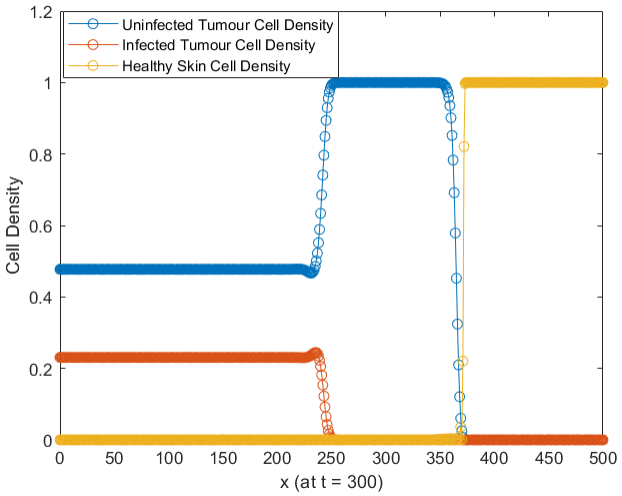

Figure 4.2: TWS connecting E_5 and E_2. The sum of the values of the blue and red curves at $x = 0$ give the total tumour cell density as $\zeta \to -\infty$, or equivalently, as $t \to \infty$. If this value is below the carrying capacity, this represents a significantly successful treatment outcome.

Figure 4.2 is obtained by solving the non-dimensionalized five-variable PDE model assuming no flux boundary conditions and initial conditions with compact supports. The above figure shows the solution at $t = 300$. This treatment outcome may be considered semi-successful as the tumour cell density approaches a value below the carrying capacity as $t \to \infty$. Biologically, the condition $\gamma < \theta$ has a clear interpretation: The virus must not be too potent at destroying tumour cells relative to its infectious capabilities, as the virus will have less available hosts for the purpose of replication. This is consistent with the results of Chapter 3. The condition $r\theta/(\theta + 1) < \gamma$ reflects that the oncolysis rate must also not be too small for this outcome to occur – this result is also consistent with Chapter 3.

We seek to bound the total tumour cell density, $U_1^* + N_1^*$ at the tumour dominant-steady state:

$$U_1^* + N_1^* = \frac{\theta - \gamma}{\theta^2 - r\theta + \theta} + \frac{\gamma - r\theta\left(\frac{\theta - \gamma}{\theta^2 - r\theta + \theta}\right)}{\theta} \leq \frac{\theta - \gamma}{\theta^2}(1 - r) + \frac{\gamma}{\theta} \leq \frac{\gamma + 1}{\theta}.$$

It can now be seen that we may improve the treatment outcome by increasing θ and ensuring that γ remains in the interval $\gamma \in (r\theta/(\theta + 1), \theta)$. This once again illustrates the delicate balance between oncolysis and infection capabilities in oncolytic virotherapy. Note that this upper bound is only clinically useful in the case $\gamma + 1 < \theta$ to ensure that the total tumour cell density does not exceed the carrying capacity.

Figure 4.3 shows that increasing θ, while ensuring that γ is appropriately bounded, results in improved treatment outcomes by reducing the long-term tumour cell density. However, interpreting this result requires some care: Simply increasing $\theta \to \infty$ may decrease the tumour burden but it must still be determined whether having an infection rate that is too large may also have toxic effects. Furthermore, the limitations of OV engineering, such as toxicity [4], must also be considered as they may impose upper bounds on θ. Unlike the no treatment case, non-monotonic transient dynamics occur in Figure 4.3. Similar oscillations were also observed in the modelling done in Chapter 3 in the case of constant θ and γ. In all cases, the healthy tissue is eventually degraded as $t \to \infty$, suggesting the need for auxiliary treatment of the skin as a complement to oncolytic virotherapy.

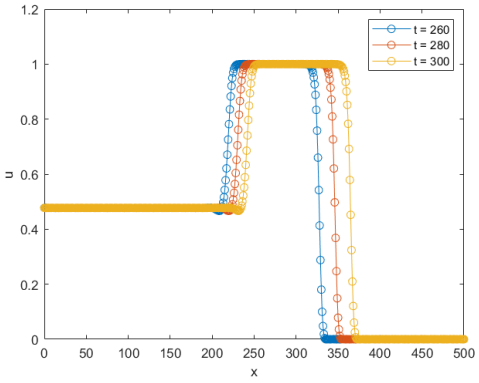

(a) Uninfected Tumour Cell Density, small θ

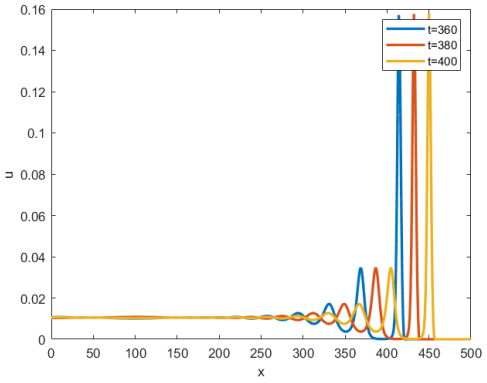

(b) Uninfected Tumour Cell Density, large θ

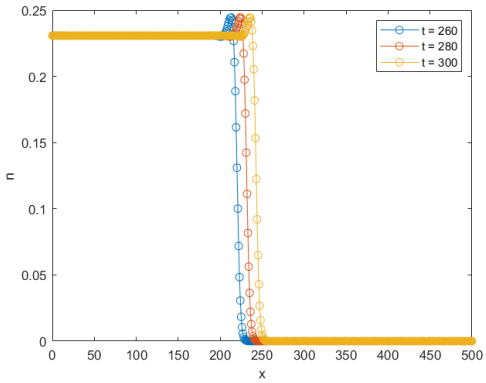

(c) Infected Tumour Cell Density, small θ

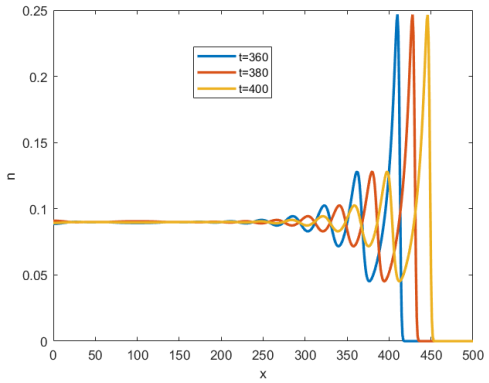

(d) Infected Tumour Cell Density, large θ

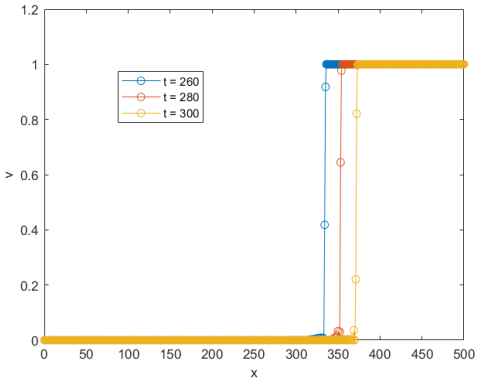

(e) Healthy Skin Cell Density, small θ

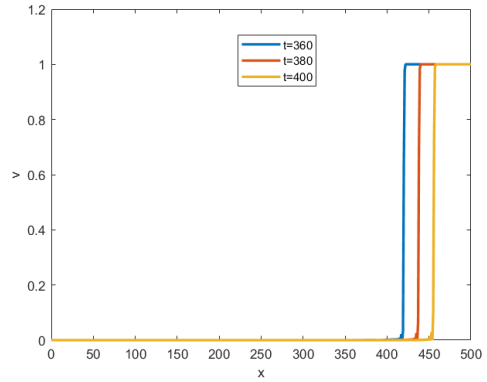

(f) Healthy Skin Cell Density, large θ

Figure 4.3: Solutions of the non-dimensionalized model at various points in time, representing travelling waves. The parameter values (excluding θ and γ) are from Table 4.2. Left column: $\theta = 1.2645$, $\gamma = 0.758$. Right column: $\theta = 10$, $\gamma = 0.5828$.

We propose that the TWS satisfying boundary conditions (4.44) represents a semi-successful treatment outcome for sufficiently large values of θ. While the tumour cells are not completely

eradicated and the healthy skin cells are eventually degraded by the tumour, we may (as previously stated) reduce the total number of tumour cells at the steady state by increasing θ. For example, in Figure 4.3, the total number of tumour cells, $u+n$, as $t \to \infty$ approaches a value of approximately 0.73 for $\theta = 1.2645$ (left column of the figure). On the other hand, increasing θ to a value of 10 results in a decrease of $u+n$ to a value of approximately 0.11 (right column of the figure). While this may lead to promising therapeutic implications, it is important to note that other parameters such as oV toxicity, must be considered. Nonetheless, the modelling once against suggests an important balance between infection rate and oncolysis rate, as in Chapter 3.

Moreover, increasing θ increases the amount of time required for the healthy skin cells to approach the healthy cell-free steady state E_1. Hence, this may be interpreted as follows: If we increase the rate at which the OV may infect the tumour cells when engineering the virus, while maintaining an appropriate bound on the oncolysis rate, we may increase the amount of time required for complete degradation of the healthy tissue.

4.3 Numerical Simulations

In this section, we consider the dimensionalized system, (4.3) - (4.5). The units of u, n, and v are cells/mm^3. We use Matlab's **pdepe** solver to perform the following simulations.

Table 4.2: PDE Model Parameters

Parameter	Parameter Name	Value	Reference
r_1	Growth Rate of Uninfected Tumour Cells	0.3954 day^{-1}	[9]
r_2	Growth Rate of Infected Tumour Cells	0.21 day^{-1}	Estimated
r_3	Regeneration Rate of Healthy Skin Cells	0.0288 day^{-1}	[8]
D_1	Uninfected Tumour Cells Diffusion Coefficient	0.00173 mm^2/day	[7]
D_2	Infected Tumour Cells Diffusion Coefficient	0.00083 mm^2/day	Estimated
K	Skin Cell Carrying Capacity	1.0×10^6 cells/mm^3	[16]
γ	Virus-Induced Death Rate	0.5115 day^{-1}	[16]
θ	Infection Rate	0.001 mm^3 (cells day)$^{-1}$	[16]
ϕ_1	Degradation due to Uninfected Tumour Cells	3.954×10^{-4} mm^3 /(cells day)	[11]
ϕ_2	Degradation due to Infected Tumour Cells	2.1×10^{-4} mm^3 /(cells day)	Estimated

Table 4.2 gives the parameter values we use to numerically integrate the PDE system. We consider a segment of skin which is 5 mm in length. Hence, we solve the system on the domain $(x, t) \in [0, 5] \times [0, t_{\max}]$. As is frequently the case in the modelling of tumour growth and spreading, we consider no flux boundary conditions [2, 10]. That is,

$$\frac{\partial u}{\partial x}(x = 0, t) = \frac{\partial n}{\partial x}(x = 0, t) = 0, \quad t > 0, \tag{4.45}$$

and

$$\frac{\partial u}{\partial x}(x = 5, t) = \frac{\partial n}{\partial x}(x = 5, t) = 0, \quad t > 0. \tag{4.46}$$

We make the natural assumption that the healthy skill cells are initially uniformly distributed

across the 5 mm segment of skin, i.e.,

$$v(x, t = 0) = v_0 \in \mathbb{R}, \quad x \in [0, 5]. \tag{4.47}$$

In our simulations, we assume that the initial tumour cell distributions have compact support. In particular, for $u_0, n_0 \in \mathbb{R}$, we define

$$u(x, t = 0) = u_0[\mathcal{H}(x - \alpha_u) - \mathcal{H}(x - \beta_u)], \quad x \in [0, 5], \tag{4.48}$$

$$n(x, t = 0) = n_0[\mathcal{H}(x - \alpha_n) - \mathcal{H}(x - \beta_n)], \quad x \in [0, 5]. \tag{4.49}$$

where $\mathcal{H}(x)$ is the Heaviside function and $0 < \alpha_i < \beta_i < 5$ for $i = u, n$. These initial conditions correspond to a tumour which is initially contained within the 5 mm skin segment, with uninfected tumour cells spanning a diameter of $\beta_u - \alpha_u$ and infected tumour cells spanning a diameter of $\beta_n - \alpha_n$. In the following simulations, we set $u_0 = 100$ and $v_0 = 10^5$.

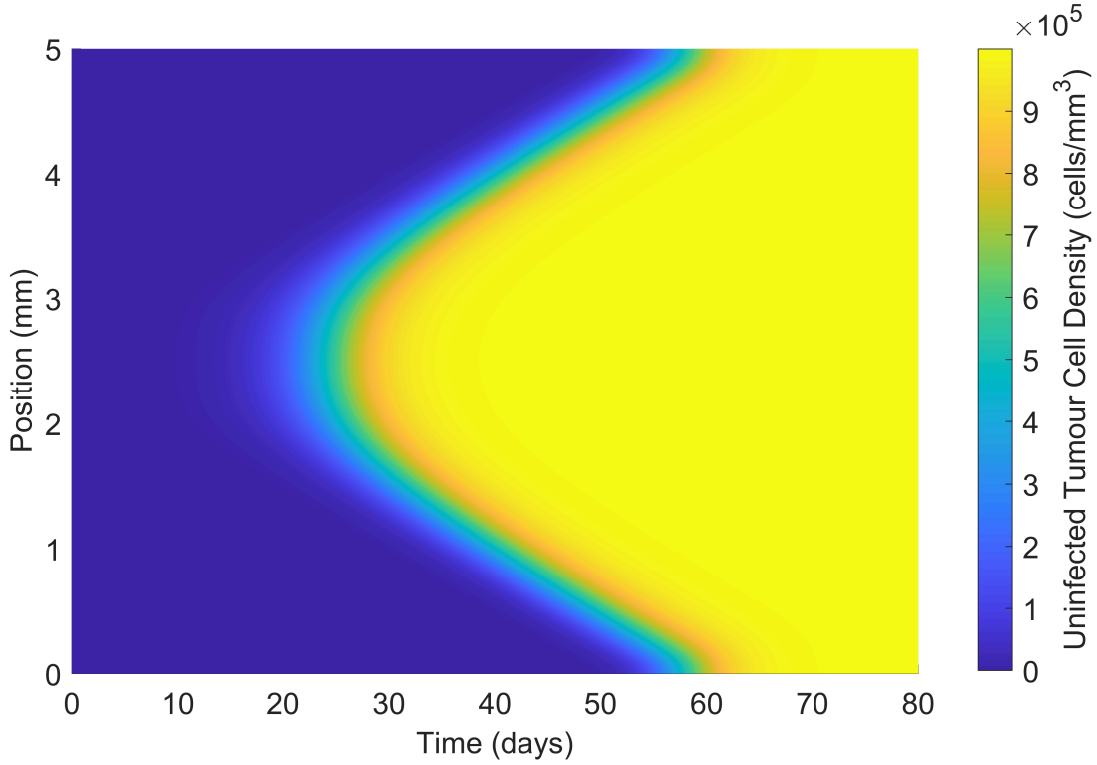

Figure 4.4: Healthy skin cell density in the case of no OV treatment. $n_0 = 0, \alpha_u = 2, \beta_u = 3$.

We begin by considering the case of no OV treatment. To do so, we set $n_0 = 0$ as there are initially no infected cancer cells in this case. Figure 4.4 shows the density of uninfected tumour cells as a function of position and time. Over the course of 80 days, there is a marked increase in the density of tumour cells, from a density of 100 cells/mm^3 to a density which approaches the carrying capacity 10^6 cells/mm^3 at each point in space. This time scale is consistent with results of other models such as [20].

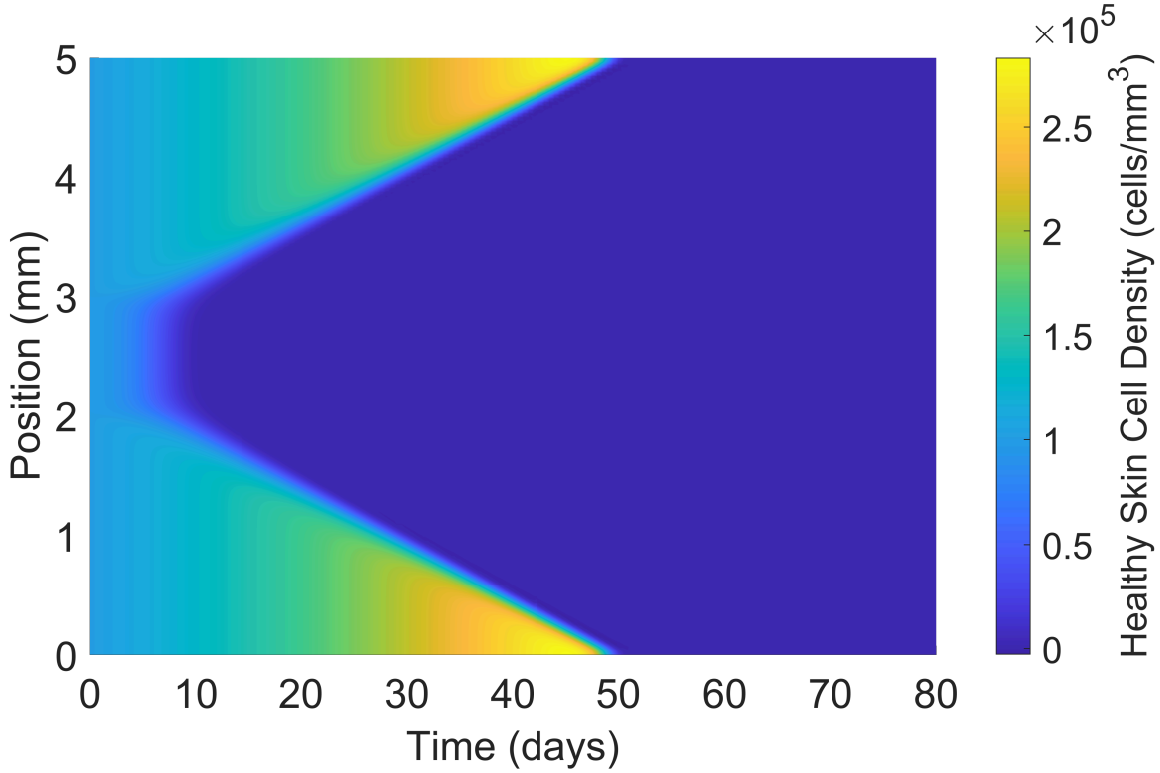

Figure 4.5: Healthy skin cell density in the case of no OV treatment. $n_0 = 0, \alpha_u = 2, \beta_u = 3$.

Figure 4.5 gives the density of healthy skin cells in the case of no OV treatment. Over time, the initially large density of healthy cells are degraded, with larger rates of degradation occurring near the centre of the tumour. Near the boundaries, the healthy skin cells continue to proliferate and approach the carrying capacity due to more limited tumour spread in these areas. This result is not unexpected as the tumour is allowed to grow without any active treatment.

The results in Figures 4.4 and 4.5 show invasion waves in the case of no treatment. The existence of this travelling wave was analytically established in Subsection 4.2.1.

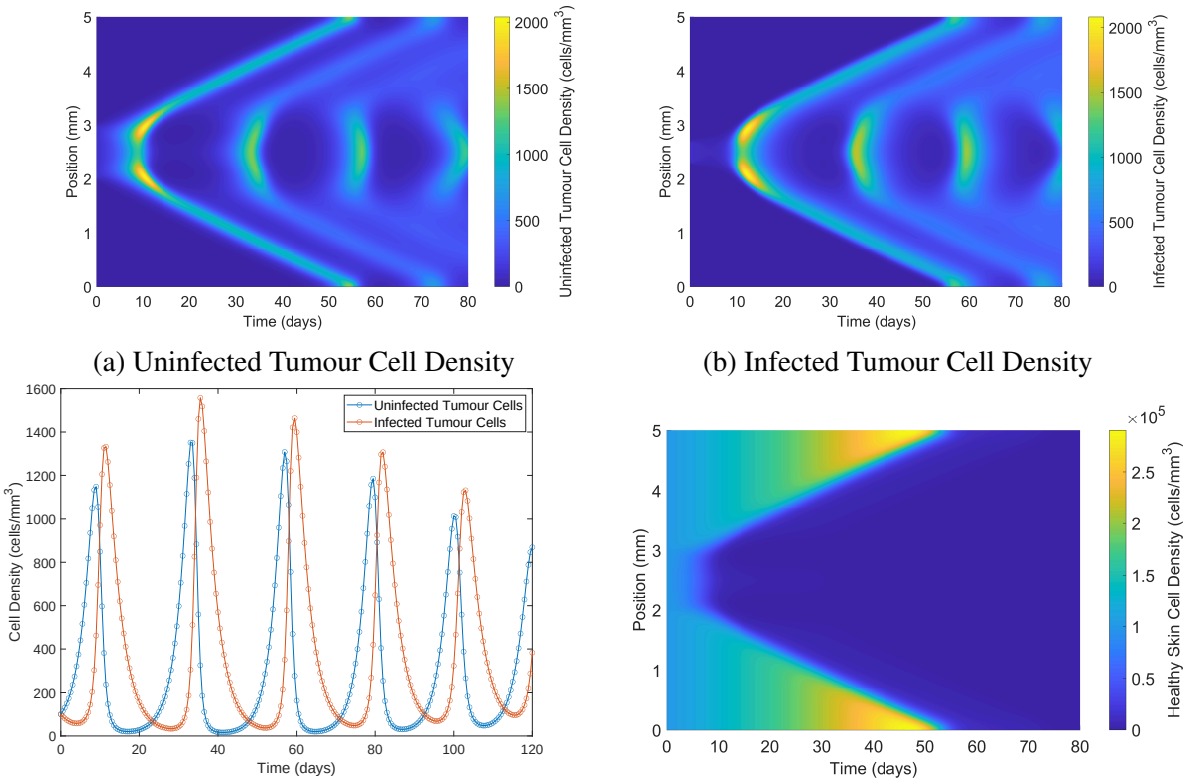

(a) Uninfected Tumour Cell Density

(b) Infected Tumour Cell Density

(c) Tumour Cell Densities at $x = 2.5$ mm

(d) Healthy Skin Cell Density

Figure 4.6: The effect of OV treatment on tumour cell dynamics.

We now consider the case of OV treatment. Figure 4.6 is obtained by setting $n_0 = 100$ cells/mm^3 in the region $2.3 < x < 2.7$. Biologically, this represents the case where an OV has been injected into a 0.4 mm diameter at the centre of the tumour. In Figure 4.6 (a), which shows the density of uninfected tumour cells, there are dampening oscillations of at any given position over the course of 80 days after initial treatment. The tumour is initially found in the $2 < x < 3$ region, a 1 mm region, and proceeds to grow and spread. A small fraction of the tumour cells are initially infected by the OV via injection at the primary site. The infected tumour cells infect the uninfected tumour cell, proliferate, then destroy the tumour cells before proceeding to infected more tumour cells. It can be seen from the figure that the virus is less effective at killing tumour cells which are further away from the centre of the initial primary lesion. While the tumour cells do continue to proliferate, the peak density reached in each wave is monotonically decreasing over the course of 80 days. Figure 4.6 (b) shows the density of tumour cells which

are infected by the OV. Qualitatively, the dynamics of the infected tumour cells mirror those of the uninfected tumour cells, with a small time lag between oscillations. These dynamics are similar to those of an ecological predator-prey system, in which the infected cells require an increase in the density of uninfected cells in order to proliferate.

In Figure 4.6 (c), we plot the evolving densities of uninfected tumour cells and infected tumour cells at the centre of the primary tumour, i.e., position $x = 2.5$, over the course of 120 days after injection. Initially, there is a growth of uninfected tumour cells while the infected tumour cells lag behind. After some time, the virus replicates and causes an increase in the number of infected tumour cells, which are subsequently destroyed via lysis. Once most of the infected cells are destroyed, the tumour is once again able to grow, creating more hosts for the virus. The virus is then once again able to replicate, infecting and killing tumour cells. This cycle continues, with a lower peak of tumour cells after every cycle. This ultimately leads to dampening oscillations, representing a favourable clinical result.

Figure 4.6 (d) shows the density of healthy skin cells in the case of OV treatment. The initial density of healthy cells begins near the carrying capacity, $v_0 = 1.0 \times 10^5$. The tumour cells cause the degradation of the healthy tissue. While the healthy tissue does regenerate, particularly during the time intervals in which the tumour cells have been destroyed by the virus, the growth rate of the healthy cell density is significantly lower than the growth rate of the tumour cells, $r3 << \min\{r_1, r_2\}$. Therefore, even in the case of OV treatment, we see a degradation of the healthy skin due to the slow recovery rate relative to the growth of the cancer. Nevertheless, when compared to Figure 4.5, it can be seen that in the same time interval, there is far greater control of the extent of the disease spread. This result implies the importance of skin regeneration in the control of melanoma. Indeed, maintaining stable healthy skin cell density impedes the spreading of the tumour cells. This model therefore leads us to suggest a greater emphasis on skin regeneration as part of the treatment. This suggestion is also supported by the existing oncology literature [18].

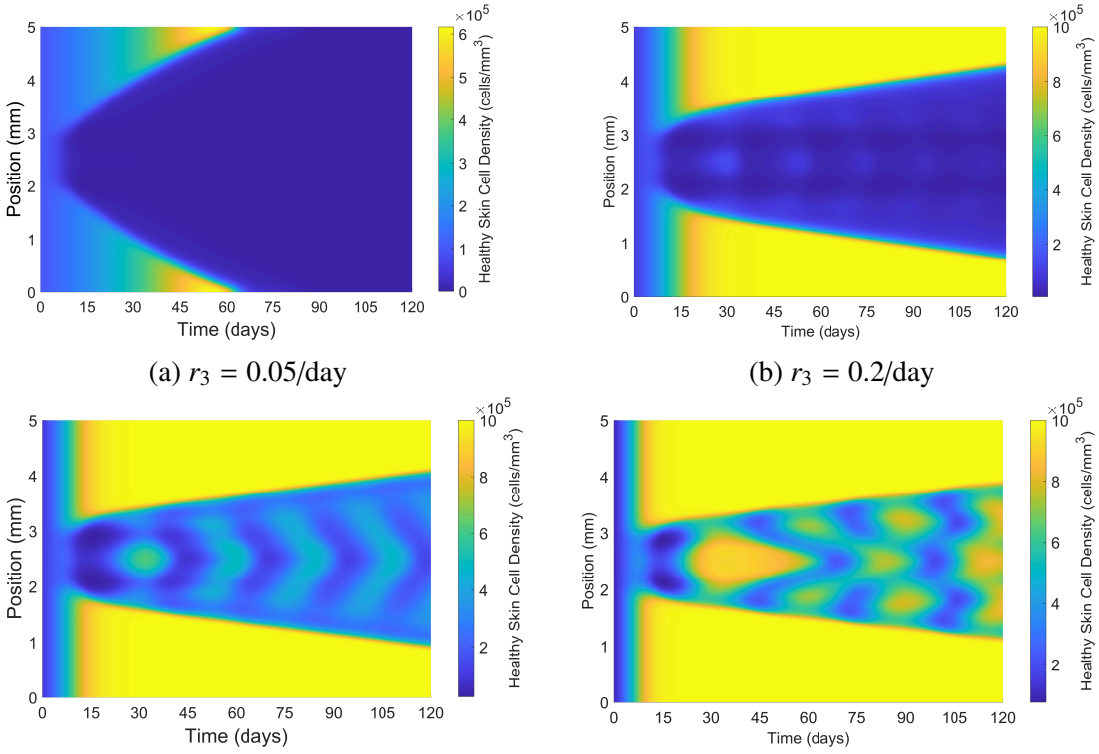

(a) $r_3 = 0.05$/day (b) $r_3 = 0.2$/day

(c) $r_3 = 0.288$/day (d) $r_3 = 0.4$/day

Figure 4.7: The effect of skin regeneration rate on healthy skin cell density.

In Figure 4.7, we consider the effect of the parameter r_3 on the tumour and skin cell densities. Biologically, r_3 represents the rate of skin regeneration and, hence, an increased r_3 may clinically be achieved through processes such as wound dressing as a complement to treatment [18]. In this sense, we may consider r_3 to be a control parameter. Figure 4.7 (a) shows the case of a low value of r_3. In this case, the tumour cells have a significant degradation effect no the healthy tissue. As r_3 is increased, Figure 4.7 (b) shows a marked decrease in the affected region of degradation over the course of 120 days. This trend continues in Figure 4.7 (c), with some regions closer to the centre even achieving some degree of regeneration around days 50, 75, and 100. In Figure 4.7 (d), there is a smaller region of degradation over the course of 120 days and a much larger fraction of the region is able to achieve regeneration, for a more sustained interval of time. These results make the significance of the regeneration rate very clear, not only in terms of healing the previously degraded skin, but of slowing down the rate of spread of the tumour cells.

As in Chapter 3, we also consider the relevance of the infection rate, θ, and the virus induced death rate, γ. The delicate interplay between these parameters can give important direction in terms of engineering effective OVs and this interplay has been the subject of mathematical modelling [1, 3]. We consider the course of treatment over an interval of 80 days, over a 5 mm region. We then compute the maximum number of tumour cells over this region, for different values of the parameters θ and γ. That is,

$$\max_{(x,t)\in[0,5]\times[0,80]} \{u(x,t) + n(x,t)\}.$$

We plot the maximum tumour cell densities in Figure 4.8.

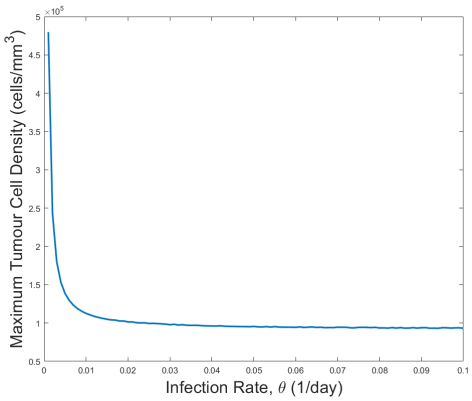

(a) The effect of increasing the infection rate. Constant virus-induced death rate, $\gamma = 0.005115$ day^{-1}.

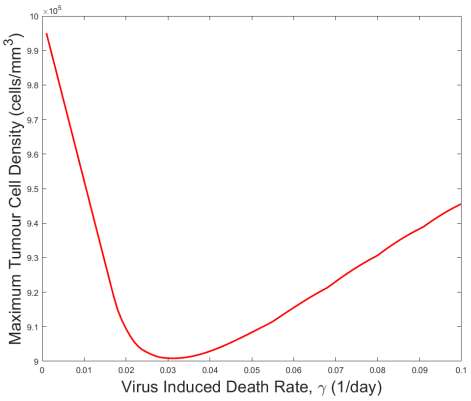

(b) The effect of increasing the virus induced death rate. Constant infection rate, $\theta = 10^{-6}$ mm^3 (cells day)$^{-1}$.

Figure 4.8: The clinical benefit of increasing the infection rate (a) eventually becomes negligible. Increasing the virus induced death rate (b) above some critical value becomes disadvantageous as infected tumour cells die faster than they may infect the uninfected tumour cells.

Figure 4.8 (a) gives the maximum tumour cell density over the course of treatment during the first 80 days as a function of the infection rate, θ. Beyond some critical value, the benefit of further increasing the infection rate becomes negligible. Figure 4.8 (b) shows maximum tumour cell density as a function of the virus induced death rate, γ. In this case, we see a minimal value of maximum tumour cell density occurs at some critical value of γ. Beyond this value, increasing the death rate results in a clinical disadvantage. Biologically, this is due to the

infected tumour cells dying faster than they are able to facilitate infection of adjacent tumour cells. These results are consistent with those of [3] and Chapter 3. The existence of a minimal value as a function of γ suggests that there may exist an optimal oncolysis rate which should be considered when engineering an OV. On the other hand, no such optimal value of θ exists. However, while there may not exist a minimizer, the simulations show that increasing θ too far beyond some threshold value results in diminishing returns in terms of maximal tumour cell density reduction.

The results of this section further enforce the significance of having a virus with an appropriate infection rate and an appropriate oncolysis rate. Furthermore, we have also established the importance of the regeneration rate of the healthy tissue and suggest the use of regenerative skin therapies as auxiliary treatment.

4.4 Conclusion and Discussion

Oncolytic virotherapy continues to show promise in the treatment of metastatic melanoma. Mathematical modelling of the spatial dynamics of OVs can be a useful tool for making clinical predictions of treatment efficacy and for making suggestions regarding genetic engineering of these viruses.

In this chapter we studied a system of partial differential equations which modelled the spread of melanoma tumour cells, both with and without treatment via an OV such as T-Vec. We have contributed to an existing body of literature in the modelling of cancer spreading dynamics. Previous work [11, 6] has been done in the modelling of melanoma growth in the presence of normal healthy cells. We have extended these results by considering the addition of a growth rate, r_3, of the healthy cells and by including a third independent variable, $n(x,t)$, representing the density of tumour cells infected by the OV. Our mathematical and computational results are consistent with both the existing oncology literature and the existing mathematical literature.

In Section 4.2, we performed a travelling wave analysis of the PDE system to study the existence of so-called *invasion waves*, representing the transition of the system from a cancer-free steady state to a healthy-cell free (or cancer dominant) steady state. We found that in the absence of treatment, even with measures taken to regenerate the healthy skin (i.e., increasing ψ), the cancer cells will asymptotically dominate via the existence of invasion waves. In the case of treatment, our results further support the idea of an appropriate balance between the infection rate and the oncolysis rate of the virus. These results were obtained both analytically and numerically. In Section 4.3, we enforced the results of Section 4.2 by numerically solving the PDE model. We also considered the rate of skin regeneration, r_3, and the impact of this parameter on treatment outcomes. Our theoretical results support the use of skin regeneration therapies, such as topical treatments, as complements to the treatment process. This is consistent with some of the existing oncology literature [18].

One of the major limitations of this modelling is the use of a one-dimensional spatial domain. To use of spherical coordinates may be used in order to obtain a greater degree of realism in this respect. Furthermore, the toxicity of OV treatment on the patient [4] should also be quantitatively considered, further imposing restrictions on parameters such as viral infection rate and oncolysis rate. Incorporating the impact of oxygen concentration of the tumour microenvironment as in chapter 3 is also a viable next step. Incorporation of conventional chemotherapy into the model may also potentially provide interesting insights regarding combination therapies.

We also suggest incorporation of lymph node modelling as in Chapter 3. To that end, we can consider some probability of spreading to the lymph node, P, as a function of total tumour cell density. Then we propose the following modifications to system (4.3) - (4.5):

$$\frac{\partial u}{\partial t} = D_1 \frac{\partial}{\partial x}\left[\left(1 - \frac{v}{K}\right)\frac{\partial u}{\partial x}\right] + r_1 u\left(1 - \frac{u+n+v}{K}\right) - \theta un - \eta \int_\Omega u(x,t)\mathrm{d}x \cdot P\left(\int_\Omega [u(x,t) + n(x,t)]\mathrm{d}x\right)$$

$$\frac{\partial n}{\partial t} = D_2 \frac{\partial}{\partial x}\left[\left(1 - \frac{v}{K}\right)\frac{\partial n}{\partial x}\right] + r_2 n\left(1 - \frac{u+n+v}{K}\right) + \theta un - \gamma n - \eta \int_\Omega n(x,t)\mathrm{d}x \cdot P\left(\int_\Omega [u(x,t) + n(x,t)]\mathrm{d}x\right)$$

$$\frac{\partial v}{\partial t} = -\phi_1 uv - \phi_2 nv + r_3 v\left(1 - \frac{u+n+v}{K}\right)$$

$$\frac{\partial u_l}{\partial t} = r_1 u_l\left(1 - \frac{u_l+n_l}{K_l}\right) - \theta u_l n_l + \eta \int_\Omega u(x,t)\mathrm{d}x \cdot P\left(\int_\Omega [u(x,t)+n(x,t)]\mathrm{d}x\right)$$

$$\frac{\partial n_l}{\partial t} = r_2 n_l\left(1 - \frac{u_l+n_l}{K_l}\right) + \theta u_l n_l - \gamma n_l - \eta \int_\Omega n(x,t)\mathrm{d}x \cdot P\left(\int_\Omega [u(x,t)+n(x,t)]\mathrm{d}x\right)$$

where u_l and n_l are, respectively, the densities of the uninfected tumour cells and the infected tumour cells at the first (sentinel) lymph node. The spatial domain of the primary lesion on the skin is given by $\Omega \subset \mathbb{R}$. The parameter η accounts for the speed of spreading to the lymph node and the carrying capacity at the lymph node is give by K_l. The analysis of this model is left to future work.

Bibliography

[1] Almuallem, N., Trucu, D., & Eftimie, R. (2021). Oncolytic viral therapies and the delicate balance between virus-macrophage-tumour interactions: A mathematical approach. *Mathematical Biosciences and Engineering*, 18(1), 764-799.

[2] Anderson, A. R., Chaplain, M. A., Newman, E. L., Steele, R. J., & Thompson, A. M. (2000). Mathematical modelling of tumour invasion and metastasis. *Computational and Mathematical Methods in Medicine*, 2(2), 129-154.

[3] Bhatt, D. K., Janzen, T., Daemen, T., & Weissing, F. J. (2022). Modelling the spatial dynamics of oncolytic virotherapy in the presence of virus-resistant tumor cells. bioRxiv.

[4] Binz, E., & Lauer, U. M. (2015). Chemovirotherapy: Combining chemotherapeutic treatment with oncolytic virotherapy. *Oncolytic Virotherapy*, 4, 39.

[5] Browning, A. P., Haridas, P., & Simpson, M. J. (2019). A Bayesian sequential learning framework to parameterise continuum models of melanoma invasion into human skin. *Bulletin of Mathematical Biology*, 81(3), 676-698.

[6] Colson, C., Sánchez-Garduño, F., Byrne, H. M., Maini, P. K., & Lorenzi, T. (2021). Travelling-wave analysis of a model of tumour invasion with degenerate, cross-dependent diffusion. *Proceedings of the Royal Society* A, 477(2256), 20210593.

[7] Gatenby, R. A., & Gawlinski, E. T. (1996). A reaction-diffusion model of cancer invasion. *Cancer Research*, 56(24), 5745-5753.

[8] Dale, P. D., Sherratt, J. A., & Maini, P. K. (1994). The speed of corneal epithelial wound healing. *Applied Mathematics Letters*, 7(2), 11-14.

[9] DePillis, L., Gallegos, A., & Radunskaya, A. (2013). A model of dendritic cell therapy for melanoma. *Frontiers in Oncology*, 3

[10] El-Hachem, M., McCue, S. W., & Simpson, M. J. (2020). A sharp-front moving boundary model for malignant invasion. *Physica D: Nonlinear Phenomena*, 412, 132639.

[11] El-Hachem, M., McCue, S. W., & Simpson, M. J. (2021). Travelling wave analysis of cellular invasion into surrounding tissues. *Physica D: Nonlinear Phenomena*, 428, 133026.

[12] Fife, P.C., *Mathematical Aspects of Reaction and Diffusion Systems*, Lecture Notes in Biomathematics, Vol.28, Springer, Berlin, New York, 1979.

[13] Gallay, T., & Mascia, C. (2022). Propagation fronts in a simplified model of tumor growth with degenerate cross-dependent self-diffusivity. *Nonlinear Analysis: Real World Applications*, 63, 103387.

[14] Hamam, H. (2017). Modelling and investigation of drug and immune therapies for cancer (Doctoral dissertation, University of Dundee).

[15] Murray, J.D. *Mathematical Biology I: An Introduction*. Third edition, Springer, New York, (2002)

[16] Malinzi, J., Ouifki, R., Eladdadi, A., Torres, D. F., & White, K. A. (2018). Enhancement of chemotherapy using oncolytic virotherapy: mathematical and optimal control analysis. arXiv preprint arXiv:1807.04329.

[17] Paiva, L. R., Binny, C., Ferreira Jr, S. C., & Martins, M. L. (2009). A multiscale mathematical model for oncolytic virotherapy. *Cancer Research*, 69(3), 1205-1211.

[18] Pavel, T. I., Chircov, C., Rădulescu, M., & Grumezescu, A. M. (2020). Regenerative wound dressings for skin cancer. *Cancers*, 12(10), 2954.

[19] Pooladvand, P., Yun, C. O., Yoon, A. R., Kim, P. S., & Frascoli, F. (2021). The role of viral infectivity in oncolytic virotherapy outcomes: A mathematical study. *Mathematical Biosciences*, 334, 108520.

[20] Wang, Z., Guo, Z., & Smith, H. (2019). A mathematical model of oncolytic virotherapy with time delay. *Mathematical Biosciences and Engineering*, 16(4), 1836-1860.

[21] Wodarz, D. (2001). Viruses as antitumor weapons: defining conditions for tumor remission. *Cancer Research*, 61(8), 3501-3507.

Chapter 5

Conclusions and Future Work

The mathematical modelling of spatial invasions can provide many useful insights in field and clinical work. In this thesis, we investigated biological invasions in two seemingly disparate contexts: the ecological problem of the spreading of invasive weeds and the oncology problem of the spreading of an invasive cancer. We considered spatial spreading as a connective tissue between the models. In all cases, we considered some notion of biological control on the spreading – invasive weeds were inhibited by competition with native plants and melanoma was inhibited by treatment via an oncolytic virus. We provided evidence concerning the importance of multiple key factors in preventing unfavourable invasion events. We found these factors to include environmental conditions, competition capabilities of native plants, infection and oncolysis capabilities of oncolytic virues, and regenerative abilities of the competing species (native plants in Chapter 2 and the healthy cell density in Chapter 4). We determined conditions on the model parameters which would lead to ecologically or clinically favourable outcomes.

In Chapter 2, we considered the spreading of an invasive weeds, *T. fluminensis*. We expanded on the work of Hogan and Myerscough [5] by taking a model of weed growth and introducing a new variable to account for competition with a native plant. Our modelling suggested that maintaining a large ratio of weed death to weed renewal is important in mitigating the damage done by the weed. We also found that an increased rate of competition between the

native plant and the weed (i.e., increased resilience of the native species) can cause a transition from a nearly extinct steady state of the system to a co-existence steady state. Furthermore, our modelling suggested that using the physical boundary as a control is more effective for faster spreading weeds – this is consistent with the existing ecological literature [6].

In Chapter 3, we developed an ordinary differential equation model of the spread of melanoma being treated by oncolytic virotherapy. An important consideration in cancer treatment is the oxygen concentration of the tumour microenvironment. We also extended the model to a regional model by incorporating spread through the lymphatic system. Our model incorporates the effect of hypoxia on treatment with an oncolytic adenovirus, such as ONYX-015. Oncolytic adenoviruses are well known for their decreased efficacy under hypoxic conditions [11]. Our modelling suggested that two important features of an oncolytic virus, the infection rate and the oncolysis rate, should be considered as functions of available oxygen concentration. For lower oxygen concentrations, preferential viruses should have increased oncolytic capabilities. However, we also found that a large infection rate of the virus is necessary so that tumour cells are not killed off faster than they may be used as hosts for viral replication. Our findings contribute to a growing body of literature regarding efficacy of engineered viruses [7, 8, 9].

In Chapter 4, we developed a continuous spatial model of tumour spreading in response to oncolytic viroterapy, based on work of prior authors [1, 2, 4]. The (main) novelty of our model was the addition of an oncolytic virus. Consistent with the results of Chapter 3, we found more evidence to further support the existence of a delicate balance between the rate at which the virus infects cancer cells and the oncolysis rate. As in Chapter 3, engineering a virus which is too potent at killing relative to its infection rate leads to negative treatment outcomes but lack of potency defeats the purpose of the treatment. We provided bounds on the oncolysis rate – these bounds depend on the infection rate and the regeneration rate of the healthy cells. This led us to further investigate the significance of the regeneration rate of healthy tissue. Our numerical investigations revealed that an increase in this regeneration rate, i.e., through auxiliary topical treatments [10]. These results were also consistent with the existing oncology literature.

How do these chapters connect? The connection between Chapters 3 and 4 is readily apparent – the spatial modelling of oncolytic virotherapy. While the models used are different, the results of each chapter are consistent with the other. The connection between Chapters 2 and 4 is in the investigation of travelling wave solutions of the PDE models. The connection between Chapters 2 and 3 lies in the incorporation of the effects of the environment. In Chapter 2, the environment is incorporated in the carrying capacity of the forest, as both the weed and the native species must share the forest. As our theoretical modelling has shown, an increased carrying capacity of the forest leads to the necessary conditions for co-existence of the species and hence precludes the possibility of extinction of the native plants. In Chapter 3, the environmental conditions are represented by the oxygen concentration of the tumour microenvironment. In this case, an increased availability of oxygen lead to more favourable treatment outcomes. These chapters both provide quantitative evidence of how improving environmental factors may lead to more favourable outcomes in which invasion does not occur.

5.1 Future Work

There is much direction regarding potential future work. From a mathematical perspective, analytically proving the existence of travelling wave solutions for the higher-dimensional models in Chapters 2 and 4 may grant further insights regarding the model parameters. From a biological perspective, we suggest considering more complex geometries in terms of the patterns of spatial spread. For Chapter 2, this means considering diffusion as well as advection as a method of spread. Furthermore, the spread of the weed is more realistically captured by considering the spread on a plane rather than on a line. In Chapter 3, a linear lattice was considered when modelling the lymphatic system. In reality, there are many different graphs which arise from the connection between lymph nodes, as more than one lymph node may be connected to any given node. The linear lattice we used does well in capturing certain connections, but considering more complex networks is an important next step. In Chapter 4, we may consider

a three-dimensional spatial domain to capture a greater degree of realism. In particular, a next step is the use of spherical coordinates in the PDE model. Finally, it has also been long speculated that oncolytic viruses may have therapeutic properties on a systemic level by triggering an immune response against the cancer cells [3]. Next steps should involve the introduction of an additional variable accounting for cytotoxic T lymphocytes (CTLs) to the models of Chapters 3 and 4. The introduction of these white blood cells into such mathematical modelling has been considered by other authors in previous work[12], but this may be extended through incorporating the oxygen dependence we considered in Chapter 3 or the cross-dependent diffusion we considered in Chapter 4. Furthermore, since CTLs are predominantly found in the lymph nodes, this is a natural extension to the regional lymph node model we proposed in Chapter 3. We leave this exploration for future work.

Bibliography

[1] Colson, C., Sánchez-Garduño, F., Byrne, H. M., Maini, P. K., & Lorenzi, T. (2021). Travelling-wave analysis of a model of tumour invasion with degenerate, cross-dependent diffusion. *Proceedings of the Royal Society A*, 477(2256), 20210593.

[2] El-Hachem, M., McCue, S. W., & Simpson, M. J. (2021). Travelling wave analysis of cellular invasion into surrounding tissues. *Physica D: Nonlinear Phenomena*, 428, 133026.

[3] Filley, A. C., & Dey, M. (2017). Immune system, friend or foe of oncolytic virotherapy?. *Frontiers in Oncology*, 7, 106.

[4] Gallay, T., & Mascia, C. (2022). Propagation fronts in a simplified model of tumor growth with degenerate cross-dependent self-diffusivity. *Nonlinear Analysis: Real World Applications*, 63, 103387.

[5] Hogan, A. B., & Myerscough, M. R. (2017). A model for the spread of an invasive weed, Tradescantia fluminensis. *Bulletin of Mathematical Biology*, 79(6), 1201-1217.

[6] James A, Molloy SM, Ponder-Sutton A, Plank MJ, Lamoureaux SL, Bourdôt GW, Kelly D. (2015), Modelling Tradescantia fluminensis to assess long term survival. *PeerJ* 3:e1013 https://doi.org/10.7717/peerj.1013

[7] Jenner, A. L., Yun, C. O., Kim, P. S., & Coster, A. C. (2018). Mathematical modelling of the interaction between cancer cells and an oncolytic virus: insights into the effects of treatment protocols. *Bulletin of Mathematical Biology*, 80(6), 1615-1629.

[8] Kim, D., Kim, H., Wu, H., & Shin, D. H. (2020). The Effect of the Infection Rate on Oncolytic Virotherapy. *Computational Biology and Bioinformatics*, 8(1).

[9] Kurozumi, K., Hardcastle, J., Thakur, R., Yang, M., Christoforidis, G., Fulci, G., ... & Kaur, B. (2007). Effect of tumor microenvironment modulation on the efficacy of oncolytic virus therapy. *Journal of the National Cancer Institute*, 99(23), 1768-1781.

[10] Pavel, T. I., Chircov, C., Rădulescu, M., & Grumezescu, A. M. (2020). Regenerative wound dressings for skin cancer. *Cancers*, 12(10), 2954.

[11] Sheng Guo, Z. (2011). The impact of hypoxia on oncolytic virotherapy. *Virus Adaptation and Treatment*, 3(1), 71-82.

[12] Wodarz, D. (2001). Viruses as antitumor weapons: defining conditions for tumor remission. *Cancer Research*, 61(8), 3501-3507.

Appendix A

Python Code: Chapter 3 Regional Model

The following is the Python code used to generate the plots in Chapter 3.

We begin with the code used to plot the solutions of both the local ((3.1) - (3.3)) and regional (system (3.34) - (3.40)) models. To obtain plots for the local model, we may set the spreading rate of tumour cells away from the primary tumour, η_0, to 0. For non-negative η_i values, the code produces plots which include lymph node involvement.

```
import numpy as np
import matplotlib.pyplot as plt
from scipy.integrate import odeint

#Parameters:

r1, r2 = 0.3954, 0.21;
K, alpha = 1e6, 1e5;
phi, beta, q1, q2 = 1e4, 5.0976, 5.47e-5, 0.5*(5.47e-5);
theta0, thetainf, k_theta = 0.005115, 2.115, 0.016
gamma0, gammainf, k_gamma = 0.1, 0.9, 0.08;

K1, K2, K3 = K/10, K/10, K/10;
alpha1, alpha2, alpha3 = alpha/10, alpha/10, alpha/10;
K_values = [K,K1,K2,K3];
```

```
16
17 eta = 0.0002; #Comment this out if eta not constant.
18 eta_values = [eta for i in range(4)] #The case with 3 lymph nodes.
19
20 #Functions:
21 def theta(x):
22
23     return thetainf*theta0/(theta0 + (thetainf - theta0)*( np.exp((-1)*
    k_theta*x)))
24
25 def gamma(x):
26
27     return gammainf*gamma0/(gamma0 + (gammainf - gamma0)*( np.exp((-1)*
    k_gamma*x) ))
28
29 def p(i,x):
30
31     Lambda = ((-1)*np.log(0.3))/K_values[i] #start at i = 0
32
33     return 1 - np.exp((-1)*Lambda*x)
34
35 def ODEs(x,t):
36
37     u, n, c, u1, n1, c1 = x[0], x[1], x[2], x[3], x[4], x[5]
38     u2, n2, c2 = x[6], x[7], x[8]
39     u3, n3, c3 = x[9], x[10], x[11]
40
41     dudt = r1*u*(1 - (u+n)/K) - ((theta(c))*n*u)/(alpha + n) - eta_values
    [0]*u*p(0,u+n) + 0.05*eta_values[1]*u1*p(1,u1+n1)
42     dndt = r2*n*(1 - (u+n)/K) + ((theta(c))*n*u)/(alpha + n) - (gamma(c))*n
     - eta_values[0]*n*p(0,u+n) + 0.05*eta_values[1]*n1*p(1,u1+n1)
43     dcdt = phi - beta*c - q1*u*c - q2*n*c
44
```

```
    du1dt = r1*u1*(1 - (u1+n1)/K1) - ((theta(c1))*n1*u1)/(alpha1 + n1) - eta_values[1]*u1*p(1,u1+n1) +  eta_values[0]*u*p(0,u+n)  + 0.05* eta_values[2]*u2*p(2,u2+n2)
    dn1dt = r2*n1*(1 - (u1+n1)/K1) + ((theta(c1))*n1*u1)/(alpha1 + n1) - (gamma(c1))*n1 - eta_values[1]*n1*p(1,u1+n1) + eta_values[0]*n*p(0,u+n) + 0.05*eta_values[2]*n2*p(2,u2 + n2)
    dc1dt =  (-1)*beta*c1 - q1*u1*c1 - q2*n1*c1

    du2dt = r1*u2*(1 - (u2+n2)/K2) - ((theta(c2))*n2*u2)/(alpha2 + n2) - eta_values[2]*u2*p(2,u2+n2) +  0.95*eta_values[1]*u1*p(1,u1+n1) + 0.05* eta_values[3]*u3*p(3,u3+n3)
    dn2dt = r2*n2*(1 - (u2+n2)/K2) + ((theta(c2))*n2*u2)/(alpha2 + n2) - (gamma(c2))*n2 - eta_values[2]*n2*p(2,u2+n2) + 0.95*eta_values[1]*n1*p (1,u1+n1) + 0.05*eta_values[3]*n3*p(3,u3+n3)
    dc2dt =  (-1)*beta*c2 - q1*u2*c2 - q2*n2*c2

    du3dt = r1*u3*(1 - (u3+n3)/K3) - ((theta(c3))*n3*u3)/(alpha3 + n3) - 0.05*eta_values[3]*u3*p(3,u3+n3) +  0.95*eta_values[2]*u2*p(2,u2+n2)
    dn3dt = r2*n3*(1 - (u3+n3)/K3) + ((theta(c3))*n3*u3)/(alpha3 + n3) - (gamma(c3))*n3 - 0.05*eta_values[3]*n3*p(3,u3+n3) + 0.95*eta_values[2]* n2*p(2,u2+n2)
    dc3dt =  (-1)*beta*c3 - q1*u3*c3 - q2*n3*c3

    return [dudt, dndt, dcdt, du1dt, dn1dt,dc1dt, du2dt, dn2dt, dc2dt, du3dt, dn3dt, dc3dt]

#Initial conditions:
u0, n0, c0, u10, n10, c10 = 10000,100, 4.3751, 0, 0, 4.375;
u20, n20, c20 = 0, 0,  4.375;
u30, n30, c30 = 0, 0,  4.375;
init_0 = [u0, n0, c0, u10, n10, c10, u20, n20, c20, u30, n30, c30];

#Numerically solving and plotting the solution of the regional model:
```

```
t = np.linspace(0,80,10000);#domain

x = odeint(ODEs, init_0,t);  #integrating

u, n, c = x[:,0], x[:,1], x[:,2];
u1, n1, c1 = x[:,3], x[:,4], x[:,5];
u2, n2, c2 = x[:,6], x[:,7], x[:,8];
u3, n3, c3 = x[:,9], x[:,10],x[:,11];

plt.plot(t,u+n,'red',label='Primary Tumour',linewidth=3);
plt.plot(t,u1+n1,'green',label='Lymph Node 1',linewidth=3);
plt.plot(t,u2+n2,'blue',label='Lymph Node 2',linewidth=3);
plt.plot(t,u3+n3,'purple',label='Lymph Node 3',linewidth=3);
plt.xlim(0)
plt.ylim(0)
plt.legend(('Primary Tumour Cell Density', 'Lymph Node 1 Cell Density', '
    Lymph Node 2 Cell Density', 'Lymph Node 3 Cell Density'),
               loc='upper right')
plt.ylabel("Cell Density (cells/mm$^3$)")
plt.xlabel("Time (days)")


```

The following code produces the heatmap in Figure 3.15. This multi-parametric analysis shows the peak tumour density value for various values of constant θ and γ over an interval of 100 days after initial OV treatment is administered.

```
t_val = 100; #Solve over this interval.
N = 100; #N+1 values of theta and gamma used.
theta_values = [0.01*i for i in range(0,N+1)];
gamma_values = [0.01*i for i in range(0,N+1)];
max_cancer_cells = [[] for i in range(0,N+1)];

i = 0;
```

```
for j in theta_values:
    theta0 = j;
    thetainf = j;

    for k in gamma_values:
        gamma0 = k;
        gammainf = k;

        x = odeint(ODEs, init_0,t);

        u = x[:,0];
        n = x[:,1];
        c = x[:,2];

        max_cancer_cells[i].append((max(u+n)));

    i = i + 1;

plt.xlabel("Virus-Induced Death Rate ($\gamma$)")
plt.ylabel("Infection Rate ($\Theta$)")

img = plt.contourf(theta_values,gamma_values,max_cancer_cells,100,cmap='
    rainbow')
plt.colorbar(img)


```

Tedi Ramaj

Curriculum Vitae

Education

2017–Present (in progress) **Ph.D. Applied Mathematics**, *Western University*, London, Ontario
Nonlinear Dynamics, Control Theory, and Mathematical Biology. Direct Entry from Master's enrollment in 2019. Supervised by Prof. Xingfu Zou.

2013–2017 **B.Sc. Mathematics**, *McGill University*, Montréal, Québec
Major Mathematics, Minor Biology

Peer-Reviewed Publications

2021/01/07 Ramaj, T. **On the Mathematical Modelling of Competitive Invasive Weed Dynamics**. Bull Math Biol 83, 13 (2021). https://doi.org/10.1007/s11538-020-00825-9

Submitted Papers

2022/10/18 **Workplace Absenteeism due to COVID-19 and Influenza: A Mathematical Model**
Co-authored with Avusuglo, Fall, Ghimire, Lee, Li, Mosleh, Sharbayta, Shi, Shin, Thommes, & Wu (Alphabetical). Submitted to the Journal of Theoretical Biology after approval from internal company reviewers.

Papers in Preparation

2022 Ramaj, T., Zou, X. **On the Treatment of Melanoma: A Mathematical Model of Oncolytic Virotherapy**, in preparation.

2022 Ramaj, T., Zou, X. **A Continuous Spatial Model of Melanoma Treatment via Oncolytic Virotherapy**, in preparation.

Relevant Teaching Experience

2022/01/01 –2022/04/30 **Course Instructor**, *Western University*, London, Ontario
Course Instructor for NMM2270B, ordinary differential equations for engineering students. Delivered lectures and tutorials. Created and graded assignments and examinations.

2017–Present **Graduate Teaching Assistant**, *Western University*, London, Ontario
Grading, leading tutorials, and holding help centre hours on various courses such as linear algebra with numerical analysis, differential equations, & calculus and probability for biology students.

2015–2017 **Mathematics Tutor**, *McGill University Tutorial Services*, Montréal, Québec
Tutoring undergraduate students in various undergraduate courses, including calculus, linear algebra, differential equations, nonlinear dynamical systems, and computer science.

Relevant Research Experience

2017–Present **Graduate Research Assistant**, *Western University*, London, Ontario
GRA in Prof. Xingfu Zou's lab group.

2014–2016 **Research Assistant**, *Netramark Corp*, Toronto, Ontario
Worked under the guidance of Dr. Joseph Geraci at Netramark Corp. Used Python to write programs relevant to Dr. Geraci's research related to the study of complex diseases.

Honours & Awards

2020/05 – 2021/04, 2021/05 – 2022/04 **Ontario Graduate Scholarship**
Research Scholarship for the study of mathematical and computational modelling of oncolytic virotherapy; granted twice.

2013 **Honour Roll 2013 Euclid Contest**
Grade 12 University of Waterloo Mathematics Contest. Scored in the top 1% of over 17000 contestants in Canada.

Conference Presentations

2021/10/04 Ramaj, T. A Mathematical Model of Melanoma Treatment via Oncolytic Virotherapy, **Fred Hutch** 5th Workshop on Virus Dynamics, Virtual Conference

2019/12/07 Ramaj, T., A Dynamical Systems Approach to Modelling Competition Between Invasive Weeds and Native Plants, 2019 Canadian Mathematical Society Winter Meeting, Toronto, Ontario

Conferences

2021/05–2021/06 Fields CQAM Thematic Program on Integrative Modeling of Emerging Infectious Disease Outbreaks., The Fields Institute for Research in Mathematical Sciences
Conference on mathematical modelling of COVID-19. Paper currently submitted with research group from conference.

2019/06 Workshop on Mathematical Ecology., *Queen's University*, Kingston, Ontario
Workshop on modelling of structured populations.

Technical & Software Skills

Programming Languages Python, Java, C++, Matlab, Mathematica, HTML, SQL
Familiarity with object-oriented programming and data structures. Experience with coding in a research setting.

Software LaTeX, Spreadsheets, Git

Research Interests

Mathematical Biology:
Oncolytic virotherapy & immunotherapy modelling, Lotka-Volterra models, invasive species dynamics, structured population dynamics, epidemiology.

Dynamical Systems:
Ordinary differential equations, partial differential equations, delay differential equations, existence of travelling wave solutions.

Computational Modelling and Simulations